Intracranial aneurysms: risk factors for development and rupture

Rachel Kleinloog

Cover	Iris Jansen | Lágrima de sangre
Layout	Renate Siebes | Proefschrift.nu
Printed by	Proefschriftmaken.nl
ISBN	978-90-393-6847-3

© 2017 Rachel Kleinloog
All rights reserved. No part of this publication may be reproduced, stored in a retrieval system, or transmitted, in any form or by any means, electronically, mechanically, by photo-copying, recording or otherwise, without the prior written permission of the author. The copyright of the published articles has been transferred to the respective journals.

Intracranial aneurysms: risk factors for development and rupture

Risicofactoren voor het ontstaan en barsten van aneurysmata in het hoofd

(met een samenvatting in het Nederlands)

PROEFSCHRIFT

ter verkrijging van de graad van doctor aan de
Universiteit Utrecht op gezag van de rector magnificus,
prof.dr. G.J. van der Zwaan, ingevolge het besluit van het
college voor promoties in het openbaar te verdedigen
op donderdag 19 oktober 2017 des middags te 4.15 uur

door

Rachel Kleinloog

geboren op 2 oktober 1985
te Delft

Promotoren:	Prof.dr. L. Regli
	Prof.dr. G.J.E. Rinkel
Copromotoren:	Dr. Y.M. Ruigrok
	Dr. B.H. Verweij

Financial support by the Dutch Heart Foundation for the publication of this thesis is gratefully acknowledged. Publication of this thesis was also financially supported by ChipSoft.

CONTENTS

1

General introduction

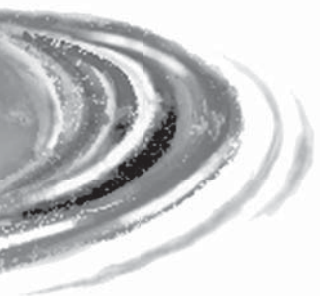

Intracranial aneurysms are acquired vascular abnormalities that arise predominantly at the bifurcations of the arteries of the circle of Willis, and occur in approximately 3% of the population.[1] Given the rising availability and quality of brain imaging, the number of incidentally discovered aneurysms is increasing.[2] The pathogenesis of intracranial aneurysms is largely unknown but we do know that genetic factors contribute to the disease. Genome-wide association studies (GWAS) of patients with intracranial aneurysms identified six genetic risk loci (4q31.23, 8q11.23-q12.1, 9p21.3, 10q24.32, 13q13.1 and 18q11.2) associated with intracranial aneurysms.[3-5] These genetic risk loci only explain a small amount of the genetic risk for intracranial aneurysms.[5] More knowledge on genes involved in aneurysms is needed and will lead to a better understanding of its pathogenesis.

Rupture of an aneurysm results in aneurysmal subarachnoid haemorrhage (aSAH), a subtype of stroke. Since aSAH often occurs at a young age and has a high case fatality and morbidity,[6] its impact is enormous, not only from the patient's perspective but also from societal and economic prospect.[7] Treatment of unruptured aneurysms can prevent rupture, but carries a risk of major complications including death, depending on age of the patient, and size and site of the aneurysm.[8-10] Preventive treatment should therefore ideally be restricted to those patients with aneurysms that have a high risk of rupture.

Risk factors identified for the development of aneurysms include female gender, cigarette smoking,[11] and hypertension.[12,13] The risk factors for aneurysm rupture include patient-related risk factors, such as higher age, female gender, history of hypertension or aSAH, and Japanese or Finish descent, and aneurysm-related risk factors, including aneurysm size, aneurysm location and symptomatic aneurysms.[14,15] Other factors that might predict aneurysm rupture include cigarette smoking,[16] and a family history of aSAH.[17] However, risk prediction for aneurysm rupture remains poor, since these risk factors stratify only between the lowest 5-year risk of rupture of 0.4%, and a risk of 17.8% when all risk factors are present.[15]

With aneurysm size being one of the most important imaging markers for rupture,[15] large aneurysms are often treated, although a considerable proportion of these aneurysms would have never ruptured.[18] Most unruptured aneurysms discovered incidentally or during screening are small,[1] with inherently small risk of rupture.[18] Consequently, these aneurysms are often left untreated. However, the relatively high prevalence of small unruptured aneurysms causes that, paradoxically, most ruptured aneurysms are small.[19,20] Therefore, better identification of rupture prone aneurysms is needed to tailor preventive treatment to those aneurysms.

This thesis focuses on identifying potential new risk factors for development and rupture of intracranial aneurysms by using today's state-of-the-art techniques. New factors associated with rupture might improve risk prediction, and improve tailored treatment of unruptured

aneurysms. Furthermore, better understanding of the pathogenesis of development and rupture of aneurysms may lead to the development of new treatment strategies in the future.

- The first aim of this thesis is to review the literature on risk factors for rupture additional to the factors currently used in clinical practice.
- The second aim of this thesis is to identify genes and pathways involved in both development and rupture of intracranial aneurysms.
- The third aim of this thesis is to investigate whether ultra-high resolution 7.0 Tesla magnetic resonance imaging (MRI) in patients with unruptured intracranial aneurysms can image potential new risk factors for rupture.

OUTLINE OF THE THESIS

Risk factors for rupture of intracranial aneurysms

As a starting point for the search for new risk factors for rupture of aneurysms, in **chapter 2**, we systematically reviewed the literature on risk factors for rupture to identify genetic, molecular, morphological and hemodynamic factors additional to the factors currently used in clinical practice.

Identification of genes and pathways involved in development and rupture of intracranial aneurysms

In **chapter 3** of this thesis, we analysed the association between aneurysm size at the time of rupture and the six genetic risk loci for intracranial aneurysms, which were identified in the genome-wide association studies on intracranial aneurysms.[3-5]
In **chapter 4**, we describe a genome-wide expression study in aneurysm wall biopsies, by using RNA sequencing methodology, to identify genes and pathways involved in development and rupture of aneurysms.

7.0 Tesla magnetic resonance imaging of intracranial aneurysms

Since several years, 7.0 Tesla MRI has become available to image the brain in humans. The ultra-high-field can increase signal-to-noise ratio, spatial resolution or imaging speed. This offers new opportunities to image those characteristics of the aneurysm, for which clinically available imaging techniques, e.g. 1.5 and 3.0 Tesla MRI, lack resolution. These characteristics might be potential risk factors for rupture.

In **chapter 5**, we assessed the feasibility to image the aneurysm wall and its thickness on 7.0 Tesla MRI. In **chapter 6**, we developed a semi-quantitative method to assess wall thickness variation on images of the vessel wall sequence used in chapter 5. This enabled us to study the relation between apparent wall thickness and wall shear stress, which might give more insight in the pathogenesis of aneurysms.
In **chapter 7**, the feasibility to quantify volume pulsation of the aneurysm during the cardiac cycle, another potential risk factor for rupture, is studied on 7.0 Tesla MRI, complemented with an aneurysm-specific accuracy analysis.

The results of this thesis are put into perspective in **chapter 8**, and future directions are discussed.

REFERENCES

1. Vlak MH, Algra A, Brandenburg R, Rinkel GJ. Prevalence of unruptured intracranial aneurysms, with emphasis on sex, age, comorbidity, country, and time period: a systematic review and meta-analysis. *Lancet Neurol.* 2011;10:626-636.
2. Gabriel RA, Kim H, Sidney S, McCulloch CE, Singh V, Johnston SC, et al. Ten-year detection rate of brain arteriovenous malformations in a large, multiethnic, defined population. *Stroke.* 2010;41:21-26.
3. Bilguvar K, Yasuno K, Niemela M, Ruigrok YM, von Und Zu Fraunberg M, van Duijn CM, et al. Susceptibility loci for intracranial aneurysm in European and Japanese populations. *Nat Genet.* 2008;40:1472-1477.
4. Yasuno K, Bakircioglu M, Low SK, Bilguvar K, Gaal E, Ruigrok YM, et al. Common variant near the endothelin receptor type A (EDNRA) gene is associated with intracranial aneurysm risk. *Proc Natl Acad Sci U S A.* 2011;108:19707-19712.
5. Yasuno K, Bilguvar K, Bijlenga P, Low SK, Krischek B, Auburger G, et al. Genome-wide association study of intracranial aneurysm identifies three new risk loci. *Nat Genet.* 2010;42:420-425.
6. Nieuwkamp DJ, Setz LE, Algra A, Linn FH, de Rooij NK, Rinkel GJ. Changes in case fatality of aneurysmal subarachnoid haemorrhage over time, according to age, sex, and region: a meta-analysis. *Lancet Neurol.* 2009;8:635-642.
7. Rivero-Arias O, Gray A, Wolstenholme J. Burden of disease and costs of aneurysmal subarachnoid haemorrhage (aSAH) in the United Kingdom. *Cost Eff Resour Alloc.* 2010;8:6-7547-8-6.
8. Alshekhlee A, Mehta S, Edgell RC, Vora N, Feen E, Mohammadi A, et al. Hospital mortality and complications of electively clipped or coiled unruptured intracranial aneurysm. *Stroke.* 2010;41:1471-1476.
9. Brinjikji W, Rabinstein AA, Nasr DM, Lanzino G, Kallmes DF, Cloft HJ. Better outcomes with treatment by coiling relative to clipping of unruptured intracranial aneurysms in the United States, 2001-2008. *AJNR Am J Neuroradiol.* 2011;32:1071-1075.
10. Naggara ON, Lecler A, Oppenheim C, Meder JF, Raymond J. Endovascular treatment of intracranial unruptured aneurysms: a systematic review of the literature on safety with emphasis on subgroup analyses. *Radiology.* 2012;263:828-835.
11. Juvela S, Poussa K, Porras M. Factors affecting formation and growth of intracranial aneurysms: a long-term follow-up study. *Stroke.* 2001;32:485-491.
12. de la Monte SM, Moore GW, Monk MA, Hutchins GM. Risk factors for the development and rupture of intracranial berry aneurysms. *Am J Med.* 1985;78:957-964.
13. Inci S, Spetzler RF. Intracranial aneurysms and arterial hypertension: a review and hypothesis. *Surg Neurol.* 2000;53:530-540.

14. Wermer MJ, van der Schaaf IC, Algra A, Rinkel GJ. Risk of rupture of unruptured intracranial aneurysms in relation to patient and aneurysm characteristics: an updated meta-analysis. *Stroke*. 2007;38:1404-1410.
15. Greving JP, Wermer MJ, Brown RD,Jr, Morita A, Juvela S, Yonekura M, et al. Development of the PHASES score for prediction of risk of rupture of intracranial aneurysms: a pooled analysis of six prospective cohort studies. *Lancet Neurol*. 2014;13:59-66.
16. Juvela S, Poussa K, Lehto H, Porras M. Natural history of unruptured intracranial aneurysms: a long-term follow-up study. *Stroke*. 2013;44:2414-2421.
17. Broderick JP, Brown RD,Jr, Sauerbeck L, Hornung R, Huston J,3rd, Woo D, et al. Greater rupture risk for familial as compared to sporadic unruptured intracranial aneurysms. *Stroke*. 2009;40:1952-1957.
18. Wiebers DO, Whisnant JP, Huston J,3rd, Meissner I, Brown RD,Jr, Piepgras DG, et al. Unruptured intracranial aneurysms: natural history, clinical outcome, and risks of surgical and endovascular treatment. *Lancet*. 2003;362:103-110.
19. Forget TR,Jr, Benitez R, Veznedaroglu E, Sharan A, Mitchell W, Silva M, et al. A review of size and location of ruptured intracranial aneurysms. *Neurosurgery*. 2001;49:1322-1325.
20. Inagawa T. Size of ruptured intracranial saccular aneurysms in patients in Izumo City, Japan. *World Neurosurg*. 2010;73:84-92.

2

RISK FACTORS FOR INTRACRANIAL ANEURYSM RUPTURE: A SYSTEMATIC REVIEW

R. Kleinloog, N. de Mul, B.H. Verweij, J.A. Post,
G.J.E. Rinkel, Y.M. Ruigrok

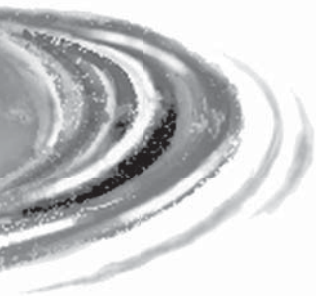

Neurosurgery. 2017: *In press*

ABSTRACT

Background: Intracranial aneurysm rupture prediction is poor, with only a few risk factors for rupture identified and used in clinical practice.

Objective: To provide an overview of all the risk factors (including genetic, molecular, morphological, and hemodynamic factors) that have potential for use in clinical practice.

Methods: We systematically searched PubMed and EMBASE and focused on factors that can be easily assessed in clinical practice, might be used for rupture prediction in clinical practice, and/or are potential targets for further research. Studies were categorized according to methodological quality, and a meta-analysis was performed, if possible.

Results: We included 102 studies describing 144 risk factors that fulfilled predefined criteria. There was strong evidence for the morphological factors irregular shape (studied in 4 prospective cohort studies of high-quality, pooled odds ratio (OR) of 4.8, 95% confidence interval (CI) 2.7–8.7), aspect ratio (pooled OR 10.2, 95% CI 4.3–24.6), size ratio, bottleneck factor, and height-to-width ratio to increase rupture risk. Moderate level of evidence was found for presence of contact with the perianeurysmal environment (pooled OR 3.5, 95% CI 1.4–8.4), unbalanced nature of this contact (pooled OR 17.8, 95% CI 8.3–38.5), volume-to-ostium ratio, and direction of the aneurysm dome (pooled OR 1.5, 95% CI 1.2–1.9).

Conclusion: Irregular aneurysm shape was identified as a risk factor with potential for use in clinical practice. The risk factors aspect ratio, size ratio, bottleneck factor, height-to-width ratio, contact with the perianeurysmal environment, volume-to-ostium ratio, and dome-direction should first be confirmed in multivariate analysis and incorporated in prediction models.

INTRODUCTION

Approximately 3% of the population harbors an unruptured intracranial aneurysm.[1] Given the rising availability and quality of brain imaging, the number of incidentally discovered aneurysms is increasing.[2] Rupture of intracranial aneurysms results in aneurysmal subarachnoid hemorrhage (aSAH), a subset of stroke that has high case fatality and morbidity, and occurs at a relatively young age compared with other types of stroke.[3,4] The incidence of aSAH is only 9 per 100 000 person-years,[5] indicating that the majority of unruptured aneurysms will never rupture. It is important to identify risk factors for rupture to tailor preventive treatment to the aneurysms that are at high risk of rupturing. The number of factors that have been assessed in cohort studies and influence the risk of rupture is limited. These are age, sex, history of hypertension or subarachnoid hemorrhage, aneurysm size, and aneurysm location.[6] Other factors that might predict aneurysm rupture include cigarette smoking[7] and a family history of aSAH.[8] These factors only explain a small proportion of the risk of rupture. Therefore, rupture risk prediction for individual patients is still poor, and consequently the search for new risk factors continues. The aim of the current study was to systematically review the literature on risk factors for rupture to identify genetic, molecular, morphological, and hemodynamic factors in addition to the factors currently used in clinical practice. We focused on factors that can be easily assessed in clinical practice and thus have the potential to be used for rupture prediction. In addition, we aimed to identify potential targets for further research, that is, re-evaluation of the risk factors in large high-quality studies and assessment of their independence in multivariate analysis followed by prediction model studies.

METHODS

For this systematic review, the PRISMA guideline was followed.

Search strategy and selection criteria

We systematically searched the PubMed and EMBASE databases until February 2015 using different combinations of the keywords (or their synonyms): "unruptured," "intracranial," "aneurysm," or "rupture" (see Box 2.1 for the full electronic search strategy). To assess eligibility of the articles found, either N.M. or R.K. screened the titles and abstracts, and, if necessary, the full text, on inclusion and exclusion criteria. If eligibility of an article was questioned by N.M., the article was reviewed by R.K., and vice versa. Any disagreement was resolved by consulting a third reviewer (Y.M.R.). Reference lists of relevant articles were searched for additional publications by R.K. and N.M. until no further publications were found. We

Box 2.1. Search strategy

Full electronic search strategy for the PUBMED database
((unruptured[tiab] OR intracranial[tiab] OR cerebral[tiab] OR brain[tiab] OR intracerebral[tiab]) AND (aneurysm*[tiab]) AND (rupture[tiab] OR growth[tiab] OR follow up[tiab]))

Full electronic search strategy for the EMBASE database
unruptured:ab,ti OR intracranial:ab,ti OR cerebral:ab,ti OR brain:ab,ti OR intracerebral:ab,ti AND aneurysm*:ab,ti AND (rupture:ab,ti OR growth:ab,ti OR follow) AND [embase]/lim

included studies that compared potential factors in (1) ruptured vs unruptured aneurysms; (2) growing vs stable aneurysms during follow-up; (3) unruptured aneurysms of different sizes. Hence, growth and size of the aneurysms were considered surrogate markers of rupture, because large aneurysms and growing aneurysms have a higher risk of rupture.[6,7] We categorized potential factors into genetic (e.g., polymorphisms, mutations), molecular, morphological, and hemodynamic factors. Studies were excluded if they were (1) reviews of the literature, conference abstracts, letters, or case reports (with ≤5 cases), (2) analyzing only mycotic or fusiform aneurysms, (3) animal models, (4) mathematical models (except models based on patient-specific data of multiple aneurysms), or (5) in languages other than English, German, French, Italian, or Spanish. Last, we excluded studies when the risk factor(s) investigated could only be determined during or after treatment of the aneurysm (e.g., intraoperative measurements or measurements in tissue samples of aneurysms obtained during surgery or at autopsy), because these factors cannot be used in the clinical decision-making of whether or not to perform a preventive treatment in unruptured aneurysms. Figure 2.1 shows a flow chart of the literature search with inclusion and exclusion criteria.

Data extraction

We extracted the following data on the methodology of the article: (1) study design being cohort or case control design, prospective or retrospective, and consecutive cases or not, (2) the population included, (3) aim of the study, (4) outcome measure, (5) sample size, (6) data analysis, and (7) data presentation. We extracted the crude data and effect estimates (odds ratio [OR] or risk ratio, and hazard ratio, if applicable) for each factor separately. If an OR was not given, we calculated the OR and its 95% CI from the crude data, if available. If none of these effect estimates was available and crude data were missing, we reported the mean and standard deviation between groups and the statistical significance of their difference, if available. If a certain risk factor was studied in the same patient population and reported upon in 2 or more different publications, we only used data from the most recent publication for further analysis. Data extraction was performed by R.K. and cross-checked by Y.M.R. (senior author).

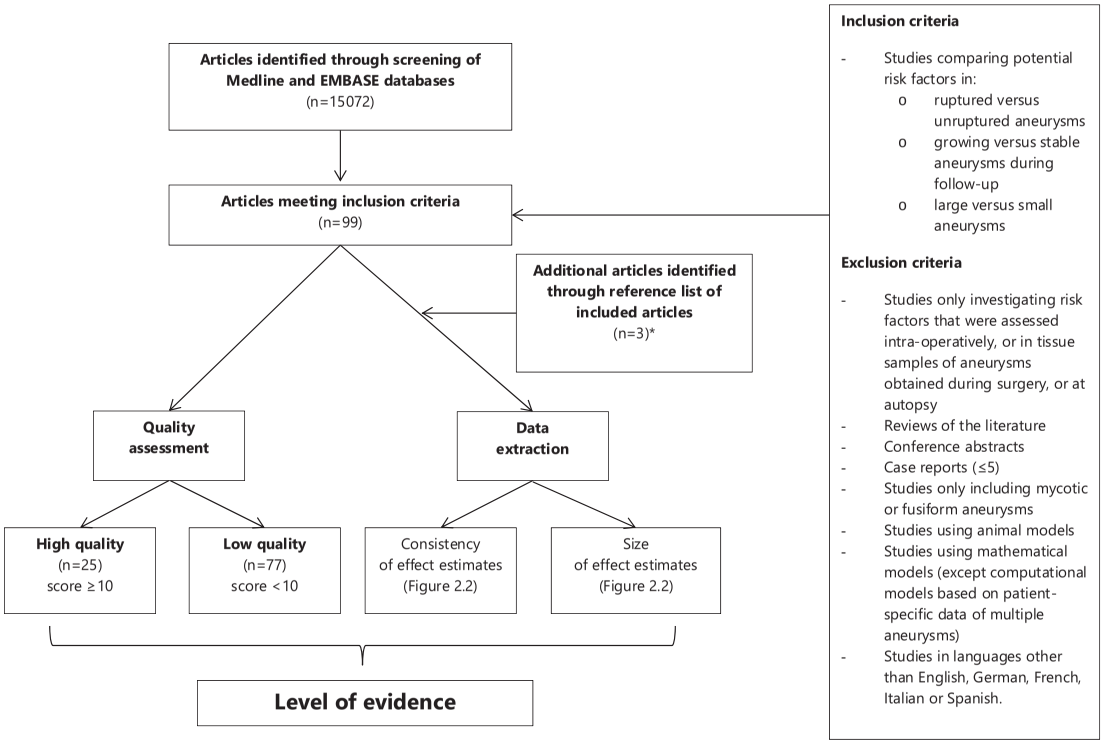

Figure 2.1. Flow chart of the literature search with in- and exclusion criteria.
* Three studies were identified through references of included articles and were not present in the original search.[16-18] The study by Nakaoka et al.[16] was missed because it only used the word "ruptured" instead of the search term "rupture." Bilguvar et al.[17] primarily analyzed genetic risk loci in aneurysms vs controls and did not report on their sub-analysis on ruptured vs unruptured aneurysms (supplied in the Supplement) in their abstract and was therefore missed in the original search. The study by Parlea et al.[18] was missed because the primary objective of the study was to characterize the geometry of simple-lobed aneurysms. Although a sub-analysis of the differences in geometry between ruptured and unruptured aneurysms was included, they did not report this in their abstract.

Table 2.1. Methodological quality score

Study methods		Points
Design	Prospective cohort of unruptured aneurysm until rupture/growth occurs (3) Retrospective cohort of unruptured aneurysm until rupture/growth occurs or a case control design with consecutive cases from a prospective database (2) Case control design with consecutive cases from a retrospective database (1) Non-consecutive case-control design (0)	3
Population	Representative group of patients with aneurysms*	3
	Baseline characteristics (age, gender, aneurysm size, aneurysm location) were described for all patients	1
Aim	The primary aim was to investigate the relationship between hemodynamic, morphological or genetic factors and aneurysm rupture, or surrogate markers of rupture: growth and size.	1
Outcome	Rupture as outcome measure (2) Growth as outcome measure (1) Size as outcome measure (0)	2
Size	• Longitudinal study design: - rupture as outcome: >10 outcomes per risk factor studied (+/- 1% rupture risk per year, >1000 patient years per risk factor)[6] - growth as outcome: >10 outcomes per risk factor studies (10% growth in 2 year, >200 patient years per risk factor)[10] • Cross-sectional study design: >10 outcomes (ruptured aneurysms) per risk factor studied (10 ruptured aneurysms per risk factor), or in case of size as surrogate marker 10 large aneurysms per risk factor.	1
Data analysis and presentation		
	Either crude numbers provided, or odds ratio/relative risk/hazard ratio with 95% CI was provided (1) Both were provided (2)	2
	Statistical analysis included multivariate analysis with inclusion of potential confounders, including aneurysm size and location.	1
	Statistical analysis included multivariate analysis, and the number of predictors studies was less than 1/10 of the total number of aneurysms	1
Total score	<10 = low quality; 10–15 = high quality	15

* A study population was considered not representative if a patient selection was made on age (other than adults), aneurysm size within the clinically relevant range (>3 mm), aneurysm location, number of aneurysms, treatment method or any treatment of the aneurysm (except for studies assessing the occurrence of growth or rupture during follow-up).

Quality assessment

Quality assessment of the studies was performed using an adapted version of a previously published methodological quality score[9] and modified for the topic of our review (Table 2.1).[6,10] Studies with scores between 10 and 15 were defined as high-quality studies, and studies with scores <10 were defined as low-quality studies. In addition, for each factor, we assessed the level of evidence for the association with aneurysm rupture by combining the consistency of the effect estimates in the different studies, the size of the effect estimates, and the methodological quality of the study. We categorized the factors as factors associated (both positive or negative) or not associated with rupture. Level of evidence was categorized into strong, moderate, low, or inconsistent level of evidence (Figure 2.2). The methodological quality and level of evidence was assessed by R.K. and cross-checked by Y.M.R. (senior author).

Potency of risk factors for clinical practice or further clinical research

We used predefined criteria for selection of those risk factors associated (both positive and negative) with rupture that can be directly used in the risk prediction of rupture in clinical practice or have potential for use after further evaluation in multivariate analysis and incorporation into prediction models (Table 2.2). Also, we predefined criteria for selection of risk factors which association with rupture should first be further confirmed in larger studies of higher quality (Table 2.2). Factors not associated with rupture were not considered relevant for use in clinical practice nor as having potential for further clinical research.

Table 2.2. Potential of risk factors associated with rupture

Potential of risk factor	Criterion
To be directly used in risk prediction of rupture in clinical practice*	Factors with strong level of evidence including evidence from >2 cohort studies of high quality with a pooled OR >2.0.
To be used in risk prediction of rupture in clinical practice after further analysis*	Factors with strong and moderate level of evidence
To be further explored in clinical research†	Risk factors associated with rupture but with low level of evidence from a single high quality study (in absence of other studies) Factors with inconsistent evidence if evidence was available from >3 low quality studies and inconsistency was based on 1 low quality study.

* To be suitable for use in clinical practice, these factors should first be tested in multivariate analysis and combined with the risk factors currently used in clinical practice in a prediction model.
† The association of these risk factors with rupture should first be further confirmed in larger high quality prospective cohort studies.

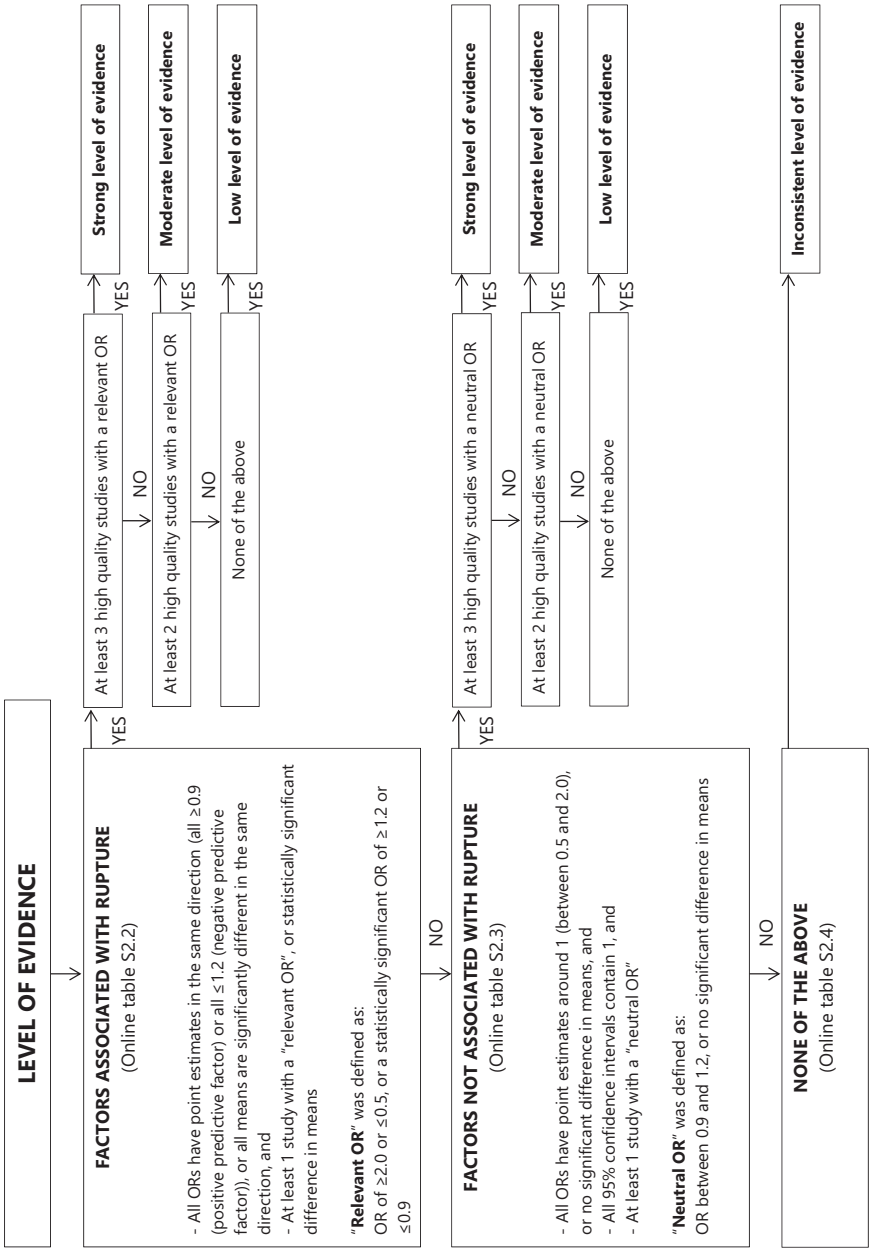

Figure 2.2. Categories for level of evidence for each risk factor.

Analyses

A formal meta-analysis was performed, if possible, by calculating a pooled OR with corresponding 95% CI for factors associated with rupture with a strong or moderate level of evidence assessed in studies that provided crude data and had limited heterogeneity in the definition for the risk factor under study. We applied a random effects model with the Mantel-Haenzsel method by using Review Manager version 5.3.[11] To assess heterogeneity of effects across the studies assessed in the meta-analysis, we used the Higgins I^2.[12] Little to moderate heterogeneity was defined as $I^2 \leq 60\%$ and substantial heterogeneity as $I^2 > 60\%$.

RESULTS

A total of 102 studies analyzing 28 812 aneurysms met our inclusion criteria (see the flow chart, Figure 2.1). These studies reported on 144 different risk factors. Of these risk factors, 12 were genetic, 18 molecular, 59 morphological, and 55 hemodynamic risk factors. Twenty-five studies fulfilled our criteria of high quality. A table with an overview of the study characteristics, including study design, number of aneurysms included, representation of the investigated population, outcome measure, and the methodological quality score of the 102 included studies, is provided in Supplementary table S2.1, as are the references of the studies included. All risk factors with their effect estimates, the methodological quality scores, and the definitions of the factors are shown in Supplementary table S2.2 (factors associated with rupture), Supplementary table S2.3 (factors not associated with rupture), and Supplementary table S2.4 (factors with inconsistent level of evidence).

Factors associated with rupture

Strong level of evidence

Strong evidence for an increased risk of aneurysm rupture was found for 5 different morphological factors: (1) irregular shape of the aneurysm (pooled OR of 4.8, 95% CI 2.7–8.7 based on 10 studies; including multilobulated shape, and the presence of blebs, see Figure 2.3), (2) larger aspect ratio (pooled OR of 10.2, 95% CI 4.3–24.6 based on 3 studies; aneurysm height divided by the diameter of the neck, see Figure 2.3), (3) larger size ratio (aneurysm height divided by the [average] parent vessel diameter), (4) higher bottleneck factor (aneurysm width divided by the diameter of the neck), and (5) height-to-width ratio (aneurysm height divided by the aneurysm width; see Figure 2.3 and Supplementary table S2.2). A pooled analysis of the ORs was not possible for the factors size ratio, bottleneck factor, and height-to-width ratio, either because of the use of different definitions (especially different or lack of cut-off values of ratio's) of the factors in different studies, because of the unavailability of ORs or crude data to calculate ORs, or both. Heterogeneity was

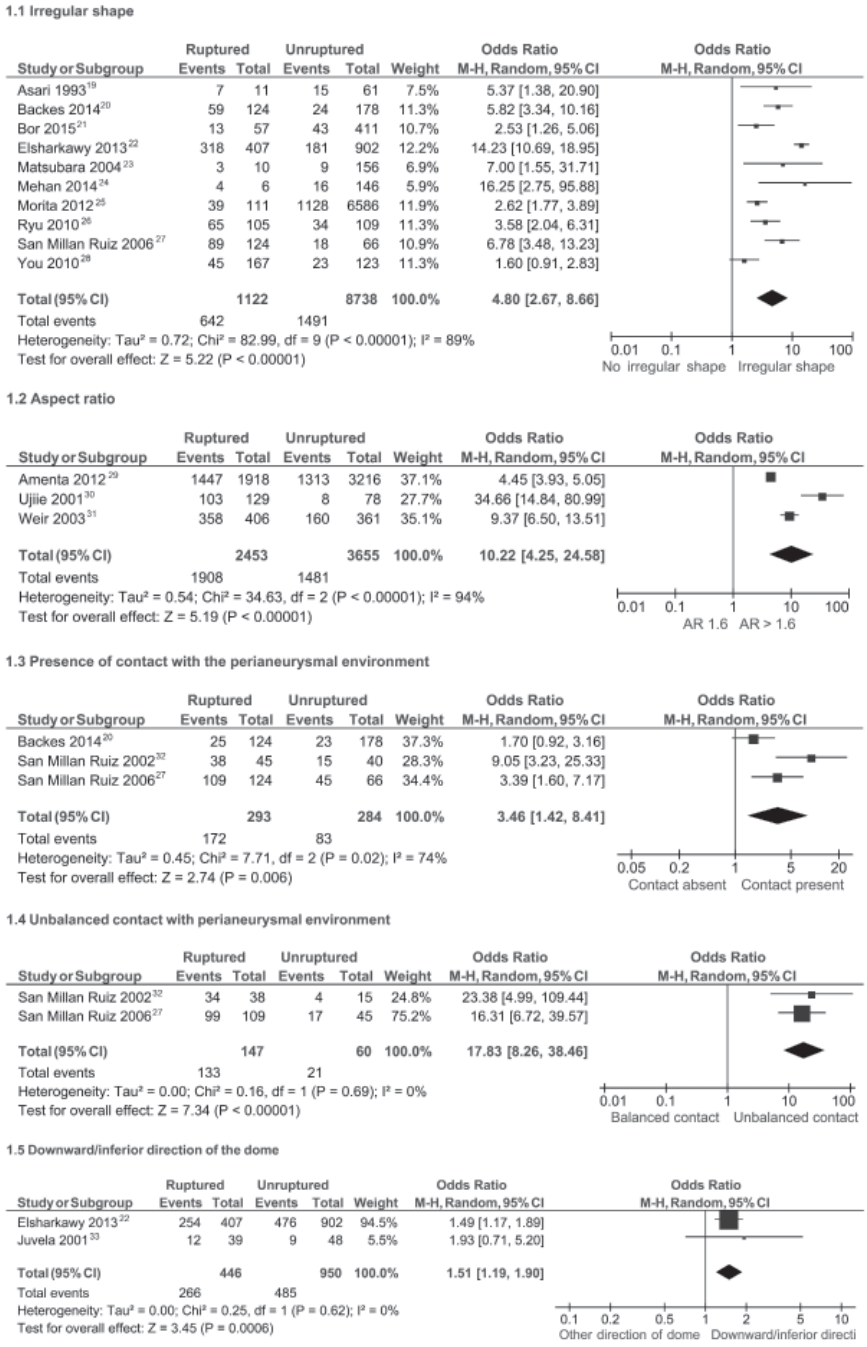

Figure 2.3. Results of the meta-analysis with the studies providing crude data for the risk factors of rupture with strong or moderate level of evidence.
For aspect ratio, we only included studies that used a cut-off of value for aspect ratio of 1.6 (with a range from 1.4–1.8) in the meta-analysis.

substantial across the studies assessing irregular shape (I^2=89%) and aspect ratio (I^2=94%). However, the heterogeneity test results can be influenced by poor precision of the estimate of between-study variance when analyzing only a small number of studies. The evidence for the risk factor irregular shape was based on >2 cohort studies of high quality with a pooled OR >2.0 and therefore has high potential and should from now on be used in risk prediction of rupture in clinical practice (Table 2.2). Aspect ratio, size ratio, bottleneck factor, and height-to-width ratio have potential for use in clinical practice after further analysis (Table 2.2).

Moderate level of evidence

Four additional morphological factors were found to have a moderate level of evidence (Supplementary table S2.2). First, the presence of contact of the aneurysm with surrounding anatomic structures, such as bone, dura mater, brain, vessels, or nerves was associated with rupture (pooled OR of 3.5, 95% CI 1.4–8.4 based on 3 studies, see Figure 2.3). Second, this contact was more often unbalanced (defined as an asymmetrical contact with the environment or contact with more than 1 anatomical structure) in ruptured aneurysms (pooled OR of 17.8, 95% CI 8.3–38.5 based on 2 studies, see Figure 2.3). Third, the volume-to-ostium ratio (ratio of the aneurysm volume to the area of the neck) was higher in ruptured aneurysms, and fourth, the downward/inferior direction of the aneurysm dome was also associated with rupture (pooled OR of 1.5, 95% CI 1.2–1.9 based on 2 studies, see Figure 2.3). A pooled analysis of the ORs in 2 or more high-quality studies was not possible for the factor volume-to-ostium ratio because of the absence of crude numbers or ORs. Heterogeneity was high for the factor presence of contact with the perianeurysmal environment (I^2=74%), while it was small for studies assessing the factor unbalanced contact with the perianeurysmal environment (I^2=0%) and the factor downward/inferior direction of the dome (I^2=0%). However, again, it should be emphasized that on analyzing only a small number of studies, the heterogeneity test results may be influenced by poor precision. All 4 factors have potential for use in clinical practice after further analysis.

Low level of evidence

There were 61 factors associated with rupture with low level of evidence (Supplementary table S2.2). Of these factors, 9 were genetic factors (including polymorphisms in the endothelial nitric oxide synthase gene, the complement factor H gene, the elastin gene, the Jun proto-oncogene, the synuclein alpha gene, the matrix metalloproteinase 1 and 9 genes, an interferon gene, and fibronectin 1 and 5'-aminolevulinate synthase 2 gene). Eight were molecular factors, including serum levels of several proteins. Twenty-two were morphological factors (including carotid intima-media thickness, intraluminal thrombus, different geometric indices, different configurations of the circle of Willis, and several variants of definitions of aneurysm shape), and 22 were hemodynamic factors (including several

blood pressure effects on the common carotid artery, different characterizations of flow, and size of the impingement of flow on the wall).

Of the factors with low level of evidence, 16 genetic, morphological, and hemodynamic risk factors fulfilled our predefined criteria (as outlined in Table 2.2) to have potential for further confirmation in future large high-quality prospective cohort studies (underlined in Supplementary table S2.2), including the 27 VNTR and G894T single nucleotide polymorphisms of the endothelial nitric oxide synthase gene, intraluminal thrombus, nonsphericity index (deviation from spherical shape), undulation index, ellipticity index (variant of aspect ratio defined with 3D variables), spherical shape, pear shape, unilateral hypoplastic A1 segment, ordinary type circle of Willis, deviated neck orifice position, flow impingement size, inflow concentration index, straight flow into the aneurysm, the smallest angle in the bifurcation on which the aneurysm is present, complex flow pattern in the aneurysm, and unstable flow pattern in the aneurysm.

Factors not associated with rupture

Factors not associated with rupture supported by strong or moderate evidence were not found (Supplementary table S2.3). There were 56 non-associated factors with low level of evidence. Of these 56 factors, 3 were genetic factors (including the polymorphisms in the genetic risk loci from the genome-wide association studies on intracranial aneurysms, and in the elastin and the endoglin gene) and 10 were molecular factors (including serum markers such as lipids, angiotensin II and renin activity, and elastase to alpha-1-antitrypsin ratio). There were 22 morphological factors (including calcification of the wall, different geometric indices, and several variants of definitions of aneurysm shape), and 21 were hemodynamic factors (including wall shear stress [WSS, the tangential force produced by blood moving across the vessel wall] in the parent artery and the ostium region, different characterizations of flow [including flow angles], and factors related to blood pressure).

Factors with inconsistent evidence

Eighteen factors had inconsistent evidence (Supplementary table S2.4). There were 6 morphological factors with inconsistent evidence, including the diameter of the aneurysm neck, the diameter of the parent artery, lateral and posterior direction of the aneurysm dome, the mean curvature norm (a measure of the predominant shape characteristic of the aneurysm surface), and bulge location (the ratio between the height from the neck plane to the maximal longitudinal diameter parallel with the neck plane to the aneurysm height). We found 12 hemodynamic factors with inconsistent evidence, including aneurysm pulsation, several definitions of WSS, energy loss (the value of collision power from hemodynamic sources divided by the aneurysm volume), and different characterizations of flow.

Of the factors with inconsistent evidence, aneurysm pulsation and maximal WSS were factors defined as having potential for further confirmation in larger high-quality prospective cohort studies (underlined in Supplementary table S2.4).

DISCUSSION

In this review, we studied 144 different risk factors for rupture and found irregular aneurysm shape as a risk factor with potential for use in clinical practice. Aspect ratio, size ratio, bottleneck factor, height-to-width ratio, contact with the perianeurysmal environment, large volume-to-ostium ratio, and dome direction also have potential for use in clinical practice but should first be confirmed in well-powered studies using multivariable analysis and incorporated in prediction models. In addition, we intended to perform a formal meta-analysis, but the large heterogeneity across the studies, the lack of crude data in many studies, and the little consistency in the definitions of the risk factors under study significantly limited the amount of data suitable for such a meta-analysis. Therefore the results should be interpreted with caution.

Irregular shape of the aneurysm had the highest potential for use in clinical practice. The validity of the meta-analysis for this risk factor is hampered by the heterogeneity across the studies assessing irregular shape. Furthermore, the availability of crude data in the studies on irregular shape was limited, which led to inclusion of only 10 of 26 studies in the meta-analysis. Despite these limitations, we still recommend the use of this risk factor in clinical practice, because the evidence for this risk factor was based on 10 high-quality studies, of which 4 were prospective cohort studies, and the pooled OR was substantial and statistically highly significant.

The evidence for the risk factor aspect ratio was derived from 10 high-quality studies, of which only 1 had a prospective cohort design. For this factor, we found a large effect size with a pooled OR of 10.2, 95% CI 4.3–24.6. However, because we again found substantial heterogeneity across studies while the pooled OR was based on only 3 of the 10 studies due to a lack of consistency in the use of a cut-off point in the different studies, this pooled OR should be interpreted with caution, and this risk factor is therefore not yet suitable for use in clinical practice. The evidence for the other 7 morphological factors was based on high-quality studies, of which none had a prospective cohort design. Furthermore, the meta-analysis of the factors presence of contact with the perianeurysmal environment, unbalanced nature of this contact, and downward/inferior direction of the dome was based on 3 or 2 studies, and, therefore, the pooled ORs of these factors should also be interpreted with caution. Most importantly, we should recognize that the 8 morphological factors associated with an increased risk of aneurysm rupture might be related to the size of the

aneurysm, a well-established risk factor,[6,13] because they are calculated with size or variants of size (e.g., height, width, and volume) as a variable. Therefore, the 8 morphological risk factors aspect ratio, size ratio, bottleneck factor, height-to-width ratio, presence of contact with the perianeurysmal environment, unbalanced nature of this contact, volume-to-ostium ratio, and a downward/inferior direction of the aneurysm dome should first be studied in a multivariate analysis and be incorporated in prediction models of rupture to assess their independence from size and from each other, and these models should be validated before implementation of these risk factors in clinical practice.

The previous systematic reviews and meta-analysis on risk factors for rupture[6,13] included only prospective cohort studies, of which the results could be directly incorporated in clinical practice and are incorporated in the current guidelines for treatment of unruptured aneurysms from the European Stroke Organization and the American Heart Association/ American Stroke Association.[14,15] This review provides an overview of all the other risk factors (including genetic, molecular, morphological, and hemodynamic factors) that have potential for use in clinical practice. Another strong aspect of our current review is the restriction to studies with factors that can be measured with easily accessible diagnostic tools (such as computed tomography angiography or magnetic resonance angiography, or from peripheral blood samples) before the aneurysm is treated. Therefore, our review also provides an overview of all potential clinically relevant risk factors and can be used as a starting point for further search for clinically relevant risk factors for rupture. Another unique aspect of our review is the assessment of the methodological quality score of each of the studies and incorporation of this score in the assessment of the potential of each risk factor, leading to a transparent and extensive overview of the available evidence for each of the risk factors.

Our study demonstrates overall poor quality of the currently available studies on genetic, molecular, morphological, and hemodynamic factors and their association with rupture of aneurysms. This poor quality led to the identification of only 1 risk factor that can be used in clinical practice and only a limited amount of risk factors with potential as a risk factor amongst a total of 144 risk factors identified, which is rather disappointing. However, the overview of the risk factors that do not have potential and should not be studied in future studies anymore also adds to the current literature. Another limitation of our study is that in our method a risk factor could only reach strong or moderate evidence if it was studied in 2 or more high-quality studies. This could have led to an overrepresentation of studies investigating factors that can be easily measured in clinical practice and therefore investigated by multiple authors, while risk factors that are not easy to measure are relatively less often studied and can therefore never reach a high level of evidence. We do not think this limits our results, because we aimed at identifying risk factors that are easy to measure in clinical practice and we also highlighted risk factors with limited level of evidence that have potential for further research. Also, we considered morphological risk factors assessed

with either computed tomography angiography, magnetic resonance angiography, or digital subtraction angiography as equal, while the quality of the measurement could have differed between these different imaging studies. At last, the risk factors identified were not evenly spread in number over the different categories we predefined (genetic, molecular, morphological, and hemodynamic factors), which can be the result of publication bias and might have led to an underestimation of potency of risk factors in 1 or more of these categories.

Irregular shape of the aneurysm should be added as a predictor of the risk of rupture to the predictors currently used in clinical practice. The morphological factors aspect ratio, size ratio, bottleneck factor, height-to-width ratio, volume-to-ostium ratio, presence of contact with the perianeurysmal environment, unbalanced nature of this contact, and a downward/inferior direction of the aneurysm dome should first be tested in multivariate analysis and confirmed in prediction models before use in clinical practice. Eighteen genetic, morphological, and hemodynamic risk factors for rupture were identified as potentially relevant for further clinical research.

REFERENCES

1. Vlak MH, Algra A, Brandenburg R, Rinkel GJ. Prevalence of unruptured intracranial aneurysms, with emphasis on sex, age, comorbidity, country, and time period: a systematic review and meta-analysis. *Lancet Neurol.* 2011;10:626-636.
2. Gabriel RA, Kim H, Sidney S, et al. Ten-year detection rate of brain arteriovenous malformations in a large, multiethnic, defined population. *Stroke.* 2010;41:21-26.
3. van Gijn J, Kerr RS, Rinkel GJ. Subarachnoid haemorrhage. *Lancet.* 2007;369:306-318.
4. Nieuwkamp DJ, Setz LE, Algra A, Linn FH, de Rooij NK, Rinkel GJ. Changes in case fatality of aneurysmal subarachnoid haemorrhage over time, according to age, sex, and region: a meta-analysis. *Lancet Neurol.* 2009;8:635-642.
5. de Rooij NK, Linn FH, van der Plas JA, Algra A, Rinkel GJ. Incidence of subarachnoid haemorrhage: a systematic review with emphasis on region, age, gender and time trends. *J Neurol Neurosurg Psychiatry.* 2007;78:1365-1372.
6. Greving JP, Wermer MJ, Brown RD Jr, et al. Development of the PHASES score for prediction of risk of rupture of intracranial aneurysms: a pooled analysis of six prospective cohort studies. *Lancet Neurol.* 2014;13:59-66.
7. Juvela S, Poussa K, Lehto H, Porras M. Natural history of unruptured intracranial aneurysms: a long-term follow-up study. *Stroke.* 2013;44:2414-2421.
8. Broderick JP, Brown RD Jr, Sauerbeck L, et al. Greater rupture risk for familial as compared to sporadic unruptured intracranial aneurysms. *Stroke.* 2009;40:1952-1957.
9. de Rooij NK, Rinkel GJ, Dankbaar JW, Frijns CJ. Delayed cerebral ischemia after subarachnoid hemorrhage: a systematic review of clinical, laboratory, and radiological predictors. *Stroke.* 2013;44:43-54.
10. Burns JD, Huston J 3rd, Layton KF, Piepgras DG, Brown RD Jr. Intracranial aneurysm enlargement on serial magnetic resonance angiography: frequency and risk factors. *Stroke.* 2009;40:406-411.
11. Review Manager (RevMan) [Computer Program]. Version 5.3. Copenhagen: The Nordic Cochrane Centre, The Cochrane Collaboration, 2014.
12. Higgins JP, Thompson SG, Deeks JJ, Altman DG. Measuring inconsistency in meta-analyses. *BMJ.* 2003;327:557-560.

13. Wermer MJ, van der Schaaf IC, Algra A, Rinkel GJ. Risk of rupture of unruptured intracranial aneurysms in relation to patient and aneurysm characteristics: an updated meta-analysis. *Stroke*. 2007;38:1404-1410.
14. Steiner T, Juvela S, Unterberg A, Jung C, Forsting M, Rinkel G. European Stroke Organization guidelines for the management of intracranial aneurysms and subarachnoid haemorrhage. *Cerebrovasc Dis*. 2013;35:93-112.
15. Thompson BG, Brown RD Jr, Amin-Hanjani S, et al. Guidelines for the Management of Patients With Unruptured Intracranial Aneurysms: A Guideline for Healthcare Professionals From the American Heart Association/American Stroke Association. *Stroke*. 2015;46:2368-2400.
16. Nakaoka H, Takahashi T, Akiyama K, et al. Differential effects of chromosome 9p21 variation on subphenotypes of intracranial aneurysm: site distribution. *Stroke*. 2010;41:1593-1598.
17. Bilguvar K, Yasuno K, Niemelä M, et al. Susceptibility loci for intracranial aneurysm in European and Japanese populations. *Nat Genet*. 2008;40:1472-1477.
18. Parlea L, Fahrig R, Holdsworth DW, Lownie SP. An analysis of the geometry of saccular intracranial aneurysms. *AJNR Am J Neuroradiol*. 1999;20:1079-1089.
19. Asari S, Ohmoto T. Natural history and risk factors of unruptured cerebral aneurysms. *Clin Neurol Neurosurg*. 1993;95:205-214.
20. Backes D, Vergouwen MDI, Velthuis BK, et al. Difference in aneurysm characteristics between ruptured and unruptured aneurysms in patients with multiple intracranial aneurysms. *Stroke*. 2014;45:1299-1303.
21. Bor ASE, Groenestege ATT, Terbrugge KG, et al. Clinical, radiological, and flow-related risk factors for growth of untreated, unruptured intracranial aneurysms. *Stroke*. 2015;46:42-48.
22. Elsharkawy A, Lehecka M, Niemela M, et al. Anatomic risk factors for middle cerebral artery aneurysm rupture: Computed tomography angiography study of 1009 consecutive patients. *Neurosurgery*. 2013;73:825-837.
23. Matsubara S, Hadeishi H, Suzuki A, Yasui N, Nishimura H. Incidence and risk factors for the growth of unruptured cerebral aneurysms: observation using serial computerized tomography angiography. *J Neurosurg*. 2004;101:908-914.
24. Mehan WA, Romero JM, Hirsch JA, et al. Unruptured intracranial aneurysms conservatively followed with serial CT angiography: Could morphology and growth predict rupture? *J Neurointervent Surg*. 2014;6:761-766.
25. UCAS Japan Investigators, Morita A, Kirino T, et al. The natural course of unruptured cerebral aneurysms in a Japanese cohort. *N Engl J Med*. 2012;366:2474-2482.
26. Ryu CW, Kwon OK, Koh JS, Kim EJ. Analysis of aneurysm rupture in relation to the geometric indices: aspect ratio, volume, and volume-to-neck ratio. *Neuroradiology*. 2011;53:883-889.
27. San Millan Ruiz D, Yilmaz H, Dehdashti AR, Alimenti A, de Tribolet N, Rufenacht DA. The perianeurysmal environment: influence on saccular aneurysm shape and rupture. *AJNR Am J Neuroradiol*. 2006;27:504-512.
28. You SH, Kong DS, Kim JS, et al. Characteristic features of unruptured intracranial aneurysms: predictive risk factors for aneurysm rupture. *J Neurol Neurosurg Psychiatry*. 2010;81:479-484.
29. Amenta PS, Yadla S, Campbell PG, et al. Analysis of nonmodifiable risk factors for intracranial aneurysm rupture in a large, retrospective cohort. *Neurosurgery*. 2012;70:693-699.
30. Ujiie H, Tamano Y, Sasaki K, Hori T. Is the aspect ratio a reliable index for predicting the rupture of a saccular aneurysm? *Neurosurgery*. 2001;48:495-503.
31. Weir B, Amidei C, Kongable G, et al. The aspect ratio (dome/neck) of ruptured and unruptured aneurysms. *J Neurosurg*. 2003;99:447-451.
32. San Millan Ruiz D, Tokunaga K, Dehdashti AR, Sugiu K, Delavelle J, Rufenacht DA. Is the rupture of cerebral berry aneurysms influenced by the perianeurysmal environment? *Acta Neurochir Suppl*. 2002;82:31-34.
33. Juvela S, Poussa K, Porras M. Factors affecting formation and growth of intracranial aneurysms: a long-term follow-up study. *Stroke*. 2001;32:485-491.

SUPPLEMENTARY MATERIAL

Supplementary tables S2.1 to S2.4, can be found online: http://hdl.handle.net/10411/MY4GN1.

3

THE ASSOCIATION BETWEEN GENETIC RISK FACTORS AND THE SIZE OF INTRACRANIAL ANEURYSMS AT TIME OF RUPTURE

R. Kleinloog, F.N.G. van 't Hof, F.J. Wolters, I. Rasing,
I.C. van der Schaaf, G.J.E. Rinkel, Y.M. Ruigrok

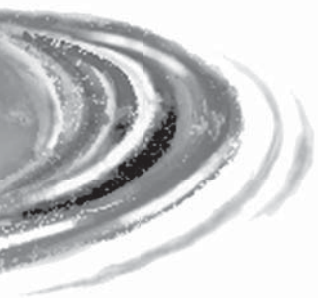

Neurosurgery. 2013;73:705-708

ABSTRACT

Background: Genetic risk factors for intracranial aneurysms may influence the size of aneurysms.

Objective: To assess the association between genetic risk factors and size of aneurysms at the time of rupture.

Methods: Genotypes of 7 independent single nucleotide polymorphisms (SNPs) of the 6 genetic risk loci identified in genome-wide association studies of patients with intracranial aneurysms were obtained from 700 Dutch patients with an aneurysmal subarachnoid hemorrhage (1997–2007) previously genotyped in the genome-wide association studies; 255 additional Dutch patients with an aneurysmal subarachnoid hemorrhage (2007–2011) were genotyped for these SNPs. Aneurysms were measured on computerized tomography angiography or digital subtraction angiography. The mean aneurysm size (with standard error) was compared between patients with and without a genetic risk factor by the use of linear regression. The association between SNPs and size was assessed for single SNPs and for the combined effect of SNPs using a weighted genetic risk score.

Results: Single SNPs showed no association with aneurysm size, nor did the genetic risk score.

Conclusion: The 6 genetic risk loci have no major influence on the size of aneurysms at the time of rupture. Because these risk loci explain no more than 5% of the genetic risk, other genetic factors for intracranial aneurysms may influence aneurysm size and thereby proneness to rupture.

INTRODUCTION

Genome-wide association studies (GWAS) of patients with intracranial aneurysms identified 6 genetic risk loci (4q31.23, 8q11.23-q12.1, 9p21.3, 10q24.32, 13q13.1 and 18q11.2) associated with the presence of intracranial aneurysms.[1-3] Previous research showed that genetic risk factors for intracranial aneurysms can vary according to different aneurysm phenotypes such as the site of aneurysms.[4] Genetic risk factors for intracranial aneurysms may also influence aneurysm size. Familial aneurysms are generally larger at the time of rupture than sporadic aneurysms, suggesting a genetic determinant for aneurysm size.[5] We investigated the association between genetic risk factors, as identified in the GWAS on intracranial aneurysms, and the size of aneurysms at the time of rupture in a large group of patients with aneurysmal subarachnoid hemorrhage (aSAH).

METHODS

Patient selection

From the 781 Dutch patients with ruptured and unruptured intracranial aneurysms who were previously included in the GWAS on intracranial aneurysms,[1,2] we included only the 700 patients with aSAH, thereby excluding the patients with unruptured aneurysms. aSAH was defined by symptoms suggestive of subarachnoid hemorrhage combined with subarachnoid blood on computerized tomography (CT) at admission and an intracranial aneurysm, proven by computerized tomography angiogram (CTA) or digital subtraction angiogram (DSA). These patients were admitted to the University Medical Center Utrecht, The Netherlands between 1997 and 2007. Furthermore, 255 additional patients with aSAH admitted between 2007 and 2011 were included. The total sample of 955 patients did not include patients with multiple aneurysms in whom the ruptured aneurysms could not be determined with certainty. Also, patients did not have fusiform or mycotic aneurysms, nor did they have aneurysms associated with underlying vascular malformations. The study was approved by the local ethics committee and subjects gave written informed consent.

Aneurysm measurement

The largest diameter of the lumen of the aneurysm was measured on CTA or DSA. If the aneurysm was multilobed or had a bleb, we measured the largest diameter through the lumen including the lobes or including the lumen of the bleb. A computer workstation was used for digitally available CTAs to measure the aneurysm in 2-dimensional view, or, if full data were available, to make standardized maximum-intensity projection images for optimal

3-dimensional view (on an Easy Vision and Extended Brilliance Workspace, Philips Medical Systems, Best, The Netherlands). In patients of whom no digital CTA was available, we used nondigital films of DSA or CTA with correction for magnification by determining the size of the aneurysm relative to the diameter of the proximal part of the internal carotid artery (just below the bifurcation) set at 4 mm.[6,7] In this analysis of nondigital films, only aneurysms present on the same projection as the carotid top could be measured leading to exclusion of aneurysms of the basilar or vertebral artery (n=3). Measurements were performed by either R.K. or F.J.W. under supervision of an experienced radiologist (I.C.v.d.S.). We were able to measure the size of the ruptured aneurysm in 624 of the 955 patients (65%); the mean size of the 624 ruptured aneurysms was 7.6 mm and the proportion of patients with an aneurysm size ≥7 mm was 48%. Aneurysm size showed a normal distribution. In 24% of the patients, measurements were performed on nondigital DSA (n=83) and nondigital CTA (n=68). The 331 patients for whom the original imaging study was unavailable were excluded from the analysis. The main reason for unavailability of original imaging studies was that patients had been treated more than 10 years ago and, accordingly, the films had been destroyed.

Genetic risk factors

We included 7 independent SNPs of the 6 genetic risk loci for intracranial aneurysms: rs6841581 (locus 4q31.23), rs10958409 and rs9298506 (locus 8q11.23-q12.1), rs1333040 (locus 9p21.3), rs12413409 (locus 10q24.32), rs9315204 (locus 13q13.1) and rs11661542 (locus 18q11.2) as found and replicated in the GWAS on intracranial aneurysms.[1-3] We retrieved the genotypes of the 6 SNPs of the 700 Dutch cases with aSAH already genotyped in the previous GWAS on Illumina CNV370-duo chips (Illumina Inc., San Diego, CA, USA).[1,2] We imputed genotypes of the risk SNP that was not genotyped in the GWAS,[1,2] using BEAGLE software version 3.0.4,[8] with the HapMap phase II CEU population as the reference panel.[9] After imputation, we removed SNPs with imputation quality below 0.1 or above 1.1. The imputation quality score (i.e., ratio of the observed variance of the allele dosage to the expected variance) was 1.0. Genotype probability scores were converted to allele dosages, ranging from 0 to 2. In the 255 additional aSAH patients, 6 SNPs (rs10958409, rs9298506, rs1333040, rs12413409 , rs9315204 and rs11661542) were genotyped using KASPar assays (KBioscience, Hertfordshire, United Kingdom) on an ABI 7900HT instrument and analyzed with SDS software (Applied Biosystems, Foster City, CA, USA). The SNP rs6841581 was genotyped using a TaqMan SNP Genotyping Assay (Applied Biosystems, Foster City, California, USA) in a LightCycler480 (Roche, Basel, Switzerland) using the TaqMan Genotyping Master Mix (Applied Biosystems). In this cohort of 255 additional patients, we observed 2% missing genotypes.

Statistical analysis

To analyze the association between genotypes and size we first compared the mean aneurysm size with standard error (SE) by using linear regression between patient groups with and without a risk allele of all SNPs separately using the allele opposed to the risk allele (as defined in the GWAS) as the reference allele.[1-3] In this analysis we corrected for sex, age at time of aSAH and family history of aSAH or intracranial aneurysms. The threshold for significance was set at $P \leq 0.007$. Then, we calculated a weighted genetic risk score (GRS) for each study patient with complete genotype information (n=568; 91%) as follows. For each SNP, the number of genotyped risk alleles (0, 1, or 2) or the estimated allele dosage after imputation (between 0 and 2) was multiplied by its effect size, defined as the natural log of the published odds ratio for that risk allele.[2,3] We summed up these effect-size weighted allele counts across all 7 SNPs to generate a GRS. The association between the GRS and aneurysm size was established by comparison of the mean aneurysm size with SE between patients with a high GRS (upper 50% percentile) and a low GRS (lower 50% percentile). Furthermore, the association of GRS and aneurysm size was also analyzed by comparing the mean aneurysm size with SE between patients in the highest GRS quartile and the lowest GRS quartile. We performed a sensitivity analysis including only patients with aneurysms measured on the computer workstation (n=473), to assess whether the less accurate measuring method of aneurysms on nondigital films might have influenced the results. Statistical analysis was performed using IBM SPSS software package version 20.0.

Power calculation

Using the sample size of 624 patients with aSAH, and under the assumption of frequencies of the risk alleles as previously reported,[2,10] a standard deviation of aneurysm size of 4 mm[11] and the threshold of nominal *P* value =0.05, the study has an acceptable power (>90%) for detecting a difference in aneurysm size of 1.5 mm between the groups with and without a genetic risk factor for all but 1 risk SNP. For the risk SNP on locus 10q24.32, the power is 57%. A detailed power calculation per genetic risk factor is provided in Supplementary table S3.1.

RESULTS

The baseline characteristics of the 624 included patients are shown in Table 3.1. In comparison of the mean aneurysm size between the patient groups with and without a risk allele, none of the risk alleles showed an association with aneurysm size (Table 3.2). In the analysis on the association between the GRS and aneurysm size, no difference was found in mean aneurysm size between patients with a high and low GRS, nor between patients in the highest and the lowest GRS quartile. The mean aneurysm size of patients with a GRS in the upper 50%

Table 3.1. Baseline characteristics of 624 patients with aneurysmal subarachnoid hemorrhage

Total number of patients	624
Mean age at time of aSAH (SD; range)	53 years (13; 16–88)
Proportion of women	(465) 75%
Family history of aSAH or intracranial aneurysms	(59) 10%
Mean size of the aneurysms (SD; range)	7.6 mm (4.2; 1.5–33.5)

aSAH, aneurysmal subarachnoid hemorrhage, SD, standard deviation.

Table 3.2. Association between risk alleles and size of ruptured intracranial aneurysms in 624 patients

Chromosome, SNP (risk allele)	Risk alleles/ Total alleles, n (%)	Mean size difference (mm) between patients with and without risk allele (95% CI)[a]	*P* value
4, rs6841581 (G)	1007/1154 (87)	-0.1 (-1.0 to 0.9)	0.89
8, rs10958409 (A)	208/1238 (17)	-0.6 (-1.2 to 0.1)	0.07
8, rs9298506 (A)	1032/1222 (84)	-0.2 (-0.8 to 0.4)	0.53
9, rs1333040 (T)	747/1244 (60)	-0.04 (-0.5 to 0.4)	0.87
10, rs12413409 (G)	1157/1240 (93)	-0.5 (-1.4 to 0.4)	0.27
13, rs9315204 (T)	272/1242 (22)	-0.1 (-0.6 to 0.5)	0.84
18, rs11661542 (C)	707/1238 (57)	-0.1 (-0.6 to 0.3)	0.61

SNP, single nucleotide polymorphism; 95% CI, 95% confidence interval; aSAH, aneurysmal subarachnoid hemorrhage.
[a] Mean size differences after correction for sex, age at the time of aSAH, and family history of aSAH or intracranial aneurysms.

percentile was 7.6 mm (SE 0.2 mm) compared with a mean aneurysm size of 7.7 mm (SE 0.2 mm) in patients with a GRS in the lower 50% percentile (mean size difference of -0.1 mm; 95% confidence interval of -1.0 to 0.9, *P*=0.82). The mean aneurysm size of patients in the highest quartile was 7.4 mm (SE 0.3 mm) compared with a mean aneurysm size of 7.7 mm (SE 0.4) in patients in the lowest quartile (mean size difference of -0.3 mm, 95% CI of -1.7 to 1.1, *P*=0.57). The sensitivity analysis performed with only those patients with aneurysms measured on the computer workstation showed comparable results.

DISCUSSION

This study shows that the 7 independent SNPs of the 6 genetic risk loci for intracranial aneurysms as identified in the GWAS are not associated with size of the aneurysm at the time of rupture, neither as single-risk alleles nor as weighted genetic risk score.

Familial aneurysms are generally larger at the time of rupture than sporadic aneurysms, suggesting a genetic determinant for aneurysm size.[5] To the best of our knowledge, this is the first study investigating the association between the SNPs of the 6 genetic risk loci as identified in the GWAS on intracranial aneurysms and aneurysm size at the time of rupture. Analyzing the SNPs of the 6 genetic risk loci identified in the GWAS on intracranial aneurysms, we did not find evidence in this study to support an association between these 6 genetic risk loci and size of aneurysms at the time of rupture. The hypothesis of a possible association between genetic risk and size at the time of rupture is, however, not rejected, because the genetic risk loci identified in the GWAS only explain approximately 5% of the genetic risk for intracranial aneurysms.[2] Aneurysm size is one of the strongest risk factors for rupture currently known.[12] A genetic risk locus associated with large size may also be involved in the mechanism of rupture of the aneurysm. Therefore, further studies should focus on identifying new genetic risk factors for aSAH. Subsequently, the newly identified genetic risk factors for aSAH should be analyzed for their association with aneurysm size.

This study has limitations. First, aSAH patients who died soon after admission could not be included in the present study because they could not be asked to participate. Our results therefore apply to a population of patients who survived the initial hours after aSAH. Only including these patients may have led to an underrepresentation of patients with large aneurysms, because large aneurysms are associated with poor outcome.[13] Second, large aneurysms are prone to contain intraluminal thrombus.[14,15] With the imaging methods used, we could only measure the lumen in the aneurysm, which could have led to an underestimation of the size of large aneurysms and an underestimation of the association between risk factors and size. Third, we had to exclude 35% of the patients because their original imaging study was unavailable, mainly because these patients had been treated more than 10 years ago, and, accordingly, the films had been destroyed. Consequently, aneurysm size could not be measured in these patients. Exclusion of these patients led to an underrepresentation of patients admitted more than 10 years ago in our cohort. We do not expect this to influence our results because it is not likely that aneurysm size or genetic risk of a cross-sectional cohort of aSAH patients changed over time. Fourth, different genotype platforms were used in the subjects admitted after 2007 and for SNP rs6841581. This could have introduced error in calling and missing genotypes. Last, the analysis of the association between genetic risk factors and size of aneurysms should ideally be assessed in a cohort of patients with unruptured aneurysms who are followed up for assessment

of growth of their aneurysm until rupture occurs instead of in a cross-sectional cohort of patients with ruptured aneurysms like our current study. However, such a follow-up study is not feasible because it would take decades of follow-up, and more importantly, would be unethical because it would withhold preventive treatment in patients with large aneurysms, and therefore a large risk of rupture.

We found that there is no association between the 6 genetic risk loci associated with presence of intracranial aneurysms as identified in the GWAS and aneurysm size at time of rupture. Because the 6 genetic risk loci explain no more than 5% of the genetic risk for the presence of aneurysms, we recommend further search for the genetic factors for aSAH and subsequent analysis of these factors with aneurysm size. When considering size as a surrogate marker of rupture, genetic risk factors associated with large size might be involved in the mechanism of rupture of aneurysms, and identification of these genetic factors can help us to further understand the pathogenesis of this complex disease.

REFERENCES

1. Bilguvar K, Yasuno K, Niemelä M, et al. Susceptibility loci for intracranial aneurysm in European and Japanese populations. *Nat Genet*. 2008;40:1472-1477.
2. Yasuno K, Bilguvar K, Bijlenga P, et al. Genome-wide association study of intracranial aneurysm identifies three new risk loci. *Nat Genet*. 2010;42:420-425.
3. Yasuno K, Bakircioglu M, Low SK, et al. Common variant near the endothelin receptor type A (EDNRA) gene is associated with intracranial aneurysm risk. *Proc Natl Acad Sci U S A*. 2011;108: 19707-19712.
4. Nakaoka H, Takahashi T, Akiyama K, et al. Differential effects of chromosome 9p21 variation on subphenotypes of intracranial aneurysm: site distribution. *Stroke*. 2010;41:1593-1598.
5. Ruigrok YM, Rinkel GJ, Algra A, Raaymakers TW, Van Gijn J. Characteristics of intracranial aneurysms in patients with familial subarachnoid hemorrhage. *Neurology*. 2004;62:891-894.
6. Gibo H, Lenkey C, Rhoton AL,Jr. Microsurgical anatomy of the supraclinoid portion of the internal carotid artery. *J Neurosurg*. 1981;55:560-574.
7. Weir B. Aneurysms affecting the nervous system. Baltimore, MD: Williams & Wilkins; 1987: 308-363.
8. Browning BL, Browning SR. A unified approach to genotype imputation and haplotype-phase inference for large data sets of trios and unrelated individuals. *Am J Hum Genet*. 2009;84:210-223.
9. International HapMap Consortium. A second generation human haplotype map of over 3.1 million SNPs. *Nature*. 2007;449:851-861.
10. Low SK, Takahashi A, Cha PC, et al. Genome-wide association study for intracranial aneurysm in the Japanese population identifies three candidate susceptible loci and a functional genetic variant at EDNRA. *Hum Mol Genet*. 2012;21:2102-2110.
11. Ohashi Y, Horikoshi T, Sugita M, Yagishita T, Nukui H. Size of cerebral aneurysms and related factors in patients with subarachnoid hemorrhage. *Surg Neurol*. 2004;61:239-245.
12. Wermer MJ, Van der Schaaf IC, Algra A, Rinkel GJ. Risk of rupture of unruptured intracranial aneurysms in relation to patient and aneurysm characteristics: an updated meta-analysis. *Stroke*. 2007;38:1404-1410.
13. Roos EJ, Rinkel GJ, Velthuis BK, Algra A. The relation between aneurysm size and outcome in patients with subarachnoid hemorrhage. *Neurology*. 2000;54:2334-2336.

14. German WJ, Black SP. Intra-aneurysmal hemodynamics: turbulence. *Trans Am Neurol Assoc.* 1954;13:163-165.
15. German WJ, Black SP. Intra-aneurysmal hemodynamics-jet action. *Circ Res.* 1955;3:463-468.

SUPPLEMENTARY MATERIAL

Supplementary table S3.1. Power calculation for comparing mean intracranial aneurysm size differences in 624 patients with and without genetic risk factors

Genetic risk factor	Expected frequency[2,10]	Power for mean aneurysm size difference of 1.5 mm (SD 4 mm)
Risk allele rs6841581 (chr. 4)	74%	98%
Risk allele rs10958409 (chr. 8)	18%	95%
Risk allele rs9298506 (chr. 8)	85%	92%
Risk allele rs1333040 (chr. 9)	63%	>99%
Risk allele rs12413409 (chr. 10)	94%	57%
Risk allele rs9315204 (chr. 13)	24%	98%
Risk allele rs11661542 (chr. 18)	54%	>99%

SD, standard deviation; chr., chromosome.

4

RNA SEQUENCING ANALYSIS OF INTRACRANIAL ANEURYSM WALLS REVEALS INVOLVEMENT OF LYSOSOMES AND IMMUNOGLOBULINS IN RUPTURE

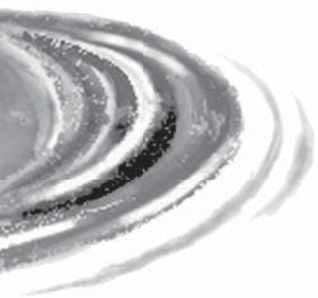

R. Kleinloog, B.H. Verweij, P. van der Vlies, P. Deelen, M.A. Swertz, L. De Muynck, P. Van Damme, F. Giuliani, L. Regli, A. van der Zwan, J.W. Berkelbach van der Sprenkel, K.S. Han, P. Gosselaar, P.C. van Rijen, E. Korkmaz, J.A. Post, G.J.E. Rinkel, J.H. Veldink*, Y.M. Ruigrok*

* These authors contributed equally.

Stroke. 2016;47:1286-1293

ABSTRACT

Background and purpose: Analyzing genes involved in development and rupture of intracranial aneurysms can enhance knowledge about the pathogenesis of aneurysms, and identify new treatment strategies. We compared gene expression between ruptured and unruptured aneurysms and control intracranial arteries.

Methods: We determined expression levels with RNA sequencing. Applying a multivariate negative binomial model, we identified genes that were differentially expressed between 44 aneurysms and 16 control arteries, and between 22 ruptured and 21 unruptured aneurysms. The differential expression of 8 relevant and highly significant genes was validated using digital polymerase chain reaction. Pathway analysis was used to identify enriched pathways. We also analyzed genes with an extreme pattern of differential expression: only expressed in 1 condition without any expression in the other.

Results: We found 229 differentially expressed genes in aneurysms versus controls and 1489 in ruptured versus unruptured aneurysms. The differential expression of all 8 genes selected for digital polymerase chain reaction validation was confirmed. Extracellular matrix pathways were enriched in aneurysms versus controls, whereas pathways involved in immune response and the lysosome pathway were enriched in ruptured versus unruptured aneurysms. Immunoglobulin genes were expressed in aneurysms, but showed no expression in controls.

Conclusions: For rupture of intracranial aneurysms, we identified the lysosome pathway as a new pathway and found further evidence for the role of the immune response. Our results also point toward a role for immunoglobulins in the pathogenesis of aneurysms. Immune-modifying drugs are, therefore, interesting candidate treatment strategies in the prevention of aneurysm development and rupture.

INTRODUCTION

Intracranial aneurysms are common with a prevalence of 3%.[1] The availability of noninvasive imaging techniques has increased, which coincided with an increase in incidental detection of aneurysms.[2] Although only a minority of aneurysms ruptures, the consequences of aneurysmal subarachnoid hemorrhage are enormous, because of the young age at which it occurs, and the high case fatality and morbidity.[3] Preventive treatment of unruptured aneurysms carries a risk of complications.[4] New treatment strategies, therefore, inhibiting the formation, growth, and rupture of aneurysms are needed. To develop such treatment strategies, we need more insight into the pathogenesis of aneurysm development and rupture. Studies investigating differences in gene expression in aneurysms versus controls and in ruptured versus unruptured aneurysms may identify genes and pathways involved in development and rupture of aneurysms. Previous studies were small and, used microarray techniques,[5-12] and extracranial instead of intracranial arteries as control.[6-9,11,12] Recent advances in sequencing methodology, such as next-generation sequencing-based RNA profiling methods, provide more accurate, sensitive, comprehensive, and reliable gene expression data than microarrays.[13] We compared differential expression of genes of a large sample of intracranial aneurysm tissue samples (n=44) to a unique control sample of intracranial arteries (n=16), and compared ruptured (n=22) to unruptured (n=21) aneurysms tissue samples using RNA sequencing, to gain insight in the pathogenesis of the development and the subsequent rupture of intracranial aneurysms.

METHODS

Patient selection and data collection

Aneurysm tissue samples were excised after complete obliteration of the aneurysm with a clip in patients aged ≥18 years undergoing neurosurgical clipping of a ruptured, or unruptured saccular intracranial aneurysm at the department of Neurology and Neurosurgery of the University Medical Center Utrecht, The Netherlands between 2010 and 2013. Patients with fusiform, mycotic and dissection aneurysms were excluded, as were patients with previous treatment of the same aneurysm. Patients with underlying diseases such as connective tissue disorders, polycystic kidney disease and arteriovenous malformations were also excluded. As controls, a tissue sample of an intracranial cortical artery was obtained from the resected brain tissue of patients aged ≥16 years who underwent surgery because of intractable epilepsy. Exclusion criteria for these control patients were a (family) history of intracranial aneurysm, subarachnoid hemorrhage or other cerebrovascular diseases, the presence of a connective tissue disease or polycystic

kidney disease, and a pathological diagnosis of a low or high grade glioma after resection. We collected characteristics for all patients and for those with aneurysms also aneurysm characteristics, including the largest diameter of the lumen of the aneurysm and the location of the aneurysm from the available imaging studies (mostly computed tomographic angiography). This study was approved by the Institutional Review Board of the University Medical Center Utrecht.

Sample collection and preparation

When complete obliteration of the aneurysm was confirmed by visual inspection and, if indicated, intraoperative IndoCyanine Green angiography, a part of the aneurysm dome distal to the clip was excised, only when this procedure was assessed to be safe by the neurosurgeon. In the controls, a part of a superficial cortical artery in the resected part of the brain was excised. There were no complications of the excision of the tissue samples. After excision, the samples were snap frozen in liquid nitrogen (<1 minute after excision) and stored at -80°C until further use. The intra-operative judgment on the rupture status of the aneurysm was considered the golden standard in case of subarachnoid hemorrhage and multiple aneurysms. Aneurysms in which the rupture status was unclear and in which the whole aneurysm could not be inspected during surgery in order to identify recent rupture, were excluded for the analysis comparing ruptured and unruptured aneurysms (n=1). Tissue samples were homogenized with zirconia/silica beads in the BeadBeater machine (BioSpec products, Inc). After homogenization, total RNA was extracted and purified using an RNeasy microkit (Catalog No. 74004, Qiagen, Valencia, CA, USA) according to the manufacturer's instructions.

Quality of the extracted RNA of the samples

A total of 82 tissue samples (60 aneurysm samples and 22 control samples) were homogenized, but only the samples with a minimum of 7 ng non-degraded RNA were selected for subsequent sequencing analysis. A total of 16 aneurysm samples (four ruptured and twelve unruptured) and six control samples had to be excluded due to insufficient amounts of RNA. An initial quality check of the extracted RNA of the samples was performed by capillary electrophoresis and RNA quantification using the LabChip GX (PerkinElmer, Waltham, MA). Of the 60 samples included, the mean total RNA concentration was 18 ng/ul (range 1–109), and 13 ng/ul (2–35) in controls, 19 ng/ul (3–109) in ruptured aneurysms and 19 ng/ul (1–77) in unruptured aneurysms (Supplementary table S4.1). The mean RNA quality score was 6.8 (range 4.2–9.3), and 7.2 (4.2–9.0) in controls, 6.7 (4.8–8.9) in ruptured aneurysm samples and 6.5 (5.1–9.3) in unruptured aneurysm samples (Supplementary table S4.1). Of two samples, the RNA quality score was not available. The RNA concentration of these samples was 5.0 and 1.2 ng/ul, and both were unruptured aneurysm samples.

Library preparation and RNA sequencing

Sequence libraries were generated from 44 aneurysm (22 ruptured, 21 unruptured, and 1 with unknown rupture status) and 16 control samples using the TruSeq mRNA sample preparation kit from Illumina (San Diego, CA) using the Sciclone NGS Liquid Handler (PerkinElmer). After an extra purification step of the libraries with the automated agarose gel separation system Labchip XT (PerkinElmer), 9 picomoles of the obtained cDNA fragment libraries were sequenced on an Illumina HiSeq2500 using default parameters (single read 1x100 bp) in randomly arranged pools of 10 or 11 samples. On an average, 14 209 239 reads were generated per sample. The number of reads passing filter ranged from 68.43 to 118.25 million. The yield ranged between 3.4 and 5.8 gigabases. We summarized the quality of the reads by using the R/Bioconductor package Rqc[14,15] producing one bar plot showing an overview of the range of quality values across all bases at each position in the reads from all the samples included in our analysis (Supplementary figure S4.1, panel A). This plot shows that the quality of our reads per position is above 30 at each position, which indicates good quality. A second plot showing the average quality pattern of reads of all the samples that were included in our analysis shows that more than 90% of the reads exceed a quality score of 30, also indicating good quality of the data (Supplementary figure S4.1, panel B).

Reads mapping

Processing of the raw data including a demultiplexing step was performed using Casava software (Illumina) with standard settings. The trimmed fastQ files where aligned to build 37 human reference genome using STAR 2.3.1[16] allowing for two mismatches. Before gene quantification SAMtools 0.1.18[17] was used to sort the aligned reads. The gene level quantification was performed by HTSeq-0.5.4[18] using --mode=union --stranded=no using Ensembl version 71 as gene annotation database. The average alignment of the reads to the human reference genome (uniquely mapped reads) was 86% (range 73–90%).

Gene expression quantification

We used R version 3.1.0[14] and Bioconductor (version 2.14) packages edgeR (version 3.6.2)[19] and limma (version 3.20.2)[20] for analysis of the gene expression data. The counts per gene for each sample obtained after alignment were used as input for the differential expression analysis. Low count genes (genes with less than 1 read per million in n of the samples, where n is the size of the smallest group of replicates) were filtered out since they have no, or little change of showing significant results in the differential expression analysis.[21] For the analysis in aneurysms versus control tissue, n was set at 16 (equivalent to the number of replicates in the smallest group, the controls), while n was set at 21 in the analysis of ruptured versus unruptured aneurysms (with unruptured aneurysms being the smallest group). To correct

for technical influences, edgeR adjusts any differential expression analysis for varying sequencing depths between samples as represented by differing library sizes. Furthermore, it calculates scale factors with the trimmed mean of M-values method, thereby normalizing for RNA composition of the sample, and creating an effective library size which is used in downstream analysis.

A generalized linear model was used to test the null hypothesis that there is no differential expression of genes between analysis groups. Age and sex of the patients were added to the model. In the model comparing aneurysms and controls, we added the rupture status, to control for genes with strong expression differences between ruptured and unruptured aneurysms. In the process of sequencing, after the first sequencing run of the samples, three pools yielded an insufficient amount of reads due to contamination of adapter-duplexes. These pools were sequenced again in a second run, and the count data of the second run was used for the differential gene expression analysis for the samples involved. Therefore, the sequencing run number was also added to the generalized linear model to correct for possible influences on the data of the different runs. Common and tagwise dispersion estimates were calculated with the Cox-Reid profile-adjusted likelihood method to be able to correct for the technical and biological variation when fitting the multivariate negative binomial model. A negative binomial generalized log-linear model, using the tagwise dispersion estimates, was fitted to the read counts for each gene and a genewise statistical test was performed for the given coefficient (either aneurysms to controls or ruptured to unruptured aneurysms). Then, a likelihood ratio test for the given coefficient in the model was performed. To correct for multiple testing, we calculated Benjamini Hochberg false discovery rates (FDR) and considered genes with an FDR-adjusted *P* value <0.05 differentially expressed.

Although the genes with low counts (genes with <1 read per million in n of the samples, where n is the size of the smallest group of replicates) are not likely to show significant results in the differential expression analysis, they can still be biologically relevant for the disease in case such genes are only expressed in 1 condition and have 0 counts in the other. We therefore performed a subanalysis of the raw count data and selected those genes that had >200 counts versus 0 counts in aneurysms versus controls and ruptured versus unruptured aneurysms.

Validation of RNA sequencing data with digital droplet polymerase chain reaction

Eight genes were selected for validation by selecting the 2 most biologically relevant top genes with overexpression and the 2 most biologically relevant top genes with underexpression in the aneurysms versus control tissue analysis and in the ruptured versus unruptured aneurysms analysis. For validation of the underexpressed genes in ruptured versus unruptured aneurysms

we initially chose the immunoglobulin gene *IGHG4*, but due to problems with the specificity of the assay of this gene, we chose keratin 17 (*KRT17*) instead. The expression of the selected genes was studied by digital polymerase chain reaction in the remaining extracted RNA of the samples included in the differential expression experiment. In 2 aneurysm samples, the amount of RNA left after RNA sequencing was insufficient leaving 20 ruptured, 21 unruptured aneurysm samples, and 16 control tissue samples for further analysis in this validation step. The QX200 Droplet Digital PCR system (Bio-Rad) was used to determine mRNA expression in the samples. First-strand complementary DNA (cDNA) was synthesized using the SuperScript® III First-Strand Synthesis Supermix for qRT-PCR kit (Invitrogen, Carlsbad, CA, USA) according to the manufacturer's instructions. Resulting cDNA was diluted by adding 79 µl nuclease-free water. Thermal cycling was performed using a 20 µl ddPCR reaction (ddPCR 2X PCR Master Mix, Bio-Rad) with 5 µl of cDNA template. Each reaction was run in duplicate and droplet counts were merged to increase the precision. Droplet counts were all within expected range (~16,000–18,000). Primary data processing was done using the QuantaSoft software. The number of positive and negative droplets is used to calculate the concentration (cDNA copies/µl ddPCR reaction) of the targets and their Poisson-based 95% confidence intervals. Further data-analysis was performed in Microsoft Excel. Two reference genes (*SCLY* and *ENOX*) were included for multi-gene normalization.[22] The normalization factor (NF) was calculated as the geometric mean of reference targets *SCLY* and *UBE4A*, and displayed high expression stability (geNorm M value of 0.49) given the heterogeneity of the samples. The absolute (cDNA copies/µl in ddPCR reaction) and relative (unit-less) concentration values and 95% confidence intervals were calculated with the QuantaSoft software in all samples and a non-template control sample. The relative difference in gene expression between aneurysms and controls or ruptured and unruptured aneurysms was analyzed with the Mann-Whitney *U* test. Genes with a *P* value of <0.05 were considered statistically significant differentially expressed.

In addition, we reviewed the existing literature investigating differences in gene expression in aneurysms for the 8 selected genes for further validation.[5-12] Furthermore, we compared the list of differentially expressed genes in our study to the full lists of differentially expressed genes in the previous studies,[5-12] when these lists were available online or could be obtained from the authors. We used the Gene Symbol, and if available the ENSEMBL ID or the Entrez gene ID to compare the lists.

Functional network analysis

To identify the biological functional pathways that were significantly over-represented by differentially expressed genes between aneurysm and control tissue samples as well as between ruptured and unruptured aneurysm samples, we analyzed which Kyoto Encyclopedia of Genes and Genomes functional pathways, and which Gene Ontology categories were enriched in our data set. We used the Bioconductor package goseq (version

1.18.0),[23] which enabled correction for gene length bias in the analysis. We used all genes with differential expression with an FDR-adjusted *P* value <0.05 as input for the analysis. Kyoto Encyclopedia of Genes and Genomes pathways with a FDR-adjusted *P* value <0.05 were considered significantly enriched. To make interpretation of the enriched GO categories possible, we reduced the number of categories by only selecting the GO terms with a total number of genes greater than 20 and smaller than 400 with a *P* value <0.01, since too small and too large categories are not very informative. Then we removed all categories with less than 5 differentially expressed genes, to remove overly-specific terms enriched by only a few genes. The resulting list of GO terms was inputed on a GOtrimming tool[24] using a strong trim threshold (which removes related terms with identical gene content) of 0.40, which calculates the similarity between a parent and child term to be able to remove a parent term with a threshold of 40%. This parent term will be removed if it contains less than or equal to 40% more genes than a child term.

RESULTS

We analyzed the transcripts of 44 aneurysm biopsies (22 ruptured, 21 unruptured and 1 with unknown rupture status) of 38 aneurysm patients (6 patients had two aneurysms treated) and 16 control biopsies of 16 control patients. Baseline characteristics of the patients and controls are shown in Table 4.1.

Aneurysm versus control tissue

Differentially expressed genes

The differential expression analysis yielded 51 genes with overexpression in aneurysms compared with controls (Figure 4.1; Supplementary table S4.2). These included the top 5 genes collagen type X (*COL10A1*), cartilage intermediate layer protein 2 (*CILP2*), 1 RNA gene affiliated with the long noncoding RNA class (ENSG00000206195), secreted frizzled-related protein 2 (*SFRP2*) and muscle excess 3 RNA-binding family member B (*MEX3B*; Table 4.2). We found 178 genes that were underexpressed in aneurysm tissue (Supplementary table S4.2), including the top 5 genes family with sequence similarity 134, member B (*FAM134B*), a gene of the solute carrier family (*SLC13A3*) which code for transporter proteins in the cell membrane, a gene involved in coagulation (*SERPIND1*), the growth regulation by estrogen in breast cancer 1 gene (*GREB1*) and a gap junction protein (*GJB6*; Table 4.2).

The overexpression of *COL10A1* and *CILP2* in aneurysm tissue, seeming the 2 most biologically relevant top genes, was confirmed in the validation experiment (*P*<0.0001), as was the underexpression of *GJB6* (*P*<0.0001) and *SERPIND1* (*P*=0.0015; Table 4.2; Figure 4.2, and Supplementary figure S4.2).

Table 4.1. Baseline characteristics of the 38 patients with aneurysm and 16 controls

	Patients with aneurysm (n=38)*	Ruptured (n=22)	Unruptured (n=21)	Control patients (n=16)
Mean age, y	53	54	53	30
Females	26	17	14	7
Current or former smoker	33	19	19	3
Aneurysm location				
MCA	-	9	17	-
ACA/ACOM	-	11	3	-
PCOM	-	2	0	-
ICA	-	0	1	-
Mean aneurysm size (range)	9 mm (3–25)	8 mm (3–25)	11 mm (5–23)	-
Mean time between rupture and surgery	-	6 d (0–20)	-	-

ACA indicates anterior cerebral artery; ACOM, anterior communicating artery; ICA, internal carotid artery; MCA, middle cerebral artery; and PCOM, posterior communicating artery.
* In 6 of the 38 patients, two biopsies of different aneurysms were obtained and analyzed, in 1 patient, the rupture status of the aneurysm was unknown.

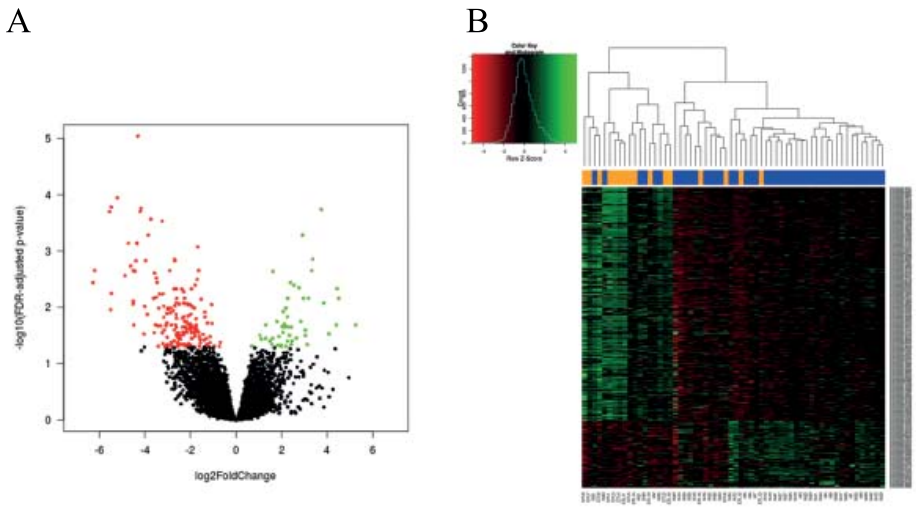

Figure 4.1. Differential expression in aneurysms versus controls visualized in a volcanoplot (A) and a heatmap (B).
A, Log2-fold changes and their corresponding *P* values of each gene were taken for construction of the volcano plot. Green dots represent upregulated genes (n=51) with false discovery rates (FDR) <0.05, whereas downregulated genes (n=178) with identical FDR are depicted in red. All other genes whose expression levels were not found to be significantly altered are in black dots.
B, Heatmap comparison of the differentially expressed genes across the 60 patients samples (16 controls and 44 aneurysms). Hierarchical clustering is shown on the top.

We were able to obtain the full lists of differentially expressed genes in aneurysms versus controls in four of the six previous gene expression studies.[6-9] In one more study, we could only compare our results to the (incomplete) list of differentially expressed genes as published in the article.[11] For one study full data was not available online and could not be obtained from the authors.[5] The 4 relevant and highly significant genes in aneurysms versus controls were not found differentially expressed in the four previous studies of which a full lists of differentially expressed genes was available,[6-9] nor in the one in which an incomplete list was available.[11] Of the total list of 229 differentially expressed genes in aneurysm versus controls identified in our study ten differentially expressed genes were previously found differentially expressed in three other studies (Supplementary table S4.3).[6,7,11] One of these genes, *COL4A6*, was found underexpressed in our and two other studies.[6,11]

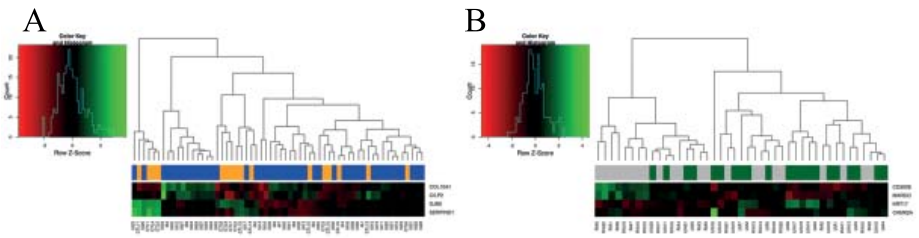

Figure 4.2. Heatmap showing the differential expression of the 8 genes used in the validation experiment.
A, Aneurysm versus controls. B, Ruptured versus unruptured aneurysms.

Table 4.2. Top 10 of differentially expressed genes in aneurysms versus controls and ruptured versus unruptured aneurysms

Ensembl ID	Gene ID (HGNC)	Location	logFC	FDR-adjusted *P* value	Validation experiment *P* value
Overexpression in aneurysms versus controls					
ENSG00000123500	COL10A1	6q21-q22	3.7	1.8 E-4	<0.0001
ENSG00000160161	CILP2	19p13.11	2.9	5.2 E-4	<0.0001
ENSG00000206195			3.7	1.3 E-3	
ENSG00000145423	SFRP2	4q31.3	3.3	2.2 E-3	
ENSG00000183496	MEX3B	15q25.2	1.6	2.3 E-3	
ENSG00000260396			2.4	3.6 E-3	
ENSG00000087494	PTHLH	12p12.1-p11.2	2.5	4.0 E-3	
ENSG00000249119	MTND6P4	5q31.1	2.8	4.5 E-3	
ENSG00000130300	PLVAP	19p13.2	4.4	4.6 E-3	
ENSG00000225210			3.2	6.9 E-3	

Table 4.2 continues on next page

Table 4.2. *Continued*

Ensembl ID	Gene ID (HGNC)	Location	logFC	FDR-adjusted *P* value	Validation experiment *P* value
Underexpression in aneurysms versus controls					
ENSG00000154153	FAM134B	5p15.1	-4.3	9.2 E-6	
ENSG00000158296	SLC13A3	20q13.12	-5.2	1.1 E-4	
ENSG00000099937	SERPIND1	22q11.21	-5.5	1.7 E-4	0.0015
ENSG00000196208	GREB1	2p25.1	-4.2	1.7 E-4	
ENSG00000121742	GJB6	13q12	-5.6	2.0 E-4	<0.0001
ENSG00000107147	KCNT1	9q34.3	-4.2	2.0 E-4	
ENSG00000151715	TMEM45B	11q24.3	-3.7	2.7 E-4	
ENSG00000164309	CMYA5	5q14.1	-3.2	3.0 E-4	
ENSG00000144550	CPNE9	3p25.3	-3.9	5.3 E-4	
ENSG00000107317	PTGDS	9q34.2-q34.3	-4.7	7.3 E-4	
Overexpression in ruptured versus unruptured aneurysms					
ENSG00000019169	MARCO	2q14.2	3.0	2.2 E-6	0.0006
ENSG00000120708	TGFBI	5q31	2.0	1.1 E-5	
ENSG00000173083	HPSE	4q21.3	2.8	4.5 E-5	
ENSG00000167850	CD300C	17q25.1	2.5	7.3 E-5	
ENSG00000186407	CD300E	17q25.1	3.2	8.4 E-5	0.0039
ENSG00000258227	CLEC5A	7q33	2.8	8.4 E-5	
ENSG00000173391	OLR1	12p13.2-p12.3	2.7	8.4 E-5	
ENSG00000170909	OSCAR	19q13.42	2.6	8.4 E-5	
ENSG00000203306			2.1	8.4 E-5	
ENSG00000268802			2.0	8.4 E-5	
Underexpression in ruptured versus unruptured aneurysms					
ENSG00000206052	DOK6	18q22.2	-2.0	1.1 E-4	
ENSG00000070808	CAMK2A	5q32	-3.1	2.0 E-4	0.1085
ENSG00000164591	MYOZ3	5q33.1	-1.8	2.8 E-4	
ENSG00000211892	IGHG4	14q32.33	-6.1	2.9 E-4	
ENSG00000129167	TPH1	11p15.3-p14	-2.7	3.3 E-4	
ENSG00000184731	FAM110C	2p25.3	-2.2	3.3 E-4	
ENSG00000128422	KRT17	17q21.2	-3.2	3.3 E-4	0.06
ENSG00000260396			-2.0	3.3 E-4	
ENSG00000124507	PACSIN1	6p21.3	-3.1	4.7 E-4	
ENSG00000181418	DDN	12q13.12	-2.9	5.2 E-4	

FDR indicates Benjamini Hochberg false discovery rates; HGNC, HUGO Gene Nomenclature Committee; and logFC, log fold change.

Functional network analysis

Functional network analysis of the 229 differentially expressed genes with an FDR-adjusted *P* value <0.05 did not identify any significant Kyoto Encyclopedia of Genes and Genomes pathways. After removal of redundant classes, 51 Gene Ontology terms were identified

(Supplementary table S4.4 for the full list), including terms related to the extracellular matrix (ECM) and transmembrane transporter activity, and terms involving blood vessel regulation.

Low count gene analysis

The subanalysis of low count genes in the raw count data yielded 3 immunoglobulin κ variable region genes (*IGKV1D-42*, *IGKV3D-15*, and *IGKV1-6*), 5 immunoglobulin heavy chain variable region genes (*IGHV3-20*, *IGHV3OR16-15*, *IGHV3-60*, *IGHV1OR15-4*,and *IGHV3-66*) and two other genes (tyrosinase [*TYR*] and a gene with Ensemble ID ENSG00000198229 but without an associated gene name) with >200 counts in aneurysm tissue and 0 counts in control tissue. None of the genes had 0 counts in aneurysms and >200 counts in control tissue.

Ruptured versus unruptured aneurysm tissue

Differentially expressed genes

The differential expression analysis identified 958 genes with overexpression in ruptured aneurysm tissue compared with unruptured aneurysm tissue (Figure 4.3; Supplementary table S4.5). The top 5 overexpressed genes included the macrophage receptor with

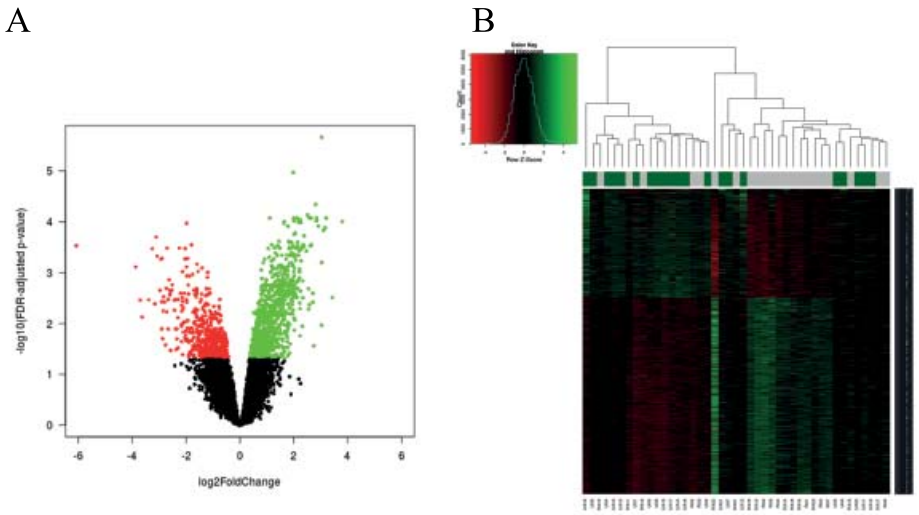

Figure 4.3. Differential expression in ruptured versus unruptured aneurysms visualized in a volcanoplot (A) and a heatmap (B).
A, Log2-fold changes and their corresponding *P* values of each gene were taken for construction of the volcano plot. Green dots represent upregulated genes (n=958) with false discovery rate (FDR) <0.05, whereas downregulated genes (n=531) with identical FDR are depicted in red. All other genes whose expression levels were not found to be significantly altered are in black dots.
B, Heatmap comparison of the differentially expressed genes across the 43 aneurysm samples (22 ruptured and 21 unruptured aneurysms). Hierarchical clustering is shown on the top.

collagenous structure gene (*MARCO*), genes involved in ECM structure (transforming growth factor β-induced [*TGFBI*], heparanase [*HPSE*]), and 2 members of CD family (*CD300C* and *CD300E*; Table 4.2). Five hundred thirty-one genes were underexpressed in ruptured aneurysms (Supplementary table S4.5). Top 5 underexpressed genes included the docking protein 6 (*DOK6*), calcium/calmodulin-dependent protein kinase type II α chain gene (*CAMK2A*), myozenin 3 (*MYOZ3*), an immunoglobulin gene (*IGHG4*) and tryptophan hydroxylase 1 (*TPH1*; Table 4.2). We also found keratin 17 (*KRT17*), a cytoskeleton protein expressed in skin, but also in blood and brain, among the top 10 genes with underexpression in ruptured versus unruptured aneurysms (Table 4.2).

The overexpression of *CD300E* (P=0.0039) and *MARCO* (*P*=0.0006) in ruptured aneurysm tissue was confirmed in the validation experiment. Comparable to the findings in the RNA sequencing analysis, we again showed underexpression of *KRT17* (*P*=0.06) and *CAMK2A* (*P*=0.1085), although for these genes the relative expression differences were not statistically significant in the validation experiment (Table 4.2; Figure 4.2, and Supplementary figure S4.2).

The full data from four previous gene expression studies comparing expression in ruptured versus unruptured aneurysms was all available.[8-10,12] Of the 4 relevant and highly significant genes in ruptured versus unruptured aneurysms, the *MARCO* gene was also found to be overexpressed in 1 previous study,[10] and the *KRT17* gene was also found to be underexpressed in the 2 most recent gene expression studies.[10,12] The other 2 relevant and highly significant genes were not found to be differentially expressed before. Of the total list of the 1489 differentially expressed genes in ruptured versus unruptured aneurysms identified in our study 463 genes were also found differentially expressed in one or more of the previous studies.[8-10,12] Of these 463 genes, 68 were found in our and in at least two of the four previous studies. The results are shown in Supplementary table S4.6.

Functional network analysis

Functional analysis of the 1489 differentially expressed genes with an FDR-adjusted *P* value <0.05 yielded 6 significant Kyoto Encyclopedia Genes and Genome pathways: lysosome, osteoclast differentiation, *Staphylococcus aureus* infection, phagosome, leishmaniasis, and Fc Y R-mediated phagocytosis (Supplementary table S4.7). After trimming, 306 Gene Ontology terms were identified (Supplementary table S4.8), including many terms involved in immune response, the terms lysosome, lysosome organization and lysosomal membrane and lumen, and terms involved in cell-cell interaction and in-cell regulation.

Low count gene analysis

The subanalysis of low count genes found immunoglobulin κ variable 1D-42 to have >200 counts in unruptured aneurysms and 0 counts in ruptured aneurysms. None of the genes had 0 counts in ruptured aneurysm tissue and >200 counts in unruptured aneurysm tissue.

DISCUSSION

This study found ECM pathways to play a role in aneurysms and pathways involved in immune response in rupture of aneurysms, and identified lysosomes as a new pathway to play a role in rupture. In addition, our results point toward a role for immunoglobulins in the pathogenesis of aneurysms because we found that immunoglobulin κ and heavy chain variable region genes were expressed in aneurysm tissue, but showed no expression in control tissue. One immunoglobulin κ variable region gene was expressed in unruptured and not in ruptured aneurysms.

The differences in gene expression found in aneurysms and controls can be the cause, but also be the result of the development of aneurysms. Because intracranial aneurysms are associated with heritable disorders of connective tissue and ECM,[25] changes in the ECM are more likely the cause of the development of aneurysms than its result. As in aneurysms and controls, the differences found in ruptured and unruptured aneurysms can be the cause, but also the result of rupture. Because the time between subarachnoid hemorrhage and clipping was >48 hours in half of our patients, the overexpression of immune response genes in ruptured versus unruptured aneurysms might also be the result of an inflammatory reaction in response to the event of rupture, instead of the cause of rupture. However, 2 previous studies compared biopsies obtained within a range of 2.6 to 24 hours[10] or 6 to 24 hours after rupture[26] and those biopsies obtained later showed no differences in gene expression,[10] nor in the degree of inflammatory cell invasion into the wall.[26] Furthermore, in a study of ruptured aneurysms from autopsy cases inflammatory cell infiltration was always found to be accompanied by fibrosis, and fibrosis was never present without an inflammatory cell infiltration, even in unruptured aneurysms.[27] Because fibrosis is considered the end result of chronic inflammatory reactions,[28] this strongly suggests that the inflammatory reaction is present before rupture.

Our study identified the expression of both light (i.e. of the κ subtype) and heavy chain immunoglobulin genes in aneurysm tissue and its complete absence in control tissue. Two previous immunohistochemistry studies already showed heavy chain immunoglobulins subtypes IgG and IgM to be present in the majority of the investigated aneurysm walls,[29,30] whereas these were only rarely found in control arteries.[29] One of these studies also found sporadic B lymphocytes (which produce immunoglobulins) in unruptured aneurysm tissue, whereas these cells were absent in control arteries.[29] The presence of immunoglobulins and B lymphocytes in the aneurysm wall suggest that the inflammatory reaction in the aneurysm wall, which is not seen in healthy control arteries, is initiated by the humoral immune response, through attraction of inflammatory cells and through complement activation.[30] Our study underlines the importance of involvement of genes of the ECM pathway in aneurysms, which was also found in a previous meta-analysis of 5 microarray studies.[31]

Furthermore, several histopathological studies have shown degradation of the ECM in intracranial aneurysm tissue.[32]

We found enrichment of the lysosome pathway in ruptured aneurysms. Lysosomes digest the degradation material from the cell. Phagosomes, another enriched pathway in ruptured aneurysms in our study, fuse with lysosomes after phagocytosis of degradation material. Enrichment of these pathways supports the notion that degradation of the components of the unruptured aneurysm wall is a process leading to rupture,[33] but may also be a response to rupture. In a previous genome-wide expression study on blood from patients with aneurysmal subarachnoid hemorrhage taken several years after the subarachnoid hemorrhage compared with blood of healthy controls the lysosome pathway was also found enriched.[34] This finding strengthens the idea that the lysosome pathway does not reflect an acute and short-lasting reaction to aneurysm rupture. Pathways found to be involved in rupture in previous studies were inflammation and immune response pathways, ECM degradation, cell adhesion, vascular remodeling, oxidative stress, turbulent bloodflow, proteases and apoptosis.[8-10,12] Our study also found immune response pathways to be involved in rupture and identified lysosomes as a new pathway. Furthermore, inflammation was a predominant characteristic of ruptured aneurysms in immunohistochemistry studies.[32]

This study has some limitations. First, aneurysm biopsies could only be taken from aneurysms treated with microneurosurgical techniques, which may induce a selection bias because certain aneurysm characteristics might make aneurysms more suitable for clipping while these characteristics are also associated with rupture.[35] Second, as controls we used cortical intracranial arteries obtained from patients with intractable epilepsy. However, we cannot be sure that the composition of these cortical arteries is similar to the composition of the basal arteries of the circle of Willis on which aneurysms arise. Furthermore, we cannot exclude the possibility that the seizures or the epileptogenic focus have altered the cortical vessels, although we found no data supporting such an influence.

There are several strengths of this study. First, we did not find larger studies investigating gene expression differences in intracranial aneurysms to date. The large sample size increased power of our study and enabled correction for possible confounders in our analysis, including sex, age, and rupture status of the aneurysm. Furthermore, we used RNA sequencing methodology, which compared with the previously used microarray technique, has the advantage of requiring less tissue mass as input material (crucial in aneurysm studies because of the small size of the biopsies) and of a genome-wide coverage, enabling the discovery of not yet identified genes involved in the disease. Finally, we used healthy intracranial arteries as controls, which are preferred above extracranial arterial tissue because of the differences in vessel wall composition between intra- and extracranial arteries.

In conclusion, we identified the lysosome pathway as a new pathway for rupture of intracranial aneurysms and found further evidence for the role of the immune response in aneurysmal rupture. Our results also point toward a role for immunoglobulins in the pathogenesis of aneurysms. Our finding that immune response pathways play a role in aneurysm rupture suggest that anti-inflammatory and immune-modifying drugs are interesting candidate therapeutics in the prevention of aneurysm rupture. The presence of immunoglobulins in aneurysm and its absence in control tissue highlights the potential role of immunoglobulin-mediated inhibition of B lymphocytes as an interesting therapeutic intervention in aneurysm development or growth. To identify patients with aneurysms showing signs of increased aneurysm wall inflammation, an imaging technique is required that is able to correctly identify those aneurysms subject to inflammation, for example, by using magnetic resonance imaging with a suitable contrast agent or high resolution vessel wall magnetic resonance imaging.[36,37]

REFERENCES

1. Vlak MH, Algra A, Brandenburg R, Rinkel GJ. Prevalence of unruptured intracranial aneurysms, with emphasis on sex, age, comorbidity, country, and time period: a systematic review and meta-analysis. *Lancet Neurol.* 2011;10:626-636.
2. Gabriel RA, Kim H, Sidney S, McCulloch CE, Singh V, Johnston SC, et al. Ten-year detection rate of brain arteriovenous malformations in a large, multiethnic, defined population. *Stroke.* 2010;41:21-26.
3. Nieuwkamp DJ, Setz LE, Algra A, Linn FH, de Rooij NK, Rinkel GJ. Changes in case fatality of aneurysmal subarachnoid haemorrhage over time, according to age, sex, and region: a meta-analysis. *Lancet Neurol.* 2009;8:635-642.
4. Brinjikji W, Rabinstein AA, Nasr DM, Lanzino G, Kallmes DF, Cloft HJ. Better outcomes with treatment by coiling relative to clipping of unruptured intracranial aneurysms in the United States, 2001-2008. *AJNR Am J Neuroradiol.* 2011;32:1071-1075.
5. Krischek B, Kasuya H, Tajima A, Akagawa H, Sasaki T, Yoneyama T, et al. Network-based gene expression analysis of intracranial aneurysm tissue reveals role of antigen presenting cells. *Neuroscience.* 2008;154:1398-1407.
6. Shi C, Awad IA, Jafari N, Lin S, Du P, Hage ZA, et al. Genomics of human intracranial aneurysm wall. *Stroke.* 2009;40:1252-1261.
7. Li L, Yang X, Jiang F, Dusting GJ, Wu Z. Transcriptome-wide characterization of gene expression associated with unruptured intracranial aneurysms. *Eur Neurol.* 2009;62:330-337.
8. Pera J, Korostynski M, Krzyszkowski T, Czopek J, Slowik A, Dziedzic T, et al. Gene expression profiles in human ruptured and unruptured intracranial aneurysms: what is the role of inflammation? *Stroke.* 2010;41:224-231.
9. Marchese E, Vignati A, Albanese A, Nucci CG, Sabatino G, Tirpakova B, et al. Comparative evaluation of genome-wide gene expression profiles in ruptured and unruptured human intracranial aneurysms. *J Biol Regul Homeost Agents.* 2010;24:185-195.
10. Kurki MI, Hakkinen SK, Frosen J, Tulamo R, von und zu Fraunberg M, Wong G, et al. Upregulated signaling pathways in ruptured human saccular intracranial aneurysm wall: an emerging regulative role of Toll-like receptor signaling and nuclear factor-kappaB, hypoxia-inducible factor-1A, and ETS transcription factors. *Neurosurgery.* 2011;68:1667-1675.
11. Yu L, Fan J, Wang S, Zhang D, Wang R, Zhao Y, et al. Gene expression profiles in intracranial aneurysms. *Neurosci Bull.* 2014;30:99-106.

12. Nakaoka H, Tajima A, Yoneyama T, Hosomichi K, Kasuya H, Mizutani T, et al. Gene expression profiling reveals distinct molecular signatures associated with the rupture of intracranial aneurysm. *Stroke*. 2014;45:2239-2245.
13. 't Hoen PA, Ariyurek Y, Thygesen HH, Vreugdenhil E, Vossen RH, de Menezes RX, et al. Deep sequencing-based expression analysis shows major advances in robustness, resolution and inter-lab portability over five microarray platforms. *Nucleic Acids Res*. 2008;36:e141.
14. R Core Team. R: A language and environment for statistical computing. R Foundation for Statistical Computing, Vienna, Austria, 2015.
15. Souza W, Carvalho B. Rqc: Quality Control Tool for High-Throughput Sequencing Data. R package version 1.2.0. Available at: https://github.com/labbcb/Rqc, 2015.
16. Dobin A, Davis CA, Schlesinger F, Drenkow J, Zaleski C, Jha S, et al. STAR: ultrafast universal RNA-seq aligner. *Bioinformatics*. 2013;29:15-21.
17. Li H, Handsaker B, Wysoker A, Fennell T, Ruan J, Homer N, et al. The Sequence Alignment/Map format and SAMtools. *Bioinformatics*. 2009;25:2078-2079.
18. Anders S, Pyl PT, Huber W. HTSeq – A Python framework to work with high-throughput sequencing data. *Bioinformatics*. 2015;31:166-169.
19. Robinson MD, McCarthy DJ, Smyth GK. edgeR: a Bioconductor package for differential expression analysis of digital gene expression data. *Bioinformatics*. 2010;26:139-140.
20. Smyth GK. Limma: linear models for microarray data. In: Gentleman R, Carey V, Dudoit S, Irizarry R, Huber W, eds. Bioinformatics and Computational Biology Solutions using R and Bioconductor. New York, NY: Springer; 2005:397-420.
21. Anders S, McCarthy DJ, Chen Y, Okoniewski M, Smyth GK, Huber W, et al. Count-based differential expression analysis of RNA sequencing data using R and Bioconductor. *Nat Protoc*. 2013;8:1765-1786.
22. Vandesompele J, De Preter K, Pattyn F, Poppe B, Van Roy N, De Paepe A, et al. Accurate normalization of real-time quantitative RT-PCR data by geometric averaging of multiple internal control genes. *Genome Biol*. 2002;3:RESEARCH0034.
23. Young MD, Wakefield MJ, Smyth GK, Oshlack A. Gene ontology analysis for RNA-seq: accounting for selection bias. *Genome Biol*. 2010;11:R14.
24. Jantzen SG, Sutherland BJ, Minkley DR, Koop BF. GO Trimming: Systematically reducing redundancy in large Gene Ontology datasets. *BMC Res Notes*. 2011;4:267.
25. Schievink WI, Michels VV, Piepgras DG. Neurovascular manifestations of heritable connective tissue disorders. A review. *Stroke*. 1994;25:889-903.
26. Kataoka K, Taneda M, Asai T, Kinoshita A, Ito M, Kuroda R. Structural fragility and inflammatory response of ruptured cerebral aneurysms. A comparative study between ruptured and unruptured cerebral aneurysms. *Stroke*. 1999;30:1396-1401.
27. Crompton MR. Mechanism of growth and rupture in cerebral berry aneurysms. *Br Med J*. 1966;1:1138-1142.
28. Wynn TA. Cellular and molecular mechanisms of fibrosis. *J Pathol*. 2008;214:199-210.
29. Chyatte D, Bruno G, Desai S, Todor DR. Inflammation and intracranial aneurysms. *Neurosurgery*. 1999;45:1137-1146.
30. Tulamo R, Frosen J, Junnikkala S, Paetau A, Pitkaniemi J, Kangasniemi M, et al. Complement activation associates with saccular cerebral artery aneurysm wall degeneration and rupture. *Neurosurgery*. 2006;59:1069-1076.
31. Roder C, Kasuya H, Harati A, Tatagiba M, Inoue I, Krischek B. Meta-analysis of microarray gene expression studies on intracranial aneurysms. *Neuroscience*. 2012;201:105-113.
32. Frosen J, Piippo A, Paetau A, Kangasniemi M, Niemela M, Hernesniemi J, et al. Remodeling of saccular cerebral artery aneurysm wall is associated with rupture: histological analysis of 24 unruptured and 42 ruptured cases. *Stroke*. 2004;35:2287-2293.
33. Hosaka K, Hoh BL. Inflammation and cerebral aneurysms. *Transl Stroke Res*. 2014;5:190-198.
34. van 't Hof FN, Ruigrok YM, Medic J, Sanjabi B, van der Vlies P, Rinkel GJ, et al. Whole Blood Gene Expression Profiles of Patients with a Past Aneurysmal Subarachnoid Hemorrhage. *PLoS One*. 2015;10:e0139352.

35. Morita A, Kirino T, Hashi K, Aoki N, Fukuhara S, et al.; UCAS Japan Investigators. The natural course of unruptured cerebral aneurysms in a Japanese cohort. *N Engl J Med*. 2012;28:2474-2482.
36. Hasan DM, Mahaney KB, Magnotta VA, Kung DK, Lawton MT, Hashimoto T, et al. Macrophage imaging within human cerebral aneurysms wall using ferumoxytol-enhanced MRI: a pilot study. *Arterioscler Thromb Vasc Biol*. 2012;32:1032-1038.
37. Kleinloog R, Korkmaz E, Zwanenburg JJ, Kuijf HJ, Visser F, Blankena R, et al. Visualization of the aneurysm wall: a 7.0-tesla magnetic resonance imaging study. *Neurosurgery*. 2014;75:614-622.

SUPPLEMENTARY MATERIAL

Supplementary tables S4.1 to S4.8 and Supplementary figures S4.1 and S4.2, can be found online: http://hdl.handle.net/10411/H580HA.

5

VISUALIZATION OF THE ANEURYSM WALL: A 7.0 TESLA MAGNETIC RESONANCE IMAGING STUDY

R. Kleinloog, E. Korkmaz, J.J.M. Zwanenburg, H.J. Kuijf, F. Visser,
R. Blankena, J.A. Post, Y.M. Ruigrok, P.R. Luijten, L. Regli,
G.J.E. Rinkel, B.H. Verweij

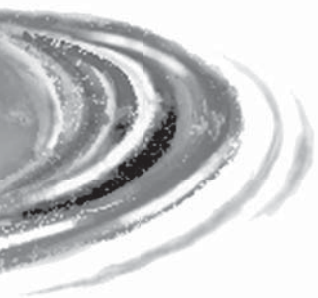

Neurosurgery. 2014;75:614-622

ABSTRACT

Background: Risk prediction of rupture of intracranial aneurysms is poor and is based mainly on lumen characteristics. However, characteristics of the aneurysm wall may be more informative predictors. The limited resolution of currently available imaging techniques and the thin aneurysm wall make imaging of wall thickness challenging.

Objective: To introduce a novel protocol for imaging wall thickness variation using ultra-high-resolution 7.0 Tesla magnetic resonance imaging (MRI).

Methods: We studied 33 unruptured intracranial aneurysms in 24 patients with a T1-weighted 3-dimensional magnetization-prepared inversion-recovery turbo-spin-echo whole-brain sequence with a resolution of 0.8 x 0.8 x 0.8 mm. We performed a validation study with a wedge phantom and with 2 aneurysm wall biopsies obtained during aneurysm treatment using ex vivo MRI and histological examination and correlating variations in MRI signal intensity with variations in actual thickness of the aneurysm wall.

Results: In vivo, the aneurysm wall was visible in 28 of the 33 aneurysms. Variation in signal intensity was observed in all visible aneurysm walls. Ex vivo MRI showed variation in signal intensity across the wall of the biopsies, similar to that observed on the in vivo images. Signal intensity and actual thickness in both biopsies had a linear correlation, with Pearson correlation coefficients of 0.85 and 0.86.

Conclusion: Unruptured intracranial aneurysm wall and its variation in thickness can be visualized with 7.0 Tesla MRI. Aneurysm wall thickness variation can now be further studied as a risk factor for rupture in prospective studies.

INTRODUCTION

Risk prediction of rupture of intracranial aneurysms is based mainly on the size of the aneurysm, with large aneurysms more prone to bleeding.[1] Most unruptured aneurysms discovered incidentally or during screening are, however, small[2] with an inherently small risk of rupture.[3] Consequently, most small aneurysms are left untreated.[3] However, most ruptured aneurysms are small, which is explained by the relatively high prevalence of small unruptured aneurysms.[4,5] Therefore, better identification of rupture-prone aneurysms is needed to tailor preventive treatment to those aneurysms. So far, studies on risk factors for aneurysm rupture have focused on the aneurysm lumen. Characteristics of the aneurysm wall are probably more important for rupture assessment; thus, imaging of the aneurysm wall seems pivotal to improve risk assessment of aneurysms. Postmortem and intraoperative studies have shown that the aneurysm wall can be very thin (0.02 to 0.50 mm)[6] with variation in thickness.[7,8] The spatial resolution of the currently available imaging techniques, including 3.0 Tesla MRI,[9] is insufficient to image the thickness of such thin structures.[10,11] Although 7.0 Tesla MRI enables imaging with increased signal-to-noise ratio and a higher spatial resolution, the resolution is still insufficient, given the typically very thin wall of aneurysms. When the vessel wall is of a similar size as or is smaller than the size of 1 voxel (resolution), partial volume effects occur, and traditional thickness measurements will therefore overestimate the actual thickness. However, variation in thickness of the vessel wall will produce a variation in signal intensity of the voxel, particularly when the signals of surrounding structures (blood on one side of the wall and cerebrospinal fluid on the other side) are low. We hypothesized that thickness variation in the aneurysm wall can be visualized as signal intensity variation with 7.0 Tesla MRI. When a recently developed sequence in which blood and cerebrospinal fluid are black is used to image the intracranial arterial wall,[12] the signal intensity variations observed across the aneurysm wall should be reflecting the amount of aneurysm wall tissue in 1 voxel and thus the actual thickness variations of the wall. In the present study, we combined in vivo imaging with ex vivo validation experiments to investigate whether the aneurysm wall can be visualized on 7.0 Tesla MRI and whether intensity variation indeed reflects variation in thickness of the aneurysm wall.

METHODS

Patient selection

Patients with unruptured intracranial aneurysms were recruited through the neurological and neurosurgical outpatient clinic at the University Medical Center Utrecht, The Netherlands between July 2011 and June 2013. Patients with contraindications for 7.0 Tesla MRI (e.g.

claustrophobia, metal objects such as dental implants or prostheses in or on the body, clips or coils used for previous aneurysm treatment) were excluded, as were patients with underlying vascular malformations such as arteriovenous malformations. All patients participating in this study gave written informed consent, and this study was approved by the Institutional Review Board of the University Medical Center Utrecht, The Netherlands.

In vivo imaging of the aneurysm wall

Imaging was performed on a 7.0 Tesla MRI scanner (Philips Healthcare, Cleveland, Ohio) with a 32-channel SENSE receive head coil and a volume transmit coil (Nova Medical, Wilmington, Massachusetts). A T1-weighted 3-dimensional magnetization-prepared inversion-recovery turbo-spin-echo (further referred to as $MR_{in\ vivo}$) sequence with whole-brain coverage, as described previously[12] and developed to image the intracranial vessel wall, was used to image the aneurysm wall. Briefly, the scan parameters were as follows: field of view, 250 x 250 x 190 mm (foot to head x anterior to posterior x right to left); acquired resolution, 0.8 x 0.8 x 0.8 mm; repetition time/inversion time/echo time, 3952/1375/37 milliseconds; and a variable-reduced refocusing flip angle scheme. The sequence was fat-suppressed using a spectral attenuated inversion-recovery pulse with 220-millisecond inversion delay. Parallel imaging with 2-dimensional sensitivity encoding was used with an acceleration factor of 6 (2 x 3, anterior to posterior x right to left), yielding a scan duration of approximately 11 minutes. In each patient, the protocol also contained a time-of-flight sequence for anatomic depiction of the aneurysm. The parameters of the time-of-flight sequence were as follows: repetition time/echo time 15/3.2 milliseconds; flip angle, 25°; field of view, 200 x 190 x 50 mm (anterior to posterior x right to left x foot to head); acquired resolution, 0.25 x 0.30 x 0.40 mm; and sensitivity encoding with an acceleration factor of 2.2 (in the right-to-left direction). The scan duration was approximately 9 minutes. One patient whose images were heavily affected by movement artifacts was excluded from further analysis, as was a second patient whose images were affected by local artifacts at the aneurysm location (resulting from a location close to the skull base).

Ex vivo imaging of the aneurysm wall

Ex vivo aneurysm wall biopsy preparation

The aneurysm wall biopsies were obtained from 2 patients who underwent clipping of their unruptured aneurysm and participated in an aneurysm wall tissue collection study. The first patient (patient 1), a 66-year-old woman, had a middle cerebral artery aneurysm with a luminal diameter of 7 mm. The second patient (patient 2), a 56-year-old man, had a large, partially thrombosed middle cerebral artery aneurysm (luminal diameter, 25 mm). A part of the aneurysm fundus distal to the clip was excised when complete obliteration

of the aneurysm was confirmed by the surgeon using visual inspection and intraoperative IndoCyanine Green angiography. The excision was performed at a location convenient for the surgeon. After excision, the wall biopsy was immediately submerged into 4% paraformaldehyde fixative in 0.1 mol/L phosphate buffer (pH 7.4) for at least 1 hour at room temperature and stored at 4°C until further preparation. For MRI, the wall biopsies were rinsed in 0.1 mol/L phosphate buffer followed by gradual infiltration with 4% gelatin (in 0.1 mol/L phosphate buffer) at 37°C. Biopsies were then embedded in fresh 4% gelatin solution in a Petri dish and left at 4°C to solidify overnight, avoiding air bubbles. Before MRI, the Petri dishes containing the gelatin-embedded biopsies were submerged in Fomblin (Solvay Solexis, Bollate, Italy), a proton-free fluid without MRI signal, to prevent artifacts at the borders.

Ex vivo MRI protocol

The wall biopsies were scanned in a single session on the 7.0 Tesla MRI using the same 32-channel head coil used for in vivo imaging. A sequence nearly identical to the in vivo sequence (further referred to as $MRI_{ex\ vivo\ 0.8\ mm}$) was used, with the following slight adjustments to the parameters for the ex vivo situation. The TI was lowered to 1100 milliseconds to null the signal from the gelatin. Because of the smaller size of the specimen, sensitivity-encoding acceleration was removed and the field of view was reduced by a factor of 2 in the right-to-left direction and 3 in the anterior-to-posterior direction, which resulted in the same scan time, turbo spin-echo train, and resolution as the in vivo protocol while avoiding potential sensitivity-encoding artifacts. We performed an additional scan with ultra-high resolution (0.18-mm isotropic voxels, further referred to as $MRI_{ex\ vivo\ 0.18\ mm}$) which was used only to align histology with the images from the $MRI_{ex\ vivo\ 0.8\ mm}$ scan. The scan parameters of the $MRI_{ex\ vivo\ 0.18\ mm}$ scan were described before[13] and this scan had an acquisition time of >3 hours.

Histological examination of aneurysm wall biopsies

After MRI, the wall biopsies were put in a 37° C incubator to liquefy the gelatin before final rinsing in 0.1 mol/L phosphate buffer. Biopsies were further processed for histology using standard procedures and embedded in paraffin in the preferred orientations to imitate the original position of the biopsies during ex vivo MRI. Then, 4-µm-thick serial sections of each sample were cut with a microtome and mounted on glass slides for hematoxylin and eosin histological staining. The serial sections of both biopsies were imaged with a light microscope with X 4 objective (Provis AX70; Olympus), and a selection of 7 sections of each biopsy was made that was evenly distributed throughout the biopsy sample and was free from microtome cutting artifacts. Nikon DXM1200 digital camera and Nikon ATC-1 software (Nikon Instruments Europe) were used to capture images of this selection of sections.

Selection of corresponding cross sections of the aneurysm wall biopsies

For each aneurysm wall biopsy, the 7 images of the selected sections of the wall were compared with 2-dimensional transversal oriented slices of the wall as obtained with the ultra-high-resolution $MRI_{ex\ vivo\ 0.18\ mm}$. From each biopsy, the cross section that showed the best alignment on the basis of its anatomy between histology and the $MRI_{ex\ vivo\ 0.18\ mm}$ was selected by visual inspection. This was done by taking into account the order of the sections of both MR slices and histological sections, thereby ensuring that the histological section and the MR slice represented the same location in the tissue. After identification of the correct slice the $MRI_{ex\ vivo\ 0.18\ mm}$, we selected the slice with the same orientation and location as the $MRI_{ex\ vivo\ 0.8\ mm}$.

Measurement of signal intensity variation on MRIs

Variation in signal intensity in the $MRI_{ex\ vivo\ 0.8\ mm}$ slice was visualized with an intensity curve showing the changes in signal intensity in a path manually drawn across the center of the aneurysm wall using MeVisLab (MeVis Medical Solutions AG, Bremen, Germany).[14] A local signal averaging was applied to correct for drawing inaccuracies. The signal intensities across the path were plotted to obtain a profile curve of the variation in signal intensity across the wall.

Measurement of actual thickness variation on histological sections

Actual thickness was measured on the histological sections using Matlab (Mathworks, Natick, Massachusetts, USA), as follows: segmentation of the tissue was performed, and the center line of the tissue was computed. Measurements were performed perpendicular to this center line to measure full thickness of the wall at multiple points across this line. The measurements were plotted to obtain a curve of the variation in actual thickness across the wall. The histological sections of biopsy 1 were all suitable for this analysis, but because there was little difference in the anatomy of these sections, we used the middle section for correlation analysis. For biopsy 2, only a part of the selected section was suitable for the correlation analysis. Because of intraoperative cutting damage, thickness measurements were not possible in the other part or in the other 6 sections of biopsy 2. In addition, histopathological examination of the selected cross sections was performed.

Correlation analysis of signal intensity curves and actual thickness curves

The curves of the variation in signal intensity and actual thickness were normalized between 0 and 1. The signal intensity curve was rescaled to have the same physical length as the histological section. The signal intensity curve was cropped to remove the extreme ends where the MRI signal started to diminish. Then, the 2 curves were aligned by maximizing the cross-correlation of the 2 curves by using Matlab. After aligning the signal intensity curve and the actual thickness curve, we correlated both data sets and calculated the Pearson

correlation coefficient. Slight tilting of the biopsies while being processed for histological examination might have compromised accurate matching with the corresponding MRI slice at the edges of the tissue. Therefore, for 1 biopsy (biopsy 1), we also compared measurements from the MRI and histological examination excluding the edges.

Wedge phantom imaging

To illustrate the basic principle that signal intensity produced by partial volume effects is related to size of the object, we performed imaging on a wedge phantom. By placing 1 end of a 6-mm-thick, 10-cm-long polymethyl methacrylate sheet on a polytetrafluorethylene strip with a thickness of 2.3 mm in a box filled with water, we created a wedge phantom with increasing thickness ranging from 0 to 2.3 mm. This phantom was scanned with the same protocol as used for the in vivo aneurysm imaging. The signal intensity variation was measured in the same way as in the ex vivo experiment with MeVisLab. Because of the large size of the phantom, we corrected the signal intensities for inhomogeneity induced by the receive coil sensitivity and the transmit field inhomogeneity. This was done by measuring a reference intensity profile of the water above the polymethyl methacrylate sheet (without partial volume effects) and dividing the intensity profile from the wedge phantom by the reference profile.

RESULTS

In vivo imaging of the aneurysm wall

In vivo images of the aneurysm wall on 7.0 Tesla MRI were obtained in 24 patients with 33 unruptured aneurysms. The size (largest luminal diameter) of the aneurysms varied from 2 to 25 mm. In 28 of the 33 aneurysms, the wall was visible because it exhibited a higher signal than cerebrospinal fluid and blood (example shown in Figure 5.1). The intensity of the wall is equal to the intensity of brain tissue and intraluminal thrombus; therefore, the parts of the wall aligning the brain or intraluminal thrombus could not be assessed. Four aneurysms were completely enclosed by surrounding tissue (brain or dura), and in one of the aneurysms, the lumen was almost completely thrombosed. In these cases, the aneurysm wall could not be distinguished at all (Figure 5.2). In all of the 28 aneurysms visible on the $MR_{in\ vivo}$ images, we detected variations in signal intensity across the aneurysm wall (Figure 5.2).

Ex vivo imaging of the aneurysm wall

$MR_{ex\ vivo\ 0.8\ mm}$ images of the 2 aneurysm wall biopsies showed a hyperintense signal similar to that observed on the $MR_{in\ vivo}$ images. When a 3-dimensional image reconstruction of the

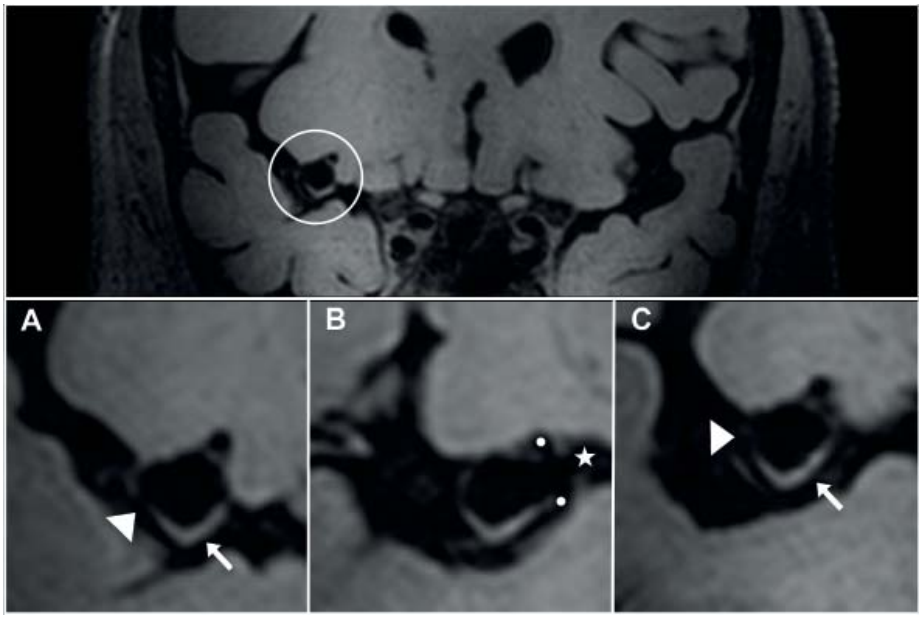

Figure 5.1. In vivo imaging of an aneurysm wall on 7.0 Tesla magnetic resonance imaging.
In vivo images of the wall of a right middle cerebral artery aneurysm with an intraluminal diameter of 7 mm (top, coronal view: aneurysm marked with a circle) show variation in signal intensity across the wall. A, magnification of the top panel showing apparently thin (low signal intensity, arrowhead) and thick (high intensity, arrow) portions of the wall. B, oblique cross section in which the lumen of the parent artery (M1 segment of the middle cerebral artery, star) and the branching arteries (M2 segments of the middle cerebral artery, dots) are visible. C, another oblique cross section of the aneurysm wall, confirming that the aneurysm is not in contact with surrounding brain tissue with its apparently thick part of the wall (arrow).

aneurysm wall was visually compared to a macroscopic picture of the biopsy, the pattern of variation in signal intensity was similar to that of variation in wall thickness (Figure 5.3). The actual thickness of the aneurysm wall, as measured by histological examination, ranged between 0.2 and 0.6 mm in biopsy 1 and 0.2 and 1.6 mm in biopsy 2. Histopathological examination of the thinnest part of biopsy 1 showed a remarkably hypocellular wall, consisting mainly of collagen, with a complete absence of endothelial lining. The thicker part showed minor hyperplasia of the intimal layer, the presence of inflammatory cells, an abundance of collagen, and an intact endothelial lining. An examination of the thick part of biopsy 2 showed a hypercellular wall without distinguishable layers with infiltration of inflammatory cells and the presence of thrombosis. Degeneration of the extracellular matrix was found, as were spindle-shaped smooth muscle cells. Some vaso vasorum were identified in the abluminal layer. The thinner parts of this biopsy were less cellular and showed disorganized collagen.

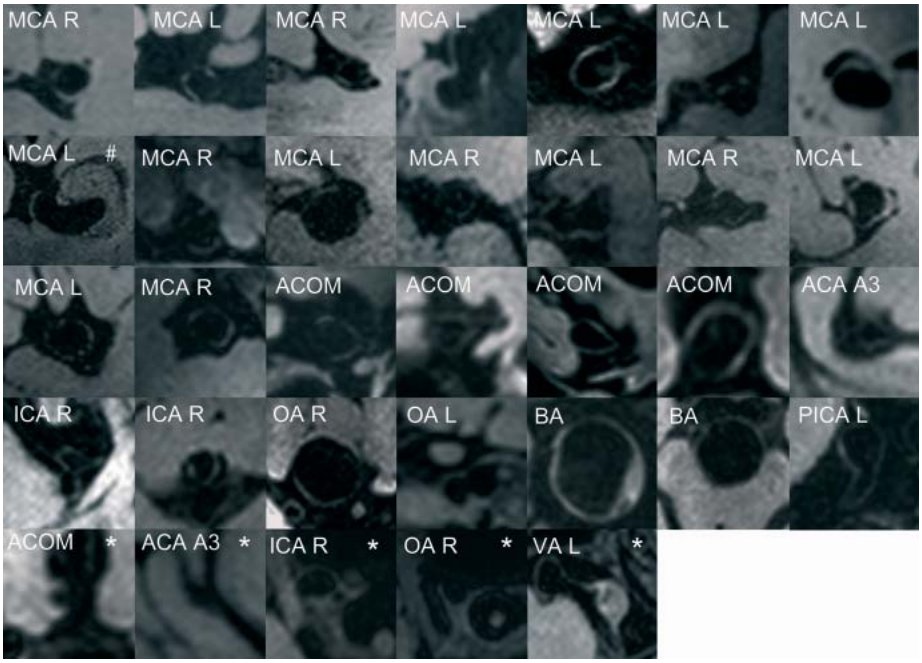

Figure 5.2. Overview of in vivo aneurysm wall imaging on 7.0 Tesla magnetic resonance imaging of all 33 unruptured intracranial aneurysms.
Locations of the aneurysms are indicated. A partially thrombosed aneurysm is indicated with a hashtag (#). An asterisk (*) indicates the aneurysms in which we were unable to assess variations in signal intensity of the wall owing to their embedment in surrounding tissue or the presence of intraluminal thrombus. ACA A3, pericallosal artery; ACOM, anterior communicating artery; BA, basilar artery; ICA, internal carotid artery; MCA, middle cerebral artery; OA, ophthalmic artery; PICA, posterior inferior cerebellar artery; VA, vertebral artery.

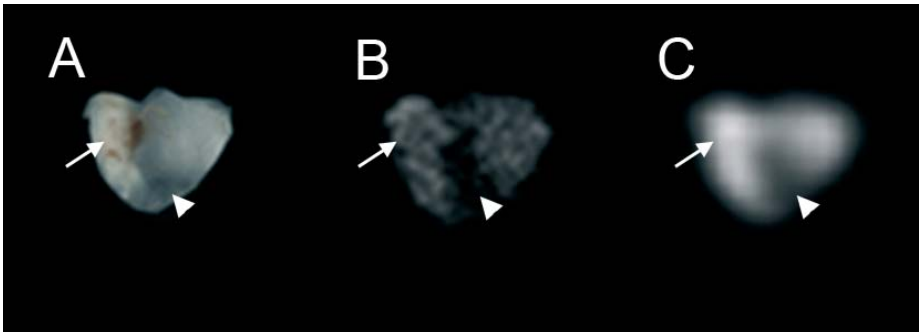

Figure 5.3. Ex vivo imaging of the aneurysm wall. Image showing the visual correlation between signal intensity and actual thickness in wall biopsy 1.
The part of the wall assumed to be thick on subsequent images is indicated with an arrow, and the thin part of the wall is indicated with an arrowhead. A, macroscopic picture of the entire biopsy in gelatin. B, screenshot of a 3-dimensional maximum-intensity projection of the 0.18-mm resolution MR images of the entire biopsy. C, screenshot of a 3-dimensional maximum-intensity projection of the ex vivo MRIs obtained with the 0.8-mm resolution vessel wall sequence.

Correlation analysis

The corresponding $MR_{ex\ vivo\ 0.8\ mm}$ images and the histological sections selected for correlation analysis by using $MR_{ex\ vivo\ 0.18\ mm}$ images are shown in Figure 5.4. The variation in actual thickness correlated with variation in signal intensity of the wall on MRI (Figure 5.5). For both biopsies, we found a linear correlation between signal intensity and actual thickness (Pearson correlation coefficient: biopsy 1, 0.85; biopsy 2, 0.86; Figure 5.5). When only the middle part of biopsy 1 was analyzed, the Pearson correlation coefficient increased to 0.97 (Figure 5.5A2).

Wedge phantom imaging

The results of the wedge phantom imaging showed that signal intensity increased linearly with thickness of the phantom until reaching a plateau at the point where the phantom size was larger than the voxel size of the sequence (Figure 5.6).

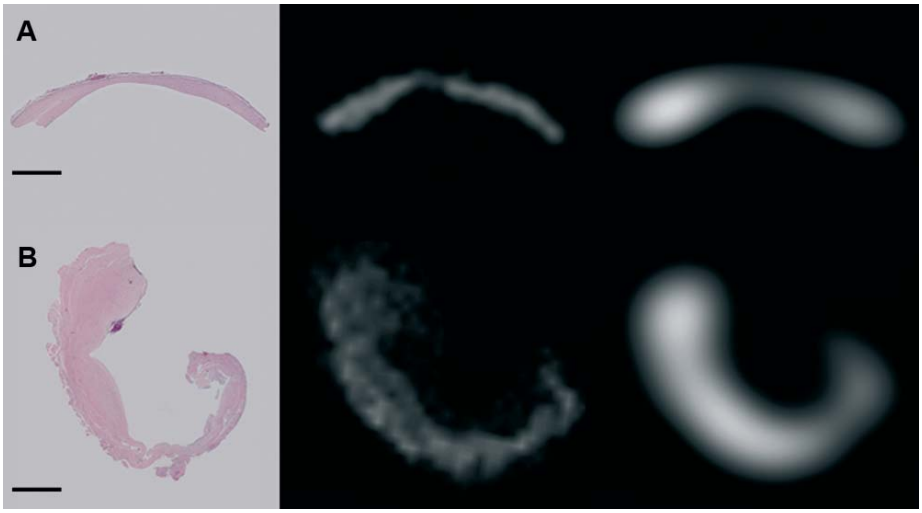

Figure 5.4. Corresponding cross sections of the 2 wall biopsies selected for the ex vivo validation study.
A, selected cross section of a middle cerebral artery aneurysm wall (wall biopsy 1). B, selected cross section of a middle cerebral artery aneurysm wall (wall biopsy 2). A slight change in configuration of biopsy 2 occurred because of a collapse of the tissue during paraffin embedment. From left to right: histological section (scale bar = 1 mm), slice of the 0.18-mm resolution MR image used for alignment of the MRI with histology, and the corresponding slice of the 0.8-mm resolution MRI.

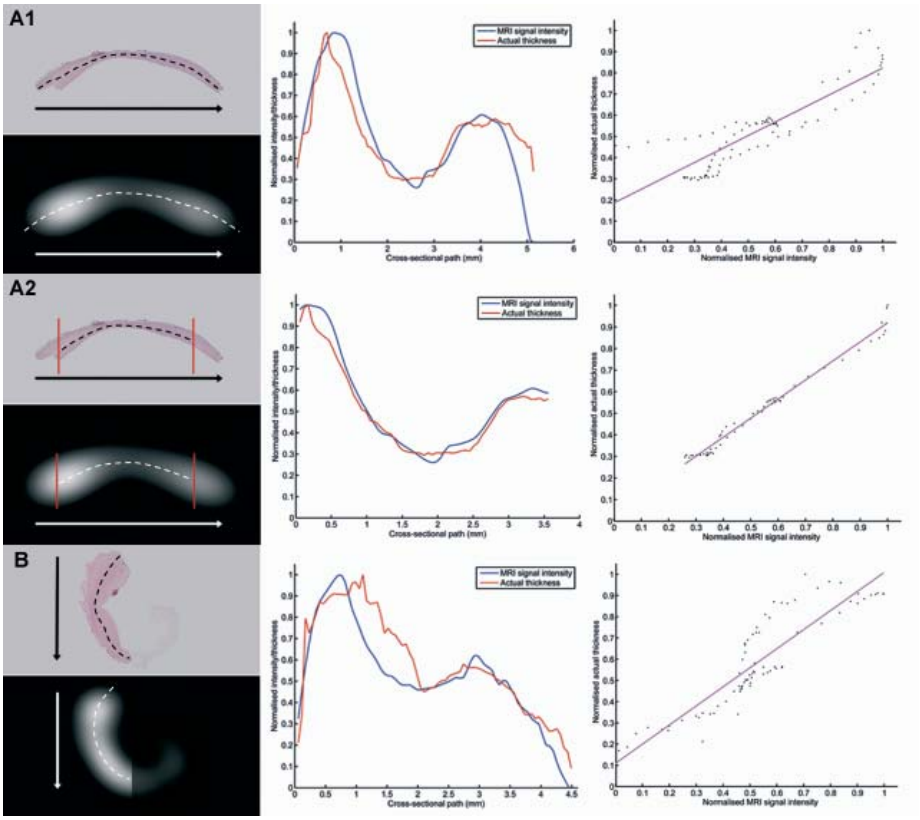

Figure 5.5. Correlation of signal intensity variation and actual thickness variation in the aneurysm wall biopsies.
From left to right: direction of the path through the center of the tissue in the histological section (top) and in the magnetic resonance imaging slice (bottom), curves of signal intensity (blue) and actual thickness (red) after normalization, and correlation between signal intensity and actual thickness. A1, correlation in wall biopsy 1; A2, correlation in the middle part of the tissue of biopsy 1. Red lines in the left panel indicate the selected region (representing the region between the peaks in intensity/thickness). B, correlation in wall biopsy 2. We excluded a part of the histological section (transparent part) of wall biopsy 2 from the measurement because intraoperative cutting damaged the tissue and a thickness measurement was not possible in that part.

DISCUSSION

The present study shows that 7.0 Tesla MRI can image intracranial aneurysm walls and assess variation in aneurysm wall thickness.

This is the first study confirming with a wedge phantom and histology data that in vivo imaging of aneurysm wall thickness variation is possible. Previously, 1 study described the imaging of unruptured aneurysm walls with a double-inversion recovery black-blood sequence on 1.5

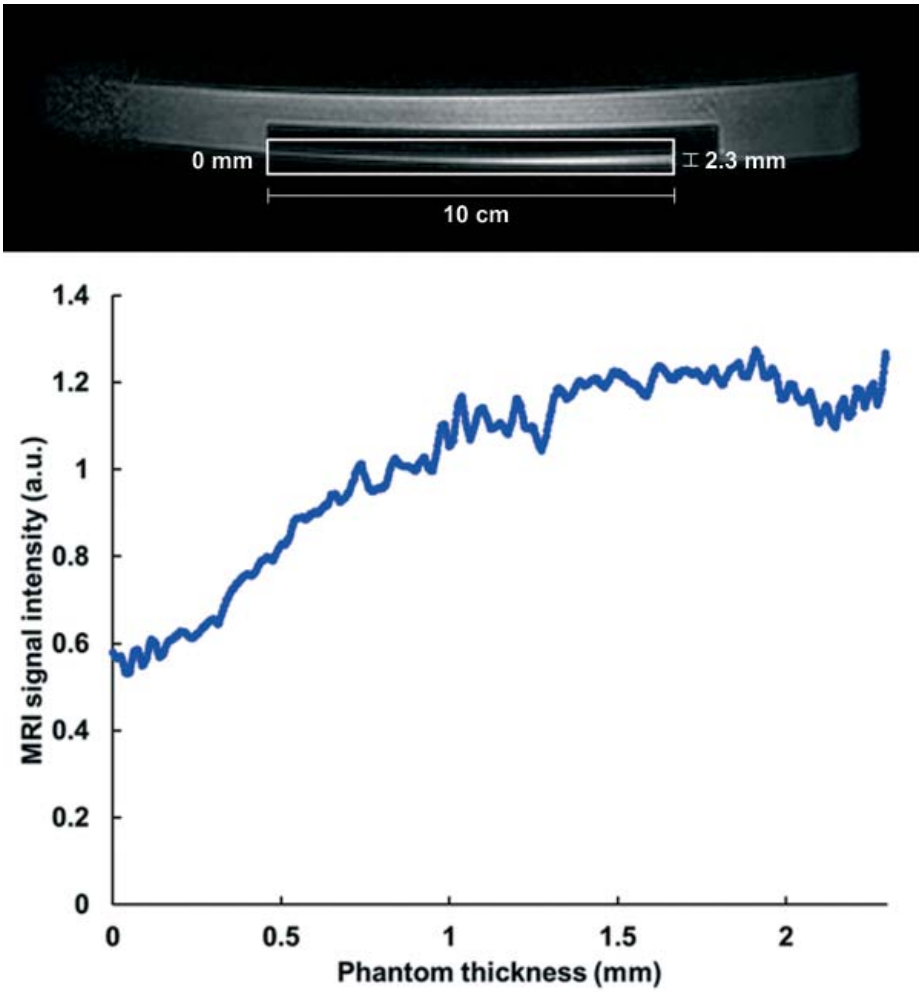

Figure 5.6. Imaging of a wedge phantom to illustrate that signal intensity produced by partial volume effects is related to the thickness of the object.
Bottom, curve of the magnetic resonance imaging signal intensity of the wedge phantom ranging in size from 0 to 2.3 mm, corrected for the inhomogeneity of the image intensity. Top, the image obtained when the polymethyl methacrylate wedge phantom (length, 10 cm) was scanned in a box with water. The water has a hyperintense signal, whereas the polymethyl methacrylate has no signal. The white box indicates the wedge on which the signal intensity measurements were performed (results of this analysis are shown in the bottom). The thickness range of the wedge is indicated. The image of the phantom is curved due to imperfect B0 shimming.

Tesla MRI with an in-plane resolution of 0.48 x 0.58 mm.[10] Spatial variations in thickness of the wall were observed, as in our study. Thickness of the wall was measured on MRI, and a mean thickness of 0.46 mm (SD, 0.05 mm) was found for the dome portion of the aneurysms. However, the method used in that study was noted to have several limitations,[11] which included

a 3-mm slice thickness that results in large partial volume effects with seeming thickness variations when the orientation of the wall changes with respect to the orientation of the long anisotropic voxels. In addition, histological verification of the MRI measurements was lacking. In our study, we refrained from measuring wall thickness on in vivo MRIs because of partial volume effects; instead, we focused on finding an alternative method. We showed that instead of measuring actual thickness, it is possible to infer thickness variations, and we validated our findings with both a wedge phantom and an ex vivo study. Furthermore, because we used isotropic voxels instead of a high in-plane resolution, the orientation of the vessel wall with respect to the image plane has only a limited influence on the signal intensity. To perform actual thickness measurements of the aneurysm wall on MRI, at least 2 full voxels without partial volume effects should represent the wall.[15] This would, for example, require an effective isotropic resolution of 0.1 mm for imaging an aneurysm wall thicker than 0.2 mm. Even with advanced imaging on 7.0 Tesla MRI, this is not feasible in vivo. Neither is this expected to be feasible on machines with stronger magnets in the near future.

Imaging with 3-dimensional T1-weighted magnetization-prepared inversion-recovery turbo-spin-echo sequence on 7.0 Tesla MRI visualized the aneurysm wall in >80% of the aneurysms and showed variation in signal intensity, reflecting variation in aneurysm wall thickness. Using a wedge phantom, we demonstrated the principle that thickness variation in a sheet/structure with subvoxel thickness can be inferred from variation in signal intensity when the signal intensities of surrounding tissues are suppressed. In aneurysms, this principle would only hold when the lumen of the aneurysm contains at least two voxels (to ensure that partial volume effects of opposite walls occur in different voxels), which would mean that aneurysms should have a diameter >3 mm. In theory, the principle that thickness variation can be inferred from variation in signal intensity would fail when the variation in composition of the wall influences the variation in intensity on MRI. The histopathological examination of the ex vivo biopsies showed a variable composition throughout the wall. However, the results of the correlation analysis of the 2 biopsies strongly suggests that, even in the presence of a variable wall composition, signal intensity reflects thickness variation for the sequence that was used in this study. This might be explained by the low contrast that is obtained with the slightly T1-weighted sequence used to image the aneurysm wall (e.g., gray and white matter have approximately the same intensity). The description of the histopathology of the different parts of the wall of the 2 biopsies included in our ex vivo validation experiment resembles the descriptions of each of the four histological wall types previously described in saccular aneurysms,[16] which are likely to reflect consecutive stages of wall degeneration proceeding to rupture. This suggests that these 2 biopsies are representative of aneurysms with wall compositions in any of the 4 consecutive stages proceeding to rupture and therefore our method should be applicable to a large range of aneurysms with different histological wall types.

Further studies should take into account some limitations of the imaging technique. First, pulsation of the aneurysm during the heart cycle in the in vivo situation can lead to blurring and signal loss of the wall, which would affect the apparent thickness. Therefore, the pulsation of the aneurysm should be assessed in a separate scan to exclude this as a confounding factor. Second, the signal of the aneurysm wall is equal to that of brain tissue; therefore, the parts of the wall aligning the brain cannot be taken into account in the assessment of thickness variation as a risk factor for rupture. It is unclear how this will influence the future analyses because it was only suggested that ruptured aneurysms are more often in contact with surrounding anatomical structures than unruptured aneurysms.[17] Third, intraluminal thrombus has approximately the same signal intensity as the aneurysm wall, and its presence may confound the assessment of the thickness variations in the wall. However, an intraluminal thrombus can easily be identified on the time-of-flight sequence because it exhibits a lower signal than the hyperintense aneurysm lumen and the surrounding brain tissue. The information obtained with a time-of-flight sequence should therefore be taken into account in analyses of the aneurysm wall with MRI. Fourth, we used fat saturation on the T1-weighted 3-dimensional magnetization-prepared inversion-recovery turbo-spin-echo sequence to decrease the influence of water-fat-shift on the images. When fat saturation is used, the signal intensity of the wall might decrease when fat is present, which would therefore influence the thickness variation measurement. However, the accumulation of lipids is thought to be limited and to occur mainly in macrophages that have infiltrated in the wall.[18] These macrophages have a scattered distribution throughout the wall, and lipids are not accumulated in a lipid core underlying the fibrous cap of a vulnerable plaque, as is known to be the case in an extracranial atherosclerotic lesion. Therefore, we do not think that the use of fat suppression significantly influenced our results. However, future studies should elucidate the role of fat deposition in the aneurysm wall and its influence on imaging of the wall. Finally, the clinical availability of 7.0 Tesla MRI is limited.

Unruptured aneurysms have a prevalence of 3% and are increasingly discovered by screening or as an incidental finding on imaging studies performed to diagnose or exclude a variety of cranial diseases.[2] Consequently, neurologists and neurosurgeons are frequently confronted with patients seeking advice about whether or not to undergo preventive treatment of their aneurysm. The answer to this question is currently based on risk factors with a limited predictive value.[1] Therefore, the need for new risk factors for rupture is great. Our study offers a new tool to study aneurysm wall thickness variation, which might be a possible risk factor for rupture, although it is still unclear whether a thin, a thick, or an irregular wall thickness is associated with rupture. The next step is to develop a standardized method in which aneurysm wall thickness variations can be quantified. Thereafter, follow up studies assessing variation in wall thickness as a risk factor for rupture can be started in patients.

REFERENCES

1. Wermer MJ, van der Schaaf IC, Algra A, Rinkel GJ. Risk of rupture of unruptured intracranial aneurysms in relation to patient and aneurysm characteristics: an updated meta-analysis. *Stroke*. 2007;38:1404-1410.
2. Vlak MH, Algra A, Brandenburg R, Rinkel GJ. Prevalence of unruptured intracranial aneurysms, with emphasis on sex, age, comorbidity, country, and time period: a systematic review and meta-analysis. *Lancet Neurol*. 2011;10:626-636.
3. Wiebers DO, Whisnant JP, Huston J,3rd, et al. Unruptured intracranial aneurysms: natural history, clinical outcome, and risks of surgical and endovascular treatment. *Lancet*. 2003;362:103-110.
4. Forget TR,Jr, Benitez R, Veznedaroglu E, et al. A review of size and location of ruptured intracranial aneurysms. *Neurosurgery*. 2001;49:1322-1325.
5. Inagawa T. Size of ruptured intracranial saccular aneurysms in patients in Izumo City, Japan. *World Neurosurg*. 2010;73:84-92.
6. Suzuki J, Ohara H. Clinicopathological study of cerebral aneurysms. Origin, rupture, repair, and growth. *J Neurosurg*. 1978;48:505-514.
7. Inagawa T, Hirano A. Autopsy study of unruptured incidental intracranial aneurysms. *Surg Neurol*. 1990;34:361-365.
8. Kadasi LM, Dent WC, Malek AM. Cerebral aneurysm wall thickness analysis using intraoperative microscopy: effect of size and gender on thin translucent regions. *J Neurointerv Surg*. 2013;5:201-206.
9. Swartz RH, Bhuta SS, Farb RI, et al. Intracranial arterial wall imaging using high-resolution 3-tesla contrast-enhanced MRI. *Neurology*. 2009;72:627-634.
10. Park JK, Lee CS, Sim KB, Huh JS, Park JC. Imaging of the walls of saccular cerebral aneurysms with double inversion recovery black-blood sequence. *J Magn Reson Imaging*. 2009;30:1179-1183.
11. Steinman DA, Antiga L, Wasserman BA. Overestimation of cerebral aneurysm wall thickness by black blood MRI? *J Magn Reson Imaging*. 2010;31:766.
12. van der Kolk AG, Hendrikse J, Brundel M, et al. Multi-sequence whole-brain intracranial vessel wall imaging at 7.0 tesla. *Eur Radiol*. 2013;23:2996-3004.
13. Korteweg MA, Zwanenburg JJ, Hoogduin JM, et al. Dissected sentinel lymph nodes of breast cancer patients: characterization with high-spatial-resolution 7-T MR imaging. *Radiology*. 2011;261:127-135.
14. Ritter F, Boskamp T, Homeyer A, et al. Medical image analysis. *IEEE Pulse*. 2011;2:60-70.
15. Shannon C. Communication in the Presence of Noise. *Proceedings of the Institute of Radio Engineers*. 1949;37:10-21.
16. Frosen J, Piippo A, Paetau A, et al. Remodeling of saccular cerebral artery aneurysm wall is associated with rupture: histological analysis of 24 unruptured and 42 ruptured cases. *Stroke*. 2004;35:2287-2293.
17. San Millan Ruiz D, Yilmaz H, Dehdashti AR, Alimenti A, de Tribolet N, Rufenacht DA. The perianeurysmal environment: influence on saccular aneurysm shape and rupture. *AJNR Am J Neuroradiol*. 2006;27:504-512.
18. Frosen J, Tulamo R, Paetau A, et al. Saccular intracranial aneurysm: pathology and mechanisms. *Acta Neuropathol*. 2012;123:773-786.

6

THINNER REGIONS OF INTRACRANIAL ANEURYSM WALL CORRELATE WITH REGIONS OF HIGHER WALL SHEAR STRESS: A 7.0 TESLA MAGNETIC RESONANCE IMAGING STUDY

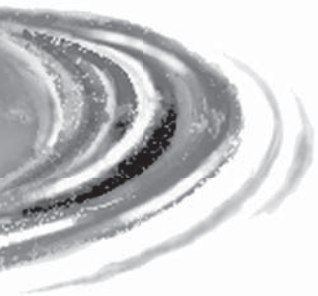

R. Blankena, R. Kleinloog, B.H. Verweij, P. van Ooij, B. ten Haken, P.R. Luijten, F. Visser, P.R. Luijten, G.J.E. Rinkel, J.J.M. Zwanenburg

American Journal of Neuroradiology. 2016;37:1310-1317

ABSTRACT

Background and purpose: Both hemodynamics and aneurysm wall thickness are important parameters in aneurysm pathophysiology. Our aim was to develop a method for semi-quantitative wall thickness assessment on in vivo 7.0 Tesla magnetic resonance images (MRI) of intracranial aneurysms for studying the relation between apparent aneurysm wall thickness and wall shear stress.

Methods: Wall thickness was analyzed in 11 unruptured aneurysms in 9 patients who underwent 7.0 Tesla MRI with a turbo spin-echo-based vessel wall sequence (0.8-mm isotropic resolution). A custom analysis program determined the in vivo aneurysm wall intensities, which were normalized to signal of nearby brain tissue and were used as measures of apparent wall thickness. Spatial wall thickness variation was determined as the interquartile range in apparent wall thickness (the middle 50% of the apparent wall thickness range). Wall shear stress was determined using phase-contrast MRI (0.5-mm isotropic resolution). We performed visual and statistical comparisons (Pearson correlation) to study the relation between wall thickness and wall shear stress.

Results: 3-dimensional colored apparent wall thickness maps of the aneurysms showed spatial apparent wall thickness variation, which ranged from 0.07 to 0.53, with a mean variation of 0.22 (a variation of 1.0 roughly means a wall thickness variation of one voxel [0.8 mm]). In all aneurysms, apparent wall thickness was inversely related to wall shear stress (mean correlation coefficient -0.35; $P<0.05$).

Conclusions: A method was developed to measure the wall thickness semi-quantitatively, using 7.0 Tesla MRI. An inverse correlation between wall shear stress and apparent wall thickness was determined. In future studies, this noninvasive method can be used to assess spatial wall thickness variation in relation to pathophysiologic processes such as aneurysm growth and rupture.

INTRODUCTION

Intracranial aneurysms may rupture; this rupture leads to subarachnoid hemorrhage (SAH). The case fatality of aneurysmal SAH has decreased during the past decades but is still around 30–40%, and almost half of the survivors remain permanently disabled.[1] The prevalence of intracranial aneurysms is approximately 3%.[2] Several risk and trigger factors for rupture have been identified,[3,4] but these factors explain only a small proportion of the risk of rupture and are insufficient to explain the pathophysiology of rupture.[5] Thus, we need more risk factors to better predict rupture, and we need to increase knowledge of pathophysiology to better understand rupture.[6] Hemodynamics play an important role in aneurysm pathophysiology because the endothelial cells are sensitive to mechanical stimuli such as stretch and wall shear stress (WSS, the frictional force on the wall caused by the blood flow).[7] Time-resolved 3D phase-contrast MRI (PCMR) can measure in vivo flow and WSS in aneurysms,[8] and a recent study showed that the use of 7.0 Tesla MRI increases the signal-to-noise ratio and improves flow visualization and quantification.[9] Aneurysm wall thickness is another interesting parameter in the pathophysiology of rupture because the wall eventually ruptures. In a previous study, we showed that it is possible to assess the spatial variation in aneurysm wall thickness by using signal intensities of the aneurysm wall on 7.0 Tesla MRI.[10] A phantom and histopathological correlation study validated that there is a linear relation between wall thickness and image intensity.[10] This development has the potential to enable noninvasive assessments of the relation between different pathophysiologic parameters and wall thickness. However, a method to quantitatively assess the wall thickness on in vivo images has not yet been developed. Therefore, we aimed to develop an algorithm to obtain semi-quantitative measurements of the wall thickness to assess the spatial variation of the apparent wall thickness within an aneurysm, and to assess the correlation between wall thickness and WSS on 7.0 Tesla MRI in patients with intracranial aneurysms.

METHODS

Patient selection

From a series of patients (18, with 20 aneurysms in total) with unruptured intracranial aneurysms from a previous study,[10] we selected the patients who underwent both a magnetization-prepared inversion-recovery turbo spin-echo (MPIR-TSE) scan for vessel wall imaging and a time-resolved PCMR scan for WSS assessment. Patients with artifacts in the PCMR due to gradient coil hardware problems were excluded as well as patients with motion artifacts on the MPIR-TSE scan. Patients in whom an insufficient amount of aneurysm wall was free from directly bordering brain tissue (<10%, based on subjective

estimation) could not be analyzed and were excluded (in total, 4 aneurysms were excluded for this reason). We performed exclusion blinded to the WSS results.

Imaging sequences

MRI was performed on a 7.0 Tesla MRI scanner (Achieva; Philips Healthcare, Best, the Netherlands) with a 32-channel receive head coil and a volume-transmit coil (Nova Medical, Wilmington, Massachusetts). A previously described[10] T1-weighted 3-dimensional MPIR-TSE sequence with whole-brain coverage was used to image the aneurysm wall.[11] Briefly, the scan parameters were as follows: acquired resolution 0.8 × 0.8 × 0.8 mm^3; field of view, 250 × 250 × 190 mm^3 (feet to head × anterior to posterior × right to left); scan duration, approximately 11 minutes. A time-resolved 3-dimensional PCMR sequence was used to determine WSS. Briefly, we used the following scan parameters[9]: acquired resolution, 0.5 × 0.5 × 0.5 mm^3; field of view, 190 × 190 x 20 mm^3 (anterior to posterior × right to left x feet to head); velocity-encoding limit, 150 cm/s for each velocity-encoding direction. Five (n=1) or six (n=10) cardiac phases were obtained, retrospectively gated, by using a peripheral pulse unit. Acquired temporal resolution ranged between 209 and 286 ms, depending on the heart rate. The scan duration was approximately 13 minutes.

Image processing

Wall thickness from intensity: theory

For walls thinner than the voxel size, the intensity on the MPIR-TSE images is proportional to the vessel wall thickness.[10] Under idealized circumstances, the observed intensity in MPIR-TSE images could be used to compute the absolute wall thickness, *w*, using a simple linear relationship:

$$w = d^{*} S_w / S_0, \qquad \text{[Eq. 6.1]}$$

where S_w is the signal for a voxel with isotropic voxel size *d*, containing the vessel wall with surrounding blood and cerebrospinal fluid (CSF). S_0 is the signal of a voxel completely filled with vessel wall. To render signal intensity a true reflection of the wall thickness (relative to the voxel size), one should have the following (long) list of requirements for a voxel with a piece of vessel wall inside: first, the partial volume effect should occur only among the vessel wall, blood, and CSF, and the signal from blood and CSF should be perfectly suppressed (Figure 6.1A). Second, the signal intensity of a voxel that is fully filled with vessel wall (S_0) should be known. Third, there should be no variation of vessel wall signal across the wall due to, for example, heterogeneous tissue composition in combination with the contrast-weighting of the MPIR-TSE sequence. Fourth, the vessel wall should be parallel with one of the sides of the voxel because oblique walls will lead to a higher filling factor than just

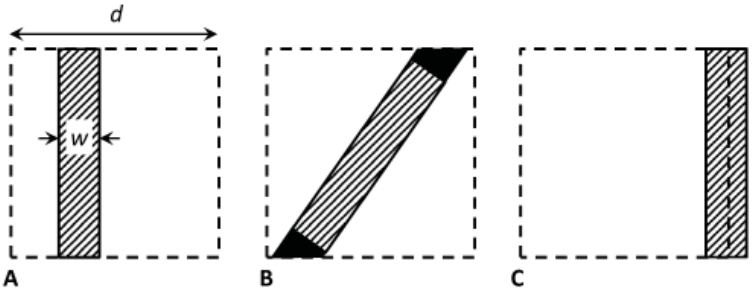

Figure 6.1.
A, Illustration of a voxel (dashed square, size d) partly filled with aneurysm wall (filled rectangle) with thickness w. In case of perfect suppression of the surrounding CSF and blood, the signal from the voxel is directly proportional to the wall thickness w, as given by Eq. 6.1.
B, If the vessel wall is oblique, the filling factor is higher, leading to a different proportionality constant between the wall thickness and the signal obtained from the voxel (extra signal is indicated by black areas).
C, If the voxel boundary falls within the vessel wall, the partial volume effect is spread over 2 voxels, leading to apparently thinner walls (less signal compared with A).

the proportion of the wall thickness to the voxel size (Figure 6.1B). Fifth, the partial volume effect of the thin vessel wall should not be divided over 2 voxels; thus, there may be no boundary of 2 voxels within the vessel wall, parallel to the vessel wall (Figure 6.1C). Last, the nominal acquired resolution of the MPIR-TSE images (0.8 mm) should be equal to the true physical resolution, without blurring due to motion or an imperfect point spread function.

Apparent wall thickness estimation algorithm

Because the above-mentioned requirements will not be met, in practice, an algorithm was developed to obtain an estimation of the ratio S_w/S_0 from the signal intensities in the vessel wall (MPIR-TSE) images, and this ratio was termed 'apparent wall thickness' (AWT). With the limitations of the requirements in mind, one might think of the AWT as a fractional thickness of the vessel wall relative to the voxel size. As a surrogate for the unknown intensity of a voxel completely filled with vessel wall, S_0, the intensity of the adjacent brain tissue, was used. Brain tissue was chosen because the vessel wall has T1 similar to that of brain tissue at 7.0 Tesla[12] and because the MPIR-TSE yields only limited T1-weighted contrast (almost no contrast between gray and white matter, Figure 6.2). A schematic overview of the analysis method, including the correlation with WSS measurements, is shown in Figure 6.2.

First, to be able to relate measurements and segmentations of either images, the MPIR-TSE images were registered to the PCMR magnitude (PC/Mag) images using a standard rigid body registration in MeVisLab (MeVis Medical Solutions, Bremen, Germany). The registration was performed on the entire image, which lead, in a minority of cases, to slightly suboptimal

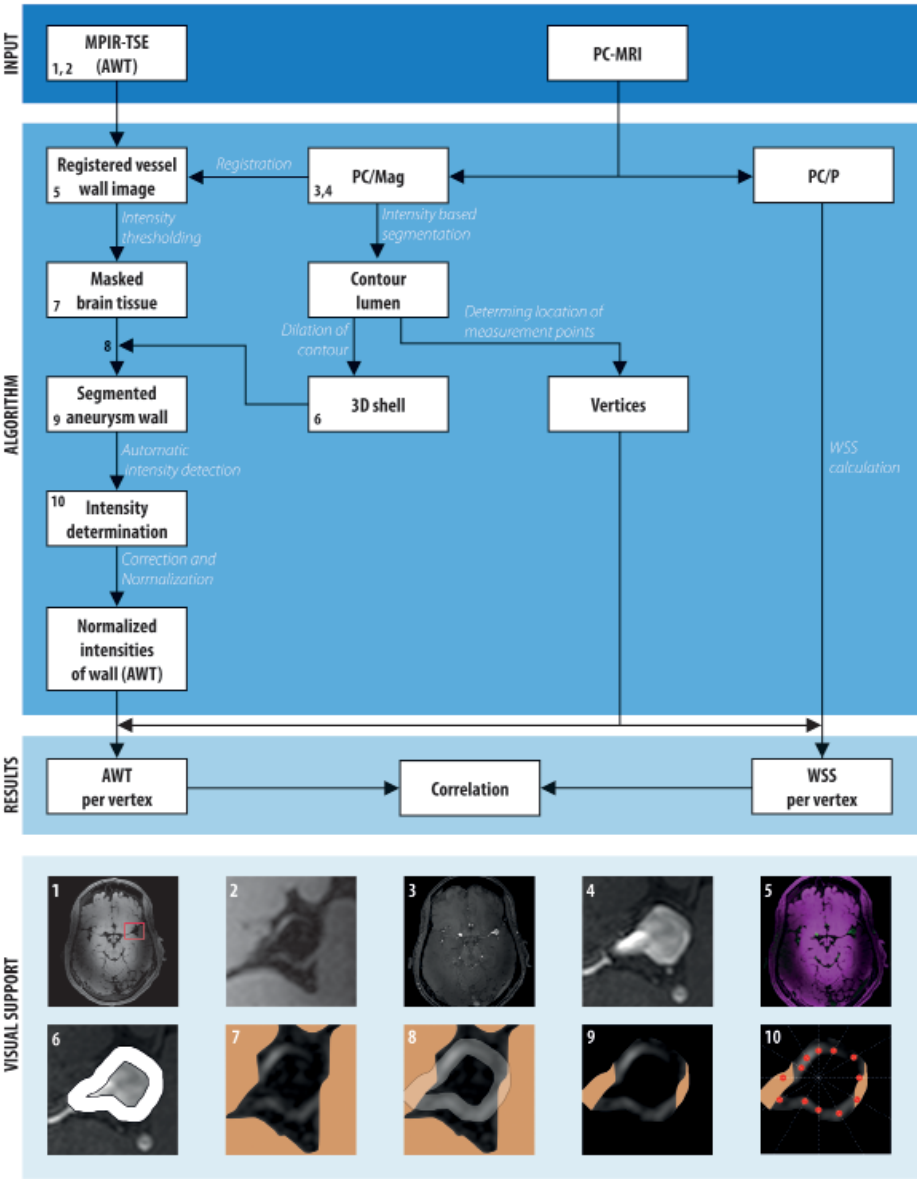

Figure 6.2. Schematic overview of the algorithm to determine the apparent wall thickness and its correlation to wall shear stress in intracranial aneurysms on 7.0 Tesla MRI.
Blocks represent in- and outputs, and arrows represent procedures within the algorithm. The numbers in the boxes refer to the visualizations of several steps at the bottom of the image: 1) MPIR-TSE image (transverse orientation); the red box indicates the area of brain tissue that is used for the correction (by fitting a second-order polynomial function to the brain tissue intensities) and normalization of the vessel wall intensities; 2) cropped MPIR-TSE image clearly showing the aneurysm wall and its varying intensity; 3) the PC/mag image used for segmentation of the aneurysm lumen; 4) cropped PC/mag

registration at the location of the aneurysm. Therefore, when automatic registration was not optimal, small manual adjustments were made. After registration, no deviations between the lumen derived from the PC/mag and the lumen of the MPIR-TSE images were observed. Second, the aneurysm lumen/wall boundary was obtained by segmentation of the PC/Mag by using a level set evolution algorithm.[13] To obtain the segmentation of the aneurysm wall on MPIR-TSE images, we dilated the contour of the segmented lumen to generate a 3-dimensional shell (region of interest) that encompassed the aneurysm wall (Figure 6.2, image panel 6). This step and the remaining postprocessing steps of the analysis method were performed in a custom built Matlab program (Mathworks, Natick, Massachusetts).

Next, the intensities of the wall within the 3-dimensional shell were automatically sampled by using radial-intensity profiles crossing the aneurysm wall in the MPIR-TSE images. Maximum intensities along the profiles within the 3-dimensional shell (i.e., where the profile crossed the aneurysm wall) were saved. The profiles were rotated with a step of 1° through all 2-dimensional sections containing the aneurysm, in transversal, sagittal, and coronal planes. Because the aneurysm wall has nearly the same intensity as brain tissue, the wall was indistinguishable from the brain tissue in areas where the aneurysm bordered the brain tissue. Therefore, a brain tissue mask based on an intensity threshold and connected components was used to avoid intensity measurements in the bordering brain tissue. Intensities of parent vessels were manually deleted, as well as intensities that were evidently located outside the wall (errors). Finally, the AWT was computed by normalizing to the local brain tissue intensity. Care was taken to use only local brain tissue to also correct for intensity inhomogeneity, which is typically present on the 7.0 Tesla MR images (see Figure 6.2, image panel 1). The inhomogeneity in local brain tissue intensity was corrected for by fitting the intensities to a second-order polynomial function, by using brain signal from a manually drawn box around the aneurysm. The brain signal was selected by removing CSF and blood signal (based on their low intensities) and the aneurysmal wall (based on the segmented 3-dimensional shell described above). The resulting fitted brain tissue intensity field was used to normalize the aneurysm wall intensities. The normalized aneurysm wall intensities were used as AWT.

image; 5) registered images: pink is MPIR-TSE; green, PC/mag; 6) 3-dimensional shell encompassing the aneurysm wall; 7) brain tissue mask; 8) overlay of 3-dimensional shell on the MPIR-TSE image with tissue mask; 9) segmented aneurysm wall; and 10) radial intensity profiles to sample vessel wall intensities (i.e. signal maxima within the 3-dimensional shell, indicated by red dots). The profiles were rotated by stepping with 1°; here only a few profiles are shown. The images are taken from aneurysm 1 (Table 6.1). PC/P indicates phase-contrast MRI phase images.

Wall shear stress calculation

Wall shear stress was determined as previously described.[14] After smoothing of the lumen/wall boundary segmentation mentioned above, a spline was fitted through the velocity values derived from PCMR phase images perpendicular to the wall. A blood viscosity of $4.0\ 10^{-3}$ $Pa \cdot s$, which is commonly used in similar algorithms,[15-17] was used in this algorithm and the wall shear stress during peak systole was used for correlation with the AWT measurements. Peak systole was defined as the cardiac timeframe with the highest average velocity in the aneurysm segmentation.

Comparison of apparent wall thickness and wall shear stress

To obtain common measurement locations for both the AWT and WSS, we divided the aneurysm lumen contour into different faces (individual surfaces) and vertices (corners of faces) by using the isosurface function in Matlab. The amount of vertices was determined by the algorithm used in the isosurface function of Matlab and depended on the size of the aneurysm. At each vertex point, the WSS was computed from the 3-dimensional velocity data, and the corresponding AWT was obtained by averaging the AWT samples that were closest to the vertex. Because the amount of vertices was much higher (approximately 10 times) than the amount of voxels on the aneurysm lumen contour, the AWT and WSS values at each vertex cannot be regarded as independent or unique measurements. Accordingly, the resolution of the AWT map (or WSS map) is determined by the resolution of the underlying MPIR-TSE images (or PCMR images), and not by the density of the vertices. Visual comparisons were made for all aneurysms, to illustrate the results of the statistical analysis. The 3-dimensional lumen contours of each aneurysm were presented, colored by an interpolated color map representing the WSS and AWT.

Statistical analyses

Spatial variation in AWT was defined as the interquartile range of the AWT within an aneurysm (i.e., the number specifies the range that contains the middle 50% of the AWT). A higher range reflects more variation in wall thickness across the aneurysm. The interquartile range was chosen to avoid the effect of outliers on the AWT variation assessment. A visual estimation of the coverage and the amount of data points were reported to give an impression of the area of the aneurysm wall that was covered by the analysis. Because the potential relation between WSS and AWT is not necessarily linear, Spearman correlation coefficients were computed to compare AWT and WSS in the aneurysms. The correlation coefficients between AWT and WSS were calculated for each individual aneurysm, after which a 1-sampled *t* test was used to test whether the mean correlation coefficient was significantly different from zero, with significance set as $P<0.05$. The correlation coefficients were weighted by the amount of measured points, to decrease the influence of aneurysms

with fewer data points. We decided to not pool all the data to calculate the overall correlation coefficient, since the amount of points was different per aneurysm. If the data were pooled, the observed correlation between WSS and AWT could be dominated by the data of the largest aneurysm. The significance of each individual correlation coefficient was not determined because the artificially high number of data points (from the high number of vertices on the lumen contour) would yield unrealistically low *P* values.

The correlation between AWT and WSS was further visualized with histograms for each aneurysm. To reduce the amount of data in these histograms, the WSS was divided into quartiles, with an equal amount of data points per quartile.

RESULTS

Population

Eighteen patients (with 20 aneurysms in total) underwent both MPIR-TSE scans and PCMR. Four patients were excluded on the basis of PCMR artifacts due to a gradient hardware problem; 1 patient due to motion artifacts on MPIR-TSE; and 4 due to an insufficient proportion of visible wall. Thus, 9 patients with in total 11 aneurysms were available for analysis. Their mean age was 59 years, and 44% were women. Baseline characteristics are shown in Table 6.1.

Apparent wall thickness and wall shear stress

Color maps of the AWT showed spatial variation in almost all aneurysms (Figure 6.3), which ranged from 0.07 to 0.53, with a mean variation of 0.22 (Table 6.1). A variation of 1.0 roughly means a thickness variation of 1 voxel. A correlation between AWT and WSS was visible in most aneurysms (Figure 6.3), particularly where the coverage and the spatial variation was high (Table 6.1). In all aneurysms, AWT and WSS were inversely correlated (though sometimes close to zero, see Table 6.1). The mean correlation coefficient was -0.35, which was significantly different from zero ($P<0.05$).

The inverse relation between AWT and WSS is also visible in the individual and pooled plots, as shown in Figure 6.4. In the lowest WSS quartile, there was more variety in AWT between different aneurysms than in the highest WSS quartile. In other words, low WSS at thinner walls was present, but high WSS at thicker walls was rarely observed (Figure 6.4, panel B).

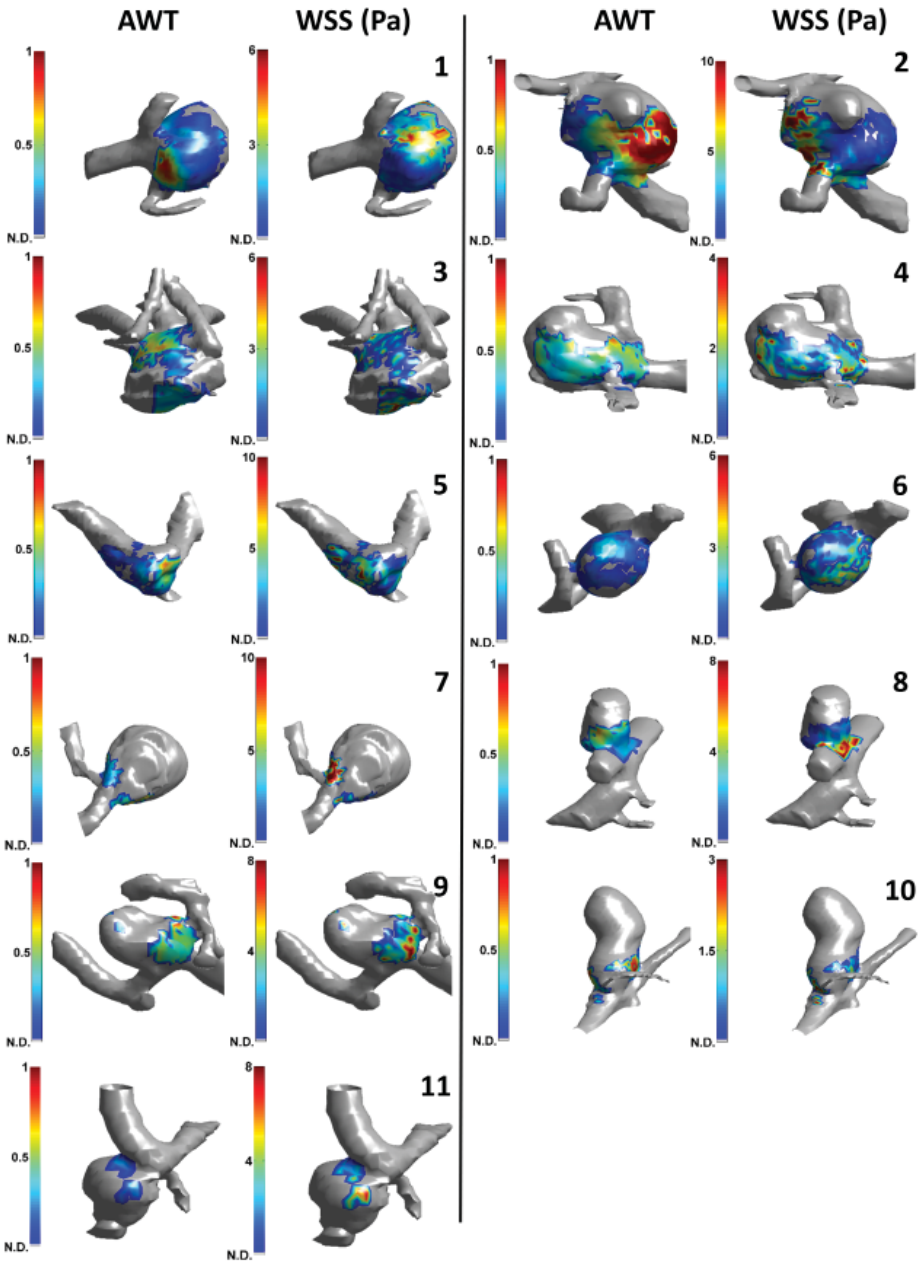

Figure 6.3. Visual comparison between apparent wall thickness and wall shear stress in intracranial aneurysms on 7.0 Tesla MRI.
A, 3-dimensional color map with AWT (left images) and 3-dimensional color map with WSS (right images) are shown. The color scaling for all AWT images is equal, while the WSS images were individually scaled as indicated by the color scale bars. Parent vessels and wall areas where no AWT data (N.D.) were available are displayed in gray. Numbers correspond to the numbering of the aneurysms in Table 6.1.

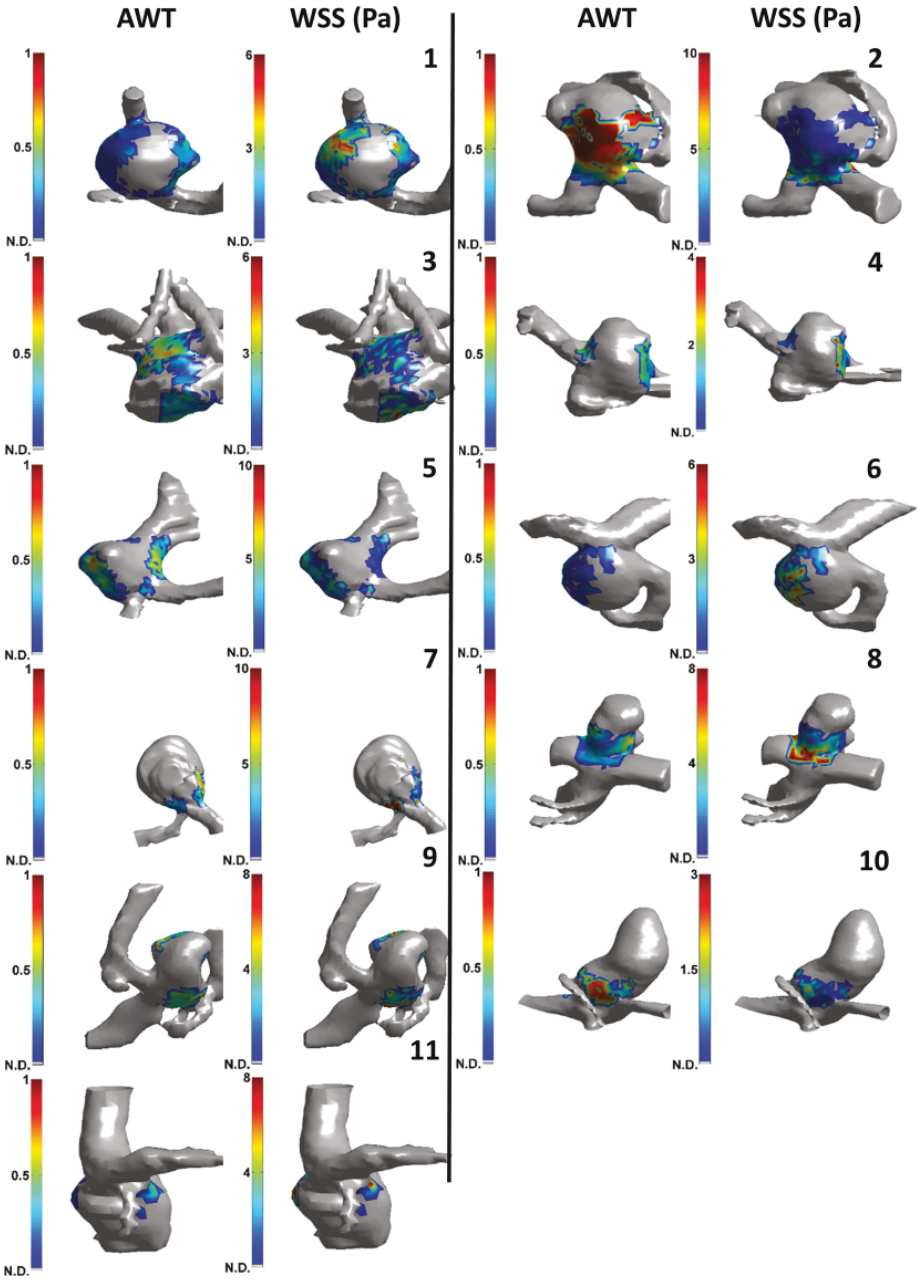

Figure 6.3. *Continued.*
B, The other side of the aneurysms shown in Figure 6.3A.

Table 6.1. Baseline characteristics and AWT results of 11 unruptured intracranial aneurysms

Aneurysm	Age, sex	Aneurysm size in mm, largest diameter (height x width in mm)	Location aneurysm	Analyzed points	Coverage[b]	AWT Heterogeneity[c]	Correlation (ρ)
1	50, M[a]	9.1 (5.9 x 6.3)	MCA	864	50–75%	0.17	-0.4
2	55, M	9.6 (6.1 x 9.6)	MCA	769	50–75%	0.53	-0.6
3	70, M	9.5 (7.8 x 7.8)	ACOM	714	25–50%	0.22	-0.1
4	64, M	10.1 (8.8 x 7.7)	MCA	466	25–50%	0.15	-0.3
5	60, F[a]	6.8 (6.0 x 4.7)	MCA	428	50–75%	0.21	-0.5
6	55, F	7.4 (6.0 x 5.8)	MCA	406	50–75%	0.11	-0.2
7	56, M	12.6 (10.1 x 9.4)	ACOM	298	<25%	0.31	-0.5
8	50, M[a]	6.4 (4.8 x 3.9)	ICA	166	25–50%	0.21	-0.5
9	74, F	6.1 (6.1 x 5.7)	ACOM	163	25–50%	0.13	-0.1
10	50, F	12.9 (12.9 x 6.3)	MCA	130	<25%	0.31	-0.3
11	60, F[a]	5.6 (4.5 x 3.9)	Pericallosal	33	<25%	0.07	-0.4

MCA indicates middle cerebral artery; ACOM, anterior communicating artery; ICA, internal carotid artery.
[a] Two aneurysms in one patient.
[b] Coverage indicates the visual estimated percentage of the area of the wall that could be analyzed.
[c] Heterogeneity is defined as the interquartile range in AWT, and reflects the spatial wall thickness variation.

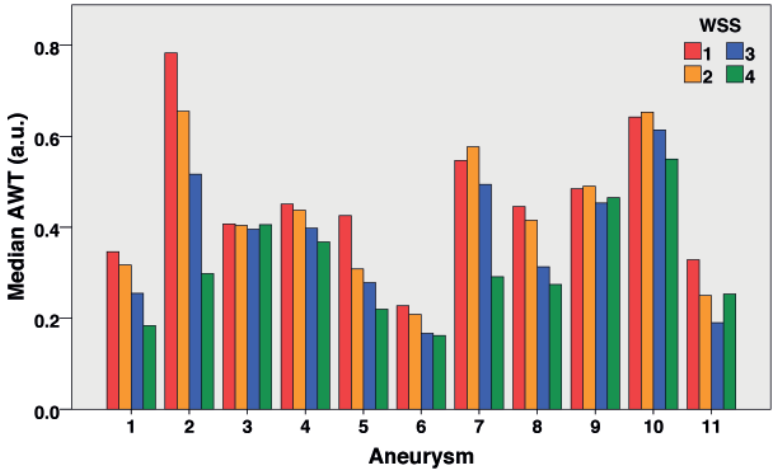

A

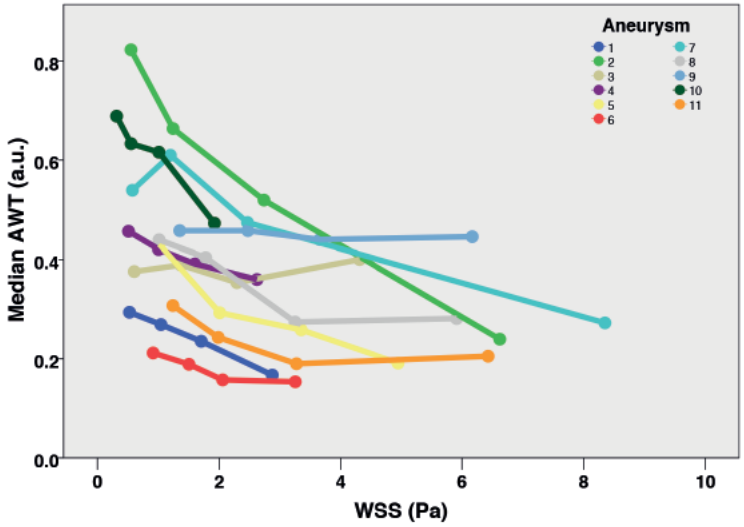

B

Figure 6.4. Comparison of apparent wall thickness and wall shear stress in intracranial aneurysms on 7.0 Tesla MRI.
A, Histogram for each aneurysm is sorted from the aneurysm with the highest amount of measurements points (n=864) to the aneurysm with the least measurement points (n=33). The 4 colors represent the WSS, divided into 4 quartiles per aneurysm with increasing WSS (1= lowest WSS quartile, 4 = highest WSS quartile).
B, AWT is plotted against WSS in all aneurysms (different colors). The dots represent the 4 WSS quartiles.

DISCUSSION

On the basis of previous work, a semi-automatic algorithm was developed to measure apparent aneurysm wall thickness from the signal intensity of the wall on 7.0 Tesla MR vessel wall images of patients with unruptured intracranial aneurysms. Semi-quantitative measurements of the wall thickness were obtained, which showed wall thickness variation in all analyzed aneurysms. Furthermore, by calculating WSS from PCMR data, we found an inverse relation between apparent wall thickness and WSS.

Our results are in contrast with the results of a previous study, which found a positive correlation between wall thickness and WSS.[18] The relation between WSS and wall thickness is probably complex and may differ between large, thick-walled aneurysms and small, thin-walled ones.[6] Kadasi et al.[18] studied predominantly smaller aneurysms because 12 of 54 aneurysms (22%) were >7 mm, and we studied relatively large aneurysms (7 of 11 (63%) were >7 mm), which might partly explain the different observations. However, the different observations can also be related to methodological differences. Kadasi et al. used intraoperative images for a dichotomous visual scoring of wall thickness, while we semi-quantitatively assessed wall thickness on noninvasive MR images. Furthermore, although they did not validate thickness measurements with ex vivo histopathological assessment, they visually assessed actual wall appearance. On the other hand, while we did validate our thickness assessments with an ex vivo study on 2 samples with heterogeneous composition,[10] we did so in the absence of flowing blood or fluid. WSS was, in our study, measured by 3-dimensional PCMR, while the previous study used computational fluid dynamics simulations, which depend on certain assumptions and boundary conditions such as rigid vessel walls and inflow velocity at the entrance of the simulated vessel segment. However, general WSS patterns should be similar for either method (computational fluid dynamics or PCMR).[14] A clear advantage of our method is the avoidance of invasive methods (such as aneurysm surgery) to obtain information on wall thickness. An elaborate study using both approaches on small and large aneurysms with ex vivo (postsurgery) validation is warranted to determine the impact of the differences in methodology.

The observed inverse correlation in the present study is consistent with the hypothesis that high WSS is associated with the process of intracranial aneurysm wall remodeling that might cause wall thinning, such as activation of proteases by mural cells, matrix degradation and apoptosis.[6] Furthermore, low WSS is associated with increased inflammatory cell infiltration and smooth muscle cell proliferation,[6,7] which may lead to wall thickening.

The WSS computations require sufficiently high velocity-to-noise ratios. We used a higher velocity-encoding (150 cm/s) than the velocity-encoding of 100 cm/s that was used by van Ooij et al.,[14] who showed good qualitative agreement between WSS measured with

PCMR and computational fluid dynamics simulations. However, the study of van Ooij et al. was performed at 3.0 Tesla, whereas we performed PCMR at 7.0 Tesla MRI, which yields a higher signal-to-noise ratio (SNR) and, therefore, improved accuracy of the velocity vector direction and magnitude.[9] Thus, we are confident that the low WSS values are of at least comparable reliability with those presented before.[14] The lumen segmentations were performed on the PC/mag images, in which the SNR depends on the blood velocity (inflow effect). The segmentations appear to be robust because no mismatches were observed with the lumens obtained from the MPIR-TSE images. Besides, comparisons of velocity direction and magnitude obtained from PCMR at 3.0 Tesla and the segmentation algorithm showed good agreement with computational fluid dynamics in regions of both high and low SNR and velocity-to-noise ratio in intracranial aneurysms.[19]

This study has several strengths. First, it uses a noninvasive method to quantify wall thickness, which provides a unique means for in vivo quantification of wall thickness variation in unruptured aneurysms. Second, the method is based on the relation between aneurysm wall thickness and image intensity, which has been validated by a phantom and histopathological correlation study.[10] Finally, the analyzed methods for WSS and wall thickness have shown to be useful in aneurysms of various sizes, providing that an appropriate SNR of the MR images is obtained and that the walls are surrounded by CSF.

Some limitations should be mentioned. First, the relation between the aneurysm wall parts bordering brain tissue and WSS could not be analyzed because measurement of thickness in these parts is not possible. Therefore, the association between thickness of wall bordering the parenchyma and WSS remains unknown. Unfortunately, this frequently concerned the apex of the aneurysm, which is especially of interest because it is known to be the predominant site of rupture. Second, the observed correlation coefficients were relatively weak, which may partly be due to noise. The influence of noise is suggested by the fact that aneurysms with larger variation in wall thickness, and thus a larger dynamic range in the AWT parameter, tended to show a stronger correlation than aneurysms with a more narrow range in AWT. Last, despite the AWT, in theory, being directly related to the absolute vessel wall thickness, it depends on too many requirements that are not met in practice to claim that we have found a tool to measure absolute wall thickness. The most important requirement is the nulling of CSF and blood. The found inverse correlation may be partly caused by imperfect nulling of blood with very low flow velocities. The MPIR-TSE is used to obtain black blood, which is based on the high flow sensitivity of the long turbo spin-echo train with low refocusing angles. However, very slow blood flow may still yield some signal. If that is the case, the wall seems thicker at locations with low velocities and thus low WSS. This feature leads to overestimation of the negative correlation. We previously validated the correlation between signal intensity and wall thickness with an ex vivo imaging experiment on an aneurysm wall of heterogeneous composition and histopathological validation, and

with a tapering phantom study, in which flow could not affect the wall thickness.[10] However, although these validation experiments show that thickness variation can explain the observed signal variation, they cannot exclude a potential additional confounding role of slow-flowing blood in the in vivo situation. The long turbo spin-echo trains with low reduced refocusing angles are very sensitive to motion, up to diffusion-related motion.[20] The refocusing angles of the MPIR-TSE sequence used in this work were very low, with a range of 12°–40°. Although we think the low refocusing angles will protect against the effect of low-flow velocities, this should be confirmed in future studies by using a dedicated phantom setup with flow or by performing additional validation studies on postoperative material from patients who have been scanned with the MPIR-TSE sequence before an operation.

The conflicting results of our study and a previous study on the relation between aneurysm wall thickness and WSS[18] call for further studies in which both approaches are applied and compared in the same patients. The presented method for in vivo wall thickness determination, in combination with the aneurysm-specific WSS, might provide a valuable means to noninvasively study how wall thickness and hemodynamic parameters are related to aneurysm growth and rupture. This study may yield new insights in the pathophysiology of intracranial aneurysms. Therefore, studies to correlate rupture of aneurysms with WSS and wall thickness may help in the search for new rupture predictors. In particular, the spatial variation in AWT might be an interesting parameter for those future studies. Whether thickness variation indicates higher rupture risks is currently unknown. Nevertheless, it seems plausible that much variation in thickness calls for a pathological wall, prone for rupture.

A method was developed to measure the wall thickness semi-quantitatively, using 7.0 Tesla MRI. An inverse correlation between wall shear stress and AWT was determined. In future studies, this noninvasive method can be used to assess spatial wall thickness variation in relation to pathophysiologic processes such as aneurysm growth and rupture.

REFERENCES

1. Nieuwkamp DJ, Setz LE, Algra A, et al. Changes in case fatality of aneurysmal subarachnoid haemorrhage over time, according Comparison of apparent wall thickness and wall shear stress to age, sex, and region: a meta-analysis. *Lancet Neurol.* 2009;8:635-642.
2. Vlak MH, Algra A, Brandenburg R, et al. Prevalence of unruptured intracranial aneurysms, with emphasis on sex, age, comorbidity, country, and time period: a systematic review and meta-analysis. *Lancet Neurol.* 2011;10:626-636.
3. Greving JP, Wermer MJH, Brown RD, et al. Development of the PHASES score for prediction of risk of rupture of intracranial aneurysms: a pooled analysis of six prospective cohort studies. *Lancet Neurol.* 2013;4422:1-8.
4. Vlak MHM, Rinkel GJE, Greebe P, et al. Trigger factors and their attributable risk for rupture of intracranial aneurysms: a case-crossover study. *Stroke.* 2011;42:1878-1882.

5. Wermer MJH, van der Schaaf IC, Algra A, et al. Risk of rupture of unruptured intracranial aneurysms in relation to patient and aneurysm characteristics: an updated meta-analysis. *Stroke*. 2007;38:1404-1410.
6. Meng H, Tutino V. High WSS or low WSS? Complex interactions of hemodynamics with intracranial aneurysm initiation, growth, and rupture: toward a unifying hypothesis. *AJNR Am J Neuroradiol*. 2014;35:1254-1262.
7. Nixon AM, Gunel M, Sumpio BE. The critical role of hemodynamics in the development of cerebral vascular disease. *J Neurosurg*. 2010;112:1240-1253.
8. Boussel L, Rayz V, Martin A, et al. Phase-contrast magnetic resonance imaging measurements in intracranial aneurysms in vivo of flow patterns, velocity fields, and wall shear stress: comparison with computational fluid dynamics. *Magn Reson Med*. 2009;61:409-417.
9. Van Ooij P, Zwanenburg JJM, Visser F, et al. Quantification and visualization of flow in the Circle of Willis: time-resolved three-dimensional phase contrast MRI at 7 T compared with 3 T. *Magn Reson Med*. 2013;69:868-876.
10. Kleinloog R, Korkmaz E, Zwanenburg JJM, et al. Visualization of the aneurysm wall: a 7.0-tesla magnetic resonance imaging study. *Neurosurgery*. 2014;75:614-622.
11. Van der Kolk AG, Hendrikse J, Brundel M, et al. Multi-sequence whole-brain intracranial vessel wall imaging at 7.0 tesla. *Eur Radiol*. 2013;23:2996-3004.
12. Koning W, Rotte A de, Bluemink J, et al. MRI of the carotid artery at 7 Tesla: Quantitative comparison with 3 Tesla. *J Magn Reson Imaging*. 2015;41:773-780.
13. Li C, Xu C, Gui C, et al. Level set evolution without re-initialization: a new variational formulation. In: Proceedings of the 2005 IEEE Computer Society Conference on Computer Vision and Pattern Recognition, San Diego, California. June 20–26, 2005:430-436.
14. Van Ooij P, Potters W V, Guédon A, et al. Wall shear stress estimated with phase contrast MRI in an in vitro and in vivo intracranial aneurysm. *J Magn Reson Imaging*. 2013;38:876-884.
15. Cebral JR, Castro M a, Appanaboyina S, et al. Efficient pipeline for image-based patient-specific analysis of cerebral aneurysm hemodynamics: technique and sensitivity. *IEEE Trans Med Imaging*. 2005;24:457-467.
16. Mut F, Löhner R, Chien A, et al. Computational hemodynamics framework for the analysis of cerebral aneurysms. *Int J Numer Method Biomed Eng*. 2011;27:822-839.
17. Shojima M, Oshima M, Takagi K, et al. Magnitude and role of wall shear stress on cerebral aneurysm: computational fluid dynamic study of 20 middle cerebral artery aneurysms. *Stroke*. 2004;35:2500-2505.
18. Kadasi LM, Dent WC, Malek AM. Colocalization of thin-walled dome regions with low hemodynamic wall shear stress in unruptured cerebral aneurysms. *J Neurosurg*. 2013;119:172-179.
19. Van Ooij P, Schneiders JJ, Marquering HA, et al. 3D cine phase-contrast MRI at 3T in intracranial aneurysms compared with patient-specific computational fluid dynamics. *Am J Neuroradiol*. 2013;34:1785-1791.
20. Weigel M, Hennig J. Diffusion sensitivity of turbo spin echo sequences. *Magn Reson Med*. 2012;67:1528-1537.

7

QUANTIFICATION OF INTRACRANIAL ANEURYSM VOLUME PULSATION WITH 7.0 TESLA MAGNETIC RESONANCE IMAGING

R. Kleinloog, J.J.M. Zwanenburg, B. Schermers, E. Krikken, Y.M. Ruigrok, P.R. Luijten, F. Visser, L. Regli, G.J.E. Rinkel, B.H. Verweij

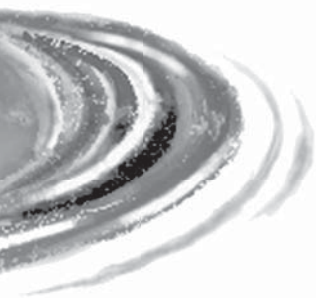

In revision

ABSTRACT

Background and purpose: Aneurysm volume pulsation is a potential predictor of intracranial aneurysm rupture. We evaluated whether 7.0 Tesla magnetic resonance imaging (MRI) can quantify aneurysm volume pulsation.

Methods: In stage I of the study, ten unruptured aneurysms in nine patients were studied using a high resolution (0.6 mm, isotropic) 3-dimensional gradient-echo sequence with cardiac gating. Semi-automatic segmentation was used to measure aneurysm volume (in mm^3) per cardiac phase. Aneurysm pulsation was defined as the relative increase in volume between the phase with the smallest volume and the phase with the largest volume. The accuracy and precision of the measured volume pulsations was addressed by digital phantom simulations, and a repeated image analysis. In stage II, the imaging protocol was optimized and nine patients with nine aneurysms were studied with and without administration of a contrast agent.

Results: The mean aneurysm pulsation in stage I was 8% (standard deviation (SD) 7%, range 2 to 27%), with a mean volume change of 15 mm^3 (SD 14 mm^3, range 3 to 51 mm^3). The mean difference in volume change for the repeated image analysis was 2 mm^3 (SD 6 mm^3). The artifactual volume pulsations measured with the digital phantom simulations were in the same magnitude as the volume pulsations observed in the patient data, even after protocol optimization in stage II.

Conclusion: Volume pulsation quantification with the current imaging protocol on 7.0 Tesla MRI is not accurate due to multiple imaging artifacts. Future studies should always include aneurysm-specific accuracy analysis.

INTRODUCTION

Intracranial aneurysms occur in approximately 3% of the population.[1] Rupture of an aneurysm results in aneurysmal subarachnoid hemorrhage, which often occurs at a young age and has a high case fatality and morbidity.[2] Current standard treatment consists of neurosurgical clipping or endovascular coiling, and can prevent rupture, but carries a 4 to 8% risk of major complications including death, depending on age of the patient, and size and site of the aneurysm.[3,4] Preventive treatment should therefore ideally be restricted to those patients that have a high risk of rupture. However, prediction of the risk of rupture of intracranial aneurysms is poor. Therefore, better predictors of rupture are needed. Volume pulsation, the change in volume during the cardiac cycle, is a potential predictor of rupture.[5] Imaging techniques used thus far in attempts to visualize volume pulsation, such as 1.5 Tesla phase-contrast MR angiography (MRA), transcranial Doppler ultrasound, 3-dimensional rotational angiography, and 4-dimensional computed tomography angiography (CTA), have various limitations, including limited signal-to-noise ratio (SNR), limited spatial resolution compared to the aneurysm volume, and/or the use of a radiation dose and/or the risk of complications.[5] Furthermore, a test of the accuracy and the precision of the volume pulsation measurement was either lacking or studies refrained from giving an error value that can be used to interpret the pulsation results for each aneurysm. Therefore, aneurysm volume pulsation is currently not used as a predictor of rupture in clinical practice. In this experimental study, we evaluated whether volume pulsation could be quantified on images obtained with 7.0 Tesla MRI, and tested accuracy and precision of the method.

METHODS

Our study consisted of two stages. In the first stage, we tested the concept of quantification of aneurysm pulsation on images obtained with 7.0 Tesla MRI, and we tested the accuracy and repeatability of the imaging analysis method. In the second stage, we implemented the lessons learned in stage I to optimize the imaging protocol and accuracy of the quantification of aneurysm pulsation.

Study population

Patients diagnosed with saccular intradural unruptured intracranial aneurysms who were either planned for treatment of their aneurysm or were in follow-up for growth of their aneurysm, were recruited through the outpatient clinic of the department of Neurology and Neurosurgery of the University Medical Center Utrecht, The Netherlands between July and December 2012 as part of an existing study focusing on imaging of the aneurysm wall

(stage I).[6] In stage II, additional patients were recruited for the purpose of the current study between February and April 2014. The diagnosis of the aneurysm was made either on CTA or 1.5 or 3.0 Tesla MRA, and the aneurysms were either incidental findings (imaging study was made for other indications), found during screening because of a positive family history of intracranial aneurysm, or symptomatic aneurysms. Patients with contraindications for 7.0 Tesla MRI (e.g. claustrophobia, metal objects such as dental implants or prostheses in or on the body) were excluded, as well as patients with aneurysms associated with vascular malformations other than aneurysms, e.g. arteriovenous malformations. In the second stage, also patients with renal insufficiency and allergy to gadolinium-based contrast agent were excluded. This study was approved by the Institutional Review Board of the University Medical Center Utrecht, The Netherlands and all participants gave written informed consent following guidelines equivalent to the National Institutes of Health guidelines.

7.0 Tesla MR Imaging

Imaging was performed on a 7.0 Tesla MRI scanner (Philips Healthcare, Cleveland, OH, USA) with a volume transmit coil and a 32 channel receive head-coil (Nova Medical, Wilmington, MA, USA). In the first stage, the volume pulsation of the aneurysm was studied by adding a 3-dimensional Turbo Field Echo sequence (further referred to as TFE) to an existing study focusing on imaging the aneurysm wall.[6] This protocol included a low resolution T1 weighted survey sequence and a time-of-flight (TOF) sequence covering the intracranial vessels from the level of the circle of Willis and upward, taking into account the location of the aneurysm.[6] It also included a previously described time-resolved 3-dimensional phase-contrast MRI (PCMR) sequence.[7] The following parameters were used in the 3-dimensional TFE sequence: TR/TE 8.2/4.4 ms, flip angle 6°, field of view 180 mm x 180 mm x 9.6 mm, an acquired spatial resolution of 0.6 mm x 0.6 mm x 0.6 mm, sensitivity encoding acceleration factor of 2.0 (RL), and an acquired temporal resolution of 90 ms, interpolated to 15 cardiac phases. The sequence was synchronized to the heart with a peripheral pulse unit and retrospective cardiac gating. The scan duration was approximately 4 minutes. The TFE sequence was oriented in either coronal or transverse orientation, and carefully positioned over the aneurysm as observed on a TOF and/or low resolution T1 weighted survey. In both the TOF and the TFE sequence, flow compensated gradients were used to prevent signal drop out from fast flowing blood. With the results of stage I, the imaging protocol was optimized. An optimized version of the TFE sequence was developed and used in the additionally recruited patients in stage II. We increased the field of view, thereby increasing signal to noise ratio and improving coverage; we shortened the TE to 2.0 ms, to decrease the influence of the flow displacement artifact; and we used a 20° flip angle to increase the contrast-to-noise-ratio (CNR) between flowing blood and static tissue. Furthermore, we performed this improved TFE sequence also after administration of Gadobutrol, a gadolinium-based contrast agent, to further increase CNR and decrease the influence of intensity fluctuations due to inflow effects.

Image analysis

Volume pulsation quantification

Image analysis was performed with the use of ANALYZE 11.0 (AnalyzeDirect, Inc., Overland Park, KS, USA), software designed to automatically segment and calculate volumes. For the cardiac phases of each slice (15 phases in the first stage of the study, 18 in the second stage), the same region of interest containing the aneurysm was chosen, using the TOF or T1 weighted survey images if necessary as 3-dimensional reference to correctly separate the aneurysm from the parent artery. Vessel segmentation (including the aneurysm) was performed by setting a signal intensity threshold. The threshold was set for each aneurysm separately, but fixed for all slices and cardiac phases of each aneurysm. Thereafter the remaining parent vessel was manually removed from the selection. Voxels selected outside the aneurysm borders due to background noise were also removed from the selection. Flow artifacts in the lumen of the aneurysm were misrecognized by the software and consequently manually included in the selection, keeping the borders of the aneurysm as selected by the software intact. The manual corrections were done slice by slice. If the signal in the last slice containing the aneurysm was of low intensity due to partial volume effects, the slice was excluded in all phases, to limit the effect of noise on the selection. For each phase of the cardiac cycle, the total volume of the aneurysm was calculated by adding up the aneurysm volumes of all slices (segmented area x slice thickness). Absolute volume pulsation was defined as the change in volume (in mm^3) between the phase of the cardiac cycle with the smallest volume and the phase with the largest volume. Relative volume pulsation was calculated with the following formula: ((maximum volume - minimum volume) / minimum volume) * 100. The size (largest diameter) of the aneurysms was measured on the TOF angiography in the first stage. In the second stage, it was measured on the improved TFE. Partially thrombosed aneurysms were excluded for the image analysis.

Repeatability of the volume pulsation quantification (stage I)

By repeating the volume measurements for the phase with the smallest and the largest volume for each aneurysm, we determined the precision of the pulsation analysis. The repeated analysis was performed by the same observer, but blinded for the initial analysis with a three-month interval between the two analyses. We evaluated the repeatability of the image analysis using the Bland-Altman method: the mean and the standard deviation (SD) of the difference between the results of the initial analysis and the results of the repeated analysis were calculated.[8] A t-distribution with a significance level of 0.05 and 9 degrees of freedom (10 measured aneurysms) was used to approximate the distribution of the 95% confidence interval (CI). Also, the Pearson correlation coefficient between the initial analysis and the repeated analysis was calculated. The repeatability analysis was only performed in stage I of this study.

Accuracy of the volume pulsation quantification (stage I)

The accuracy of the volume pulsation analysis is expected to depend on four different factors: the CNR (between blood and surroundings) of the images, signal intensity fluctuations in the gated TFE sequence due to inflow effects, aneurysm size, and blood flow artifacts.

CNR, signal intensity fluctuations and aneurysm size

In images with low CNR, the difference in intensity between the aneurysm and the background can be small. When using a signal intensity based segmentation method, the aneurysm volumes in these low CNR images could be overestimated. These artifactual volume changes resulting from signal fluctuations and low CNR, are due to a change in the detection of the border, and, thus depend on the size of the aneurysm or object. Some systematic signal fluctuations over the heartbeat that are intrinsic to the acquisition method cannot be excluded, although these fluctuations were minimized by using cardiac gating in the TFE sequence, which means that the signal was maintained in steady state while waiting for the next electrocardiogram-R wave. Such signal fluctuations could be interpreted as a volume change by our segmentation method. First, the dependence of the inaccuracy of the volume pulsation analysis of both CNR and signal fluctuations was studied by static digital phantom simulations. Second, the interaction of aneurysm volume with CNR and signal fluctuations was studied with static digital phantom simulations. Third, to estimate the (aneurysm-specific) inaccuracy in the pulsation analysis of the aneurysms in this study, the CNR and intensity fluctuations were measured for each aneurysm. Next, for each aneurysm a pulsating digital phantom was made, with the same volume, CNR, intensity fluctuation and volume pulsation as measured in the patient data. The volume pulsation measurement in this phantom was compared with the given volume pulsation. The difference between the given and the measured volume pulsation was called the absolute observed artifactual pulsation. See Supplementary material for further details.

Flow displacement artifact

In image acquisition, the timing difference between the moment of phase encoding (right after excitation) and the moment of frequency encoding (approximately at t=TE), will lead to the flow displacement artifact.[9] We assessed the influence of this artifact by combining the TFE images from stage I with images containing blood flow velocity data (obtained with the time-resolved 3-dimensional PCMR sequence, only available in stage I, see Supplementary material for further details).

Imaging protocol optimization (stage II)

Volume pulsation quantification on images obtained with the improved TFE were analyzed with the same analysis tool used in stage I. As in stage I, the accuracy of the volume pulsation analysis method was addressed in pulsating phantoms. For both the improved TFE and the

gadolinium enhanced improved TFE patient data, pulsating phantoms were made to estimate the (aneurysm-specific) inaccuracy in the pulsation. The volume pulsation measurement in the phantom was compared with the given volume pulsation. This difference yielded the absolute observed artifactual pulsation.

RESULTS

Stage I. Volume pulsation quantification, repeatability and accuracy of the analysis

In stage I, we included nine patients with ten unruptured aneurysms. Characteristics of the aneurysms are given in Table 7.1. The size of the aneurysms ranged from 3 to 19 mm with a mean size of 9 mm (SD 4 mm). The mean aneurysm volume change was 15 mm^3 (SD 14 mm^3, range 3 to 51 mm^3), and the mean volume pulsation was 8% (SD 7%, range 2 to 27%). Figure 7.1 shows the 15 images obtained during the cardiac cycle of one cross-section of an aneurysm, and a video of this pulsating aneurysm is provided as Supplementary video. The repeatability analysis yielded a correlation coefficient of 0.95 (Figure 7.2). The mean of the difference between the results of the initial pulsation analysis and the results of the repeated pulsation analysis was 2 mm^3 (SD 6 mm^3, 95% CI -12 to 15, Figure 7.2). The absolute observed pulsation in a static digital phantom (used as measure for the inaccuracy of the analysis) was found to increase quickly below a CNR of approximately 6, and increased with increasing signal intensity fluctuations (see Supplementary material for further details and figures). The mean CNR of aneurysms in the patient study was 5 (range 1 to 8) while the mean intensity fluctuation was 3% (SD 1.6%). Both the effects of CNR and intensity fluctuations were size dependent, with increasing relative inaccuracy with decreasing phantom volumes. The mean absolute observed artifactual pulsation in the pulsating digital phantoms (used as measure for the inaccuracy of the analysis) was 2.0 mm^3 (SD 1.6 mm^3, range 0.2 to 5.4 mm^3). The pulsation observed as a result of the flow displacement artifact was higher than the actual pulsation measured in the six available patient data sets (see Supplementary table S7.3). The mean absolute artifactual pulsation due to the flow displacement artifact was 11 mm^3 (SD 6.3 mm^3, range 5 to 22 mm^3, Table 7.1 and Supplementary table S7.1).

Stage II. Results after imaging protocol optimization

In stage II, we included nine patients with nine aneurysms. Characteristics of the aneurysms are given in Table 7.2. The size of the aneurysms ranged from 2 to 14 mm with a mean size of 8 mm (SD 4 mm). The mean aneurysm volume change on the improved TFE was 38 mm^3 (SD 31 mm^3, range 2 to 88 mm^3), and the mean volume pulsation was 39% (SD 24%,

Table 7.1. Baseline characteristics and pulsation of the ten unruptured intracranial aneurysms in stage I

Aneurysm number	Aneurysm size in mm, largest diameter (heightxwidth)	Age, sex	Location aneurysm	Imaging sequence	Minimum volume (mm^3)	Maximum volume (mm^3)	Relative volume pulsation (%)	Absolute volume pulsation (mm^3)	Absolute observed artifactual pulsation (mm^3)#
1	2.8 (1.8x1.6)	56, F	Pericallosal	TFE	12	15	25	3	1.3
2	5.6 (4.5x3.9)	60, F*	Pericallosal	TFE	70	75	7	5	1.9
3	6.1 (6.1x5.7)	74, F	ACOM	TFE	92	98	7	6	3.1
4	6.8 (6.0x4.7)	60, F*	MCA	TFE	56	64	14	8	0.7
5	8.7 (6.1x7.7)	72, F	PICA	TFE	308	327	6	19	-0.2
6	9.3 (6.6x8.2)	56, F	ACOM	TFE	292	303	4	11	1.1
7	9.6 (6.1x9.6)	55, M	MCA	TFE	285	298	5	13	5.4
8	10.1 (8.8x7.7)	64, M	MCA	TFE	276	298	8	22	-0.4
9	12.9 (12.9x6.3)	50, F	MCA	TFE	312	324	4	12	2.6
10	18.6 (14x15.8)	53, F	Basilar	TFE	2078	2128	2	50	3.5

* Two aneurysms in one patient. MCA indicates middle cerebral artery; ACOM, anterior communicating artery; PICA, posterior inferior cerebellar artery. # The absolute observed artifactual pulsation is the difference between the absolute volume pulsation and the volume pulsation of the aneurysm-specific digital phantom, and is a measure for the inaccuracy of the volume pulsation analysis (see Supplementary material for further details).

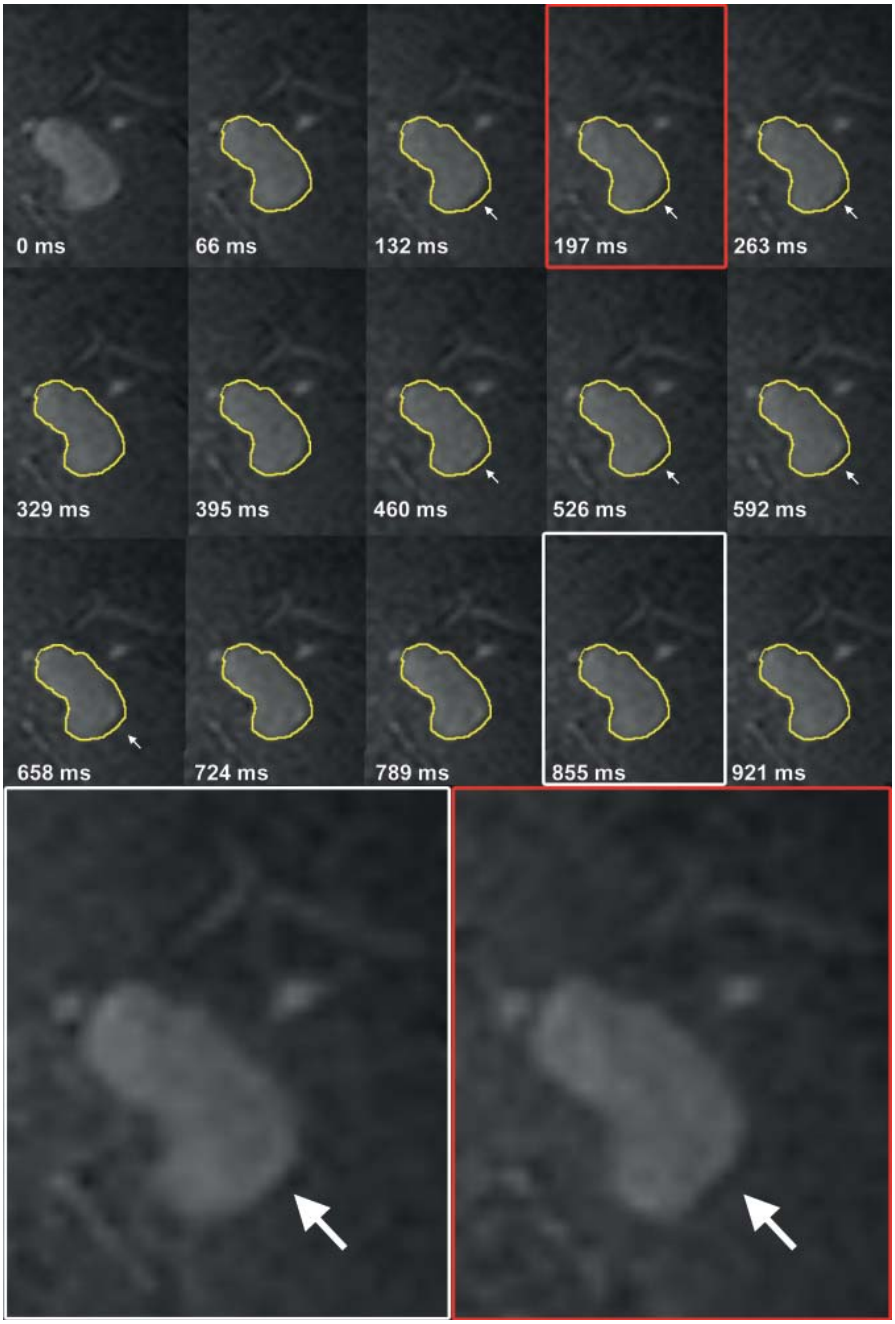

Figure 7.1. Coronal cross-section of a left middle cerebral artery aneurysm for each of the 15 phases of the cardiac cycle (heart rate 60 beats per minute).
The contour of the aneurysm at 0 ms is shown in yellow on all other time points. The white arrows indicate the area of pulsation in this cross-section. Magnification of two phases shows the deformation of the aneurysm at one side of the dome.

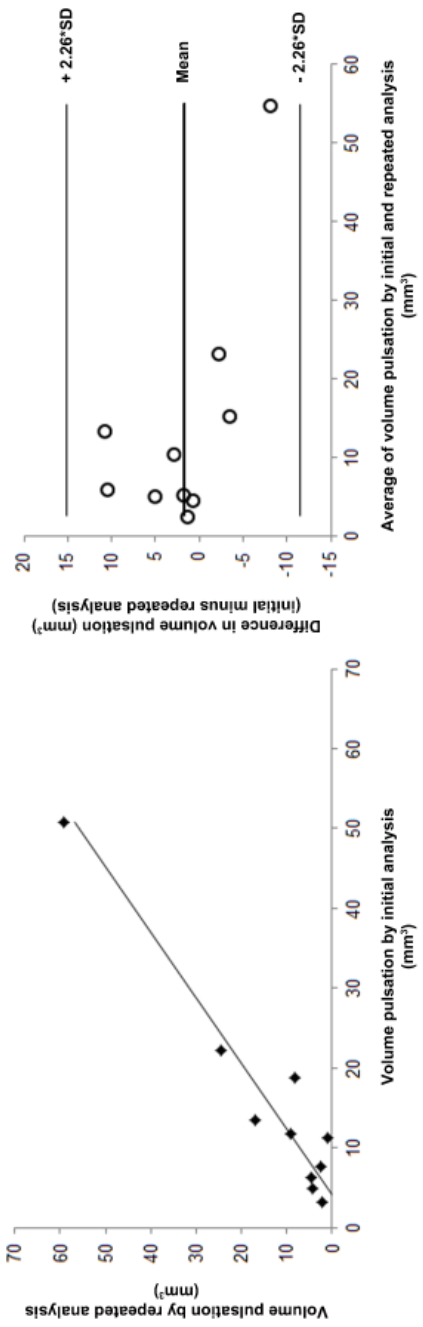

Figure 7.2. Repeatability of the image analysis method.
Left: scatterplot showing the correlation between the measured volume pulsation obtained with the repeated image analysis vs. the results from the initial analysis. Right: Bland-Altman plot of the same data. SD indicates standard deviation.

range 14 to 73%). In one patient, the image acquisition of the contrast enhanced improved TFE failed. The mean aneurysm volume change on the contrast enhanced improved TFE in the remaining eight aneurysms was 14 mm^3 (SD 9 mm^3, range 1 to 25 mm^3), and the mean volume pulsation was 15% (SD 11%, range 4 to 36%). The mean CNR was 23 (SD 7) in the improved TFE and 28 (SD 8) in the gadolinium enhanced improved TFE, while the mean intensity fluctuation was 23% (SD 7%) in the improved TFE and 15% (SD 6%) in the gadolinium enhanced improved TFE. The mean absolute observed artifactual pulsation in the pulsating digital phantoms (used as measure for the inaccuracy of the analysis) was 13 mm^3 (SD 9 mm^3, range 1 to 27 mm^3, Table 7.2 and Supplementary table S7.2).

DISCUSSION

This study shows that quantification of volume pulsation of unruptured intracranial aneurysms is feasible when using a semi-automatic segmentation method on high resolution 7.0 Tesla MR images. However, the accuracy of the quantification of volume pulsation is influenced by the CNR, intensity fluctuations, aneurysm size and most importantly by the flow displacement artifact. Our study shows that the artifactual volume pulsation due to these influences is of the same magnitude as the volume pulsations observed in the patient data, even after optimization of the imaging sequences and adding contrast agent.

Two previous studies quantified pulsation in unruptured aneurysms by the use of a ECG-gated CTA.[10,11] These studies found a volume pulsation in the range of 3 to 18% with a mean of 8% (SD 5%),[10] and in the range of 1 to 15% with a mean of 5% (SD 4%),[11] which compares well with our findings. Accuracy and precision analyses were performed in both CTA studies. The first study found a mean of 8% volume pulsation in aneurysms, which was considered substantial in comparison with a 2% volume change found in bone tissue.[10] In the second study, a large and static phantom (a syringe filled with saline) was imaged to study the artificial volume pulsation, and it was concluded that its volume change of <0.248% was an insignificant artifact.[11] However, in the current study, we showed that inaccuracy increases with decreasing phantom size, and therefore their accuracy analysis might underestimate the artifactual pulsation, because the phantom used was much larger than the aneurysms studied. The second study measured an interobserver discrepancy in the repeated measurement of 5 aneurysms of 11.9 mm^3 (SD 17.6 mm^3) which was considered acceptable, given a mean expansion volume of all aneurysms of 27.87 mm^3 (SD 60.53 mm^3).[11] Both studies refrained from giving an error value that can be used to interpret the pulsation results for each aneurysm. Our study shows that the error is influenced by multiple artifacts and is aneurysm specific, which makes it difficult to compare the accuracy of 7.0 Tesla MRI with the reported CTA accuracies. Furthermore, CTA has its own technique-specific artifacts which should be taken into account when analyzing accuracy of the pulsation measurement.[5]

Table 7.2. Baseline characteristics and pulsation of the nine unruptured intracranial aneurysms in stage II

Aneurysm number	Aneurysm size in mm, largest diameter (heightxwidth)	Age, sex	Location aneurysm	Imaging sequence	Minimum volume (mm^3)	Maximum volume (mm^3)	Relative volume pulsation (%)	Absolute volume pulsation (mm^3)	Absolute observed artifactual pulsation (mm^3)*
11	2.0 (2.0x1.6)	53, F	MCA	TFEi	3	4	73%	2	-
				CE TFEi	2	3	36%	1	2
12	6.2 (5.1x3.3)	58, F	MCA	TFEi	68	90	31%	21	-
				CE TFEi	96	104	8%	8	1
13	5.4 (4.8x4.4)	70, M	ACOM	TFEi	44	75	70%	31	-
				CE TFEi	78	96	23%	18	13
14	5.7 (5.7x3.1)	47, F	MCA	TFEi	62	79	28%	17	-
				CE TFEi	70	78	11%	8	9
15	8.7 (8.1x6.0)	39, M	MCA	TFEi	134	153	14%	19	-
				CE TFEi	NA	NA	NA	NA	NA
16	8.7 (7.9x5.4)	70, M	ACOM	TFEi	91	149	64%	58	-
				CE TFEi	114	138	22%	25	27
17	9.4 (8.7x6.7)	53, M	ACOM	TFEi	188	215	14%	27	-
				CE TFEi	256	265	4%	9	10
18	12.3 (8.1x8.0)	70, M	ACOM	TFEi	206	289	41%	84	-
				CE TFEi	166	191	15%	25	24
19	13.7 (10.9x8.7)	51, M	ACOM	TFEi	419	507	21%	88	-
				CE TFEi	581	603	4%	22	25

MCA indicates middle cerebral artery; ACOM, anterior communicating artery; TFEi, the improved version of the Turbo Field Echo sequence to image pulsation used in stage II; CE, contrast enhanced. * The absolute observed artifactual pulsation is the difference between the absolute volume pulsation and the volume pulsation of the aneurysm-specific digital phantom, and is a measure for the inaccuracy of the volume pulsation analysis (see Supplementary material for further details).

This study has some limitations. First, we used a signal intensity based threshold to segment the aneurysm volume, but also showed that signal intensity fluctuations have a considerable influence on the accuracy of the volume pulsation analysis. Future studies should use an analysis method which is insensitive to signal intensity fluctuations throughout the cardiac cycle. For example, a recently published automatic segmentation method used for quantification and visualization of pulsation from ECG-gated CTA data, uses the local deformation of image structures in all cardiac phases, which may be less dependent on the actual intensity.[10] By using such an automated method, the effects of manual correction are also eliminated, and the precision of the measurement may be increased. Second, our estimate of aneurysm-specific inaccuracy was based on patient-specific measurements of CNRs and intensity fluctuations. Although care was taken to obtain representative values, one should note that both the CNR and intensity fluctuations may be variable along the border of the aneurysm. Also, the CNR measurements were likely influenced by intensity fluctuations. Since there was no separate noise acquisition in the MRI protocol, we used the SD of the region of interest over the cardiac cycles, which may have led to an underestimation of the actual CNR (and, thus, to a slightly worse inaccuracy than actually present). Nonetheless, the accuracy analysis shows that aneurysm-specific inaccuracies should be determined, and that an increase in the signal-to-noise ratio of the images should be achieved to improve the accuracy. Third, our restricted field of view led to incomplete imaging of the largest aneurysm of 19 mm in stage I of the study, and the subsequent pulsation only accounts for the imaged part. We were not able to expand the field of view due to a fixed scan protocol and therefore fixed scantime. In the second stage of this study, we were able to increase the field of view to prevent this lack of coverage. Last, the clinical availability of 7.0 Tesla MRI is still limited but expected to increase in the future.

The strength of this study is the use of an advanced high resolution imaging method to quantify pulsation in aneurysms, combined with a thorough accuracy analysis. All previous studies showed a single value for the inaccuracy, sometimes obtained from a large stable phantom. The phantom simulations in our study give insight in the relative contributions of different sources of measurement errors, and their combined effect in a patient-specific way, which can stimulate future improvement on each of these aspects. An advantage of MRI over CTA is the lack of radiation for MRI. Furthermore, the ultra-high resolution of MRI combined with its ability to discriminate the aneurysm wall from its lumen, provides a unique opportunity to search for new markers of rupture.

In conclusion, quantification of intracranial aneurysm pulsation seemed to be feasible with 7.0 Tesla MRI, but even after optimization of the imaging protocol the artifactual volume pulsations as a result of intensity fluctuations, the limited CNR, aneurysm size, and the flow displacement artifact have the same magnitude as the volume pulsations observed in the patient data. The current imaging protocol on 7.0 Tesla MRI is therefore of limited

use in studying pulsation as a risk factor for rupture. Future studies should always include an aneurysm-specific accuracy analysis.

REFERENCES

1. Vlak MH, Algra A, Brandenburg R, et al. Prevalence of unruptured intracranial aneurysms, with emphasis on sex, age, comorbidity, country, and time period: a systematic review and meta-analysis. *Lancet Neurol.* 2011;10:626-636.
2. Nieuwkamp DJ, Setz LE, Algra A, et al. Changes in case fatality of aneurysmal subarachnoid haemorrhage over time, according to age, sex, and region: a meta-analysis. *Lancet Neurol.* 2009;8:635-642.
3. Brinjikji W, Rabinstein AA, Nasr DM, et al. Better outcomes with treatment by coiling relative to clipping of unruptured intracranial aneurysms in the United States, 2001-2008. *AJNR Am J Neuroradiol.* 2011;32:1071-1075.
4. Naggara ON, Lecler A, Oppenheim C, et al. Endovascular treatment of intracranial unruptured aneurysms: a systematic review of the literature on safety with emphasis on subgroup analyses. *Radiology.* 2012;263:828-835.
5. Vanrossomme AE, Eker OF, Thiran JP, et al. Intracranial Aneurysms: Wall Motion Analysis for Prediction of Rupture. *AJNR Am J Neuroradiol.* 2015;36:1796-1802.
6. Kleinloog R, Korkmaz E, Zwanenburg JJ, et al. Visualization of the aneurysm wall: a 7.0-tesla magnetic resonance imaging study. *Neurosurgery.* 2014;75:614-622.
7. van Ooij P, Zwanenburg JJ, Visser F, et al. Quantification and visualization of flow in the Circle of Willis: time-resolved three-dimensional phase contrast MRI at 7 T compared with 3 T. *Magn Reson Med.* 2013;69:868-876.
8. Bland JM, Altman DG. Applying the right statistics: analyses of measurement studies. *Ultrasound Obstet Gynecol.* 2003;22:85-93.
9. Larson TC, 3rd, Kelly WM, Ehman RL, et al. Spatial misregistration of vascular flow during MR imaging of the CNS: cause and clinical significance. *AJNR Am J Neuroradiol.* 1990;11:1041-1048.
10. Firouzian A, Manniesing R, Metz CT, et al. Quantification of Intracranial Aneurysm Morphodynamics from ECG-gated CT Angiography. *Acad Radiol.* 2013;20:52-58.
11. Kuroda J, Kinoshita M, Tanaka H, et al. Cardiac cycle-related volume change in unruptured cerebral aneurysms: a detailed volume quantification study using 4-dimensional CT angiography. *Stroke.* 2012;43:61-66.

SUPPLEMENTARY MATERIAL

The Supplementary material, including Supplementary tables S7.1 to S7.3, can be found online: http://hdl.handle.net/10411/LLNJ9E.

Supplementary video

Video showing volume pulsation of a middle cerebral artery aneurysm. Coronal cross-section of a left middle cerebral artery aneurysm. Repetitive movie of the 15 phases of the cardiac cycle, showing volume pulsation of this aneurysm. The Supplementary video can be found online: http://hdl.handle.net/10411/LLNJ9E.

8

General discussion

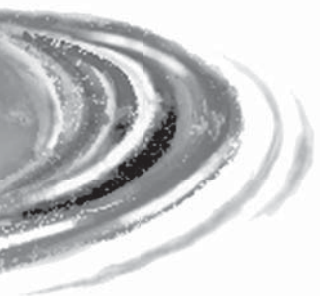

In this chapter, the findings of this thesis are put into perspective, and future directions are presented.

Rupture of an intracranial aneurysm causes aneurysmal subarachnoid haemorrhage (aSAH), a subtype of stroke with a poor prognosis which mainly affects middle-aged women,[1,2] and has high economic burden and a large impact on the patients personal life.[3] The overall one-year risk of rupture of unruptured aneurysms is 1.4%, indicating that the majority of unruptured aneurysms never ruptures nor causes symptoms.[4] The risk of rupture differs between individuals with the lifetime risk of rupture in the general population being the highest for those with a positive family history for aSAH and for persons ≥35 years who smoke(d) and are hypertensive.[5]

Because treatment to prevent rupture, including neurosurgical clipping and endovascular coiling, carries a risk of major complications,[6-8] in the ideal situation we would only treat those aneurysms that are definitely going to rupture in the near future. However, as only few risk factors for rupture are available in clinical practice,[4] our ability to predict the risk of rupture is limited.

There are several approaches to improve rupture prediction and eventually decrease the incidence of aSAH. First, identifying more risk factors for rupture enables better selection of patients with high risk of rupture for preventive treatment. Second, more knowledge on the pathogenesis of rupture enables identification of markers reflecting steps in the process of rupture, and these markers can then be used in risk prediction. Furthermore, with this knowledge on rupture pathogenesis new noninvasive treatment strategies that prevent aneurysm development or rupture could be developed, and added to invasive treatment options. Last, more knowledge on the factors involved in development of aneurysms enables screening for aneurysms in individuals with high risk of development of aneurysms. This may increase the detection rate of aneurysms in the general population and will give an opportunity to perform treatment of these newly identified unruptured aneurysms, to prevent rupture.

Risk factors for rupture of intracranial aneurysms

In current clinical practice, the decision whether or not to preventively treat an unruptured aneurysm is discussed in a multidisciplinary meeting in which both patient- and aneurysm-specific factors are considered.[9,10] These factors are summarised in prediction models such as the so called PHASES score.[4] This score was constructed by performing a pooled analysis of individual data from six prospective cohort studies on risk of rupture of unruptured aneurysms. The score includes six risk factors for rupture: population (with higher risk in

Japanese and Finnish populations); the presence of hypertension; age ≥70 years; aneurysms ≥7 mm; earlier aSAH from another aneurysm; and site of the aneurysm (with higher risk for middle cerebral artery location and even higher risk for anterior and posterior cerebral artery location). Treatment of the aneurysm is advised to those patients in which the risk of rupture based on the PHASES score is higher than the risk of the procedure (either neurosurgical clipping or endovascular coiling). The full score (≥12) accounts for a predicted 5-year risk of rupture of 17.8% (95% confidence interval of 15.2 to 20.7%). This shows that rupture risk prediction is poor, with more than 80% of the rupture risk still unexplained. In **chapter 2** of this thesis, 144 additional risk factors for rupture were identified in a systematic review of the literature, but only one risk factors was found to be suitable for use in clinical practice additional to the PHASES score: the morphological risk factor irregular shape. Therefore, when using the PHASES score[4] to predict the rupture risk of an unruptured aneurysm, the physician should take into account that the calculated risk is probably higher for aneurysms with an irregular shape, and lower for those with a regular shape, but the extent by which the absolute risks change through the morphology is unknown. The evidence for other morphological risk factors, including aspect ratio, size ratio, bottleneck factor, height-to-width ratio, contact with the perianeurysmal environment, large volume-to-ostium ratio, and dome direction was based on ≤1 prospective study, and therefore the value of these factors should first be confirmed in multivariate analysis and incorporated in prediction models. These multivariate models should also include the already established risk factors included in the PHASES score,[4] enabling determination of the additional value of new risk factors.

Only one genetic risk factor with potential for further study was identified in **chapter 2**, the 27 VNTR and G894T single nucleotide polymorphisms of the endothelial nitric oxide synthase (*eNOS*) gene, a gene which is involved in smooth muscle cell proliferation, platelet aggregation and white blood cell adhesion in the vessel wall via the molecule nitric oxide.[11] No other genetic or molecular factors with strong or moderate evidence, or potential for further study were found. This is probably the result of the design of the studies included in the review, which were hypothesis driven, while a hypothesis free approach (which was used in the genome-wide association study (GWAS) on intracranial aneurysms)[12-14] is more suitable for a complex disease such as intracranial aneurysms. However, the GWAS on intracranial aneurysms did not include enough patients to analyse ruptured versus unruptured aneurysms, indicating that a larger GWAS is necessary to find genetic variants associated with rupture. Another explanation for the lack of evidence for genetic risk factors for rupture found in **chapter 2** may be the exclusion of studies investigating risk factors in aneurysm wall biopsies. Although the study of these biopsies has brought us more insight in the pathogenesis of aneurysm rupture,[15-19] risk factors which can only be measured after the aneurysm is preventively clipped, cannot be used in risk prediction. Recent studies suggest that imaging techniques to obtain information on the aspect of the wall and processes

occurring in the wall, without taking biopsies of the tissue, might become available soon.[20-24] **Chapter 2** shows that studies on the association of hemodynamic factors with rupture are conflicting and that there is a lack of high quality studies, with consequently limited level of evidence for the identified risk factors. However, wall shear stress (WSS) is thought to be an important determinant of endothelial cell function (e.g. proliferation and apoptosis) and its gene expression.[25] When the normal hemodynamic stress on the wall changes, remodelling of the aneurysm wall can occur, which might lead to critical thinning of the wall and eventually rupture. This can occur either via high WSS, which promotes increased release of nitric oxide in the wall, leading to extensive remodelling by internal elastic lamina fragmentation and cell loss,[26] or via low WSS, promoting atherothrombosis and inflammation of the wall.[27] Computational Fluid Dynamics (CFD) is currently the preferred method to measure flow and WSS and calculate the different hemodynamic factors. It has high resolution, and is based on images obtained with digital subtraction angiography (DSA) or computed tomography angiography (CTA), which are widely available imaging techniques. However, the method requires a few assumptions, including rigid vessel walls and pulsatile flow conditions obtained from healthy individuals, which might not correctly reflect the actual situation in an individual patient. Furthermore, the computations are complex and time-consuming, making them only suitable to be performed in specialised centres. This might explain the lack of large high quality studies on hemodynamic risk factors for rupture. Alternatively, flow and WSS can be measured with 3-dimensional phase-contrast magnetic resonance imaging (MRI). Clinical availability of ultra-high resolution MRI might accelerate advances in this field, e.g. by improving imaging of hemodynamic factors with 3-dimensional phase-contrast MRI with the same resolution as CFD.[28,29]

If future studies identify new risk factors of rupture, their independence from the currently available risk factors should be studied before these new risk factors have potential to be used in clinical practice. In the ideal situation, a prospective cohort study including a large sample of patients with unruptured aneurysm followed until rupture occurs should be conducted. However, this is unethical, because guidelines advise treatment in aneurysms with a high risk of rupture.[9,10] The best alternative would be to follow patients with unruptured aneurysms that are not selected for preventive treatment either because the risk of rupture of their aneurysm is low, the risk of treatment is high due to co-morbidities, or because they reject the option of preventive treatment, until growth of their aneurysm occurs. Although the process of growth of an aneurysm is different to the process of rupture, growth is associated with rupture,[30] and the risk factors for each of these processes show overlap.[31] Therefore, growth can be seen as a surrogate marker of rupture.

IDENTIFICATION OF GENES AND PATHWAYS INVOLVED IN DEVELOPMENT AND RUPTURE OF INTRACRANIAL ANEURYSMS

Better understanding of the genes and pathways involved in development and rupture of aneurysms can lead to better risk prediction, and to identification of new treatment strategies. In the GWAS on intracranial aneurysms six genetic risk loci associated with intracranial aneurysms were identified.[12-14] We do not know whether these risk loci are associated with development of aneurysms, aneurysm rupture or both. In a sub-analysis of one of the GWAS on intracranial aneurysms,[32] no association was found between the genetic risk loci and rupture status, probably because of the low number of patients with unruptured aneurysms included (18% of the patients). A meta-analysis of the results of the GWAS on intracranial aneurysms,[12-14] and more recent results,[33,34] including an analysis of ruptured versus unruptured aneurysms, is ongoing, and might identify genetic risk alleles associated with rupture. In **chapter 3** of this thesis, no association between the six genetic risk loci identified in the GWAS and size of the aneurysm was found. Since the six risk loci only explain a small amount of the genetic risk of aneurysms, this result does not exclude that there is an association of genetic factors with size or rupture of aneurysms. A new and larger GWAS in which genetic variation is analysed in ruptured and unruptured aneurysms and aneurysms of different sizes as surrogate marker for rupture, might identify new genetic risk factors for rupture of aneurysms.

In **chapter 4** of this thesis, gene expression in aneurysms versus controls and in ruptured versus unruptured aneurysms was compared to increase knowledge on the genes involved in the pathogenesis of development and rupture of aneurysms. Extracellular matrix (ECM) pathways were found in the analysis of aneurysms versus controls, indicating that these pathways play a role in aneurysm development. It is thought that changes in the ECM, including intimal hyperplasia and degeneration of the internal elastic lamina, lead to development of an aneurysm.[35] These changes are probably the result of a combination of genetic predisposition, hemodynamic stress on the wall, and aging of the wall. How these factors interact, and which of the factors initiates the process is still unclear. Identification of the expression of both light and heavy chain immunoglobulin genes in aneurysm tissue and its complete absence in control tissue, suggests the involvement of the humoral immune response in development of aneurysms. A recent animal study showed that lymphocyte-deficient mice had significantly fewer aneurysm formation than wild-type mice,[36] which further supports the role of the humoral immune response in aneurysm development. Whether the humoral immune response is the primary cause of inflammation in the aneurysm wall is yet unclear.

The lysosome pathway was identified as a new pathway involved in rupture of aneurysms in **chapter 4**. Disturbance of the normal activity of lysosomes in the aneurysm wall might lead

to remodelling of intercellular substances (such as collagen, elastin and proteoglycans),[37] and consequently to rupture.

Inflammation is thought to play an important role in the process of rupture.[38,39] In **chapter 4**, immune response pathways were found to be differentially expressed between ruptured and unruptured aneurysms. Ultimately, one would like to develop treatment strategies to prevent aneurysm development and rupture. Anti-inflammatory drugs could therefore be an interesting target for therapy. Recent studies suggest that acetylsalicylic acid, an inexpensive and easy accessible anti-inflammatory drug, may decrease the overall rate of aneurysm rupture.[40,41] A prospective, randomised open label trial is soon to be started to assess whether acetylsalicylic acid in combination with intensive blood pressure treatment compared to standard care, decreases the risk of growth and rupture of aneurysms.[42]

The results of our gene expression study enhance knowledge on pathogenesis of intracranial aneurysms, but cannot yet be used in clinical practice for rupture risk prediction, nor to select individuals at high risk of development of aneurysms for screening. One of the reasons is that the gene expression was studied in aneurysm wall tissue, which cannot be used for risk prediction in clinical practice before (neurosurgical) treatment is performed. There is some evidence that disruption of the ECM is present not only in aneurysms, but also in skin and unaffected intra- and extracranial arteries.[43,44] This may imply that aneurysms are not a localised disease, but rather represent a more general disease of the ECM. If presence of aneurysms is a generalised disease of ECM, we might be able to find potential markers of development or rupture of aneurysms in other tissues than the aneurysm wall. Therefore, a future study should investigate whether the genes that were found differentially expressed between aneurysms and controls, and ruptured and unruptured aneurysms, are also differentially expressed in other, more accessible locations, such as the peripheral blood or the skin. If we can prove that aneurysms is a generalised disease of the ECM, we might be able to use patients' skin or blood to test for biomarkers of development and rupture of aneurysms in the future. Furthermore, in our gene expression study, we analysed aneurysm biopsies (containing different cell types) as a whole, and we therefore do not know in which cell type the genes we found are differentially expressed. Also, gene expression coming from a single cell type will be diluted by the presence of other cell types and therefore relevant gene expression can be missed when analysing a tissue as a whole. Studying gene expression in specific cell types isolated from the aneurysm biopsies, such as smooth muscle cells, endothelial cells and several types of inflammatory cells, can also give more insight in the mechanisms of development and rupture of aneurysms.

7.0 TESLA MAGNETIC RESONANCE IMAGING OF INTRACRANIAL ANEURYSMS

MRI is a widely used technique to image the brain and its vascular structures. It is a noninvasive technique, especially because off its lack of radiation dose, which is able to image tissue in great detail and with high contrast. Furthermore, it is capable of giving information on both the lumen, wall, and surrounding of the aneurysm, all in one session. Currently, most centres have either 1.5 Tesla MRI or 3.0 Tesla MRI available for diagnostic purposes. For small lesions such as aneurysms, these field strengths are sufficient for detection of the aneurysm, and for measurement of crude parameters, such as the size of the aneurysm. If, however, more details are required, for example on the aspect of the wall of the aneurysm,[45,46] 1.5 and 3.0 Tesla MRI have insufficient resolution. An increasing number of research centres worldwide have access to ultra-high resolution 7.0 Tesla MRI scanners. These scanners have the advantage of giving higher signal-to-noise-ratio and contrast-to-noise-ratio, without prolonging scan time. This means that we are able to image aneurysm characteristics in greater detail,[47,48] and to image characteristics which we were not able to image before. Now that it is possible to image patients with aneurysms on 7.0 Tesla MRI for research purposes, we can start investigating the purpose of this improved imaging technique for clinical practice.

In this thesis, I experimented with 7.0 Tesla MR imaging of the aneurysm wall (**chapter 5**), flow and WSS in aneurysms (**chapter 6**), and pulsatility of the aneurysm (**chapter 7**). Actual rupture of an aneurysm is thought to occur when stress on some part of the wall exceeds the strength of the tissue.[49] Strength decreases when the aneurysmal wall elongates and becomes thinner.[50] Simulated aneurysm models show that the deformation and stress on the wall are inversely correlated to wall thickness, in other words, increased stress and deformation correlates with thinner wall.[51] Simulation of spatial variations in thickness of the wall demonstrated that a local thinning of the aneurysm wall led to a local bulge-out (bleb) and a local stress concentration.[51] In **chapter 2**, irregular shape (including blebs) was found to be associated with rupture. These findings suggest that thin portions of the wall are prone to rupture. **Chapter 5** showed that imaging of the aneurysm wall is possible with 7.0 Tesla MRI, and that MRI signal intensity variation reflects actual wall thickness variation. Subsequently, in **chapter 6**, a semi-automatic segmentation method was developed to quantify wall thickness variation of the complete aneurysm, with exception of the parts of the wall aligning the brain, because the signal of the wall is equal to that of brain tissue and, therefore, the signal intensity of parts of the wall aligning the brain cannot be measured. To be able to compare wall thickness between different patients, the intensity of the brain surrounding the aneurysm was used as a reference for calculating the wall thickness variation from the MRI signal, hereby assuming that the signal from the brain is stable between patients. This method now enables the study of the association between wall thickness and rupture in vivo. A large prospective study in which aneurysm wall thickness variation on 7.0

Tesla MRI is studied as a risk factor for rupture (with growth of the aneurysm as surrogate marker of rupture) should be designed to confirm this association.

In **chapter 4**, it was confirmed that inflammation of the aneurysm wall is a likely determinant of rupture. Previous studies have suggested that wall enhancement is associated with instability (including large aneurysm size) and rupture of the aneurysm wall,[52-54] or can identify the site of rupture.[24,54] In light of these results, the proposed prospective study on wall thickness variation and its association with rupture on 7.0 Tesla MRI can be combined with a study on the association of enhancement of the aneurysm wall (as surrogate marker for wall inflammation) with rupture, for example by performing an extra MRI sequence after administration of a contrast agent. When performing this study, one should keep in mind that we do not know whether wall enhancement after administration of a contrast agent is truly reflecting wall inflammation. Therefore, in the ideal situation, imaging findings should be correlated with findings of histopathological examination of the wall. This is however very challenging, since tissue of the aneurysm wall can only be obtained during neurosurgical clipping and only a small part of the wall can be obtained, which makes it very difficult to study the walls histopathological structure at the exact location of the enhancement on MRI. A study combining high resolution imaging and post-mortem histological examination of the wall in an aneurysm animal model, might find further evidence for the assumption that wall enhancement correlates with wall inflammation.

The tool to quantify wall thickness variation of the aneurysm developed in **chapter 6**, also enables the study of the association between wall thickness and other characteristics, such as WSS, which might give more insight in the pathogenesis of aneurysms. In **chapter 6**, an inverse association between wall thickness variation and WSS was found. This finding is consistent with the hypothesis that high WSS leads to wall remodelling (including activation of proteases, ECM degradation and apoptosis) which might lead to wall thinning; and low WSS is associated with increased inflammation and smooth muscle cell proliferation, which might lead to wall thickening.[55] However, the amount of aneurysms studied in **chapter 6** was small, and the results are in contrast to the findings of a previous study,[56] indicating the need for further study of the association between wall thickness and WSS.

In **chapter 2** of this thesis, inconsistent evidence was found for the association of aneurysm pulsation with aneurysm rupture. However, because the evidence was based on >3 low quality studies and the inconsistency of this factor was based on 1 low quality study, we classified this factors as having potential for further study. We found that quantification of aneurysm pulsation is not accurate on 7.0 Tesla MRI, even after optimisation of the study protocol, due to the influence of contrast-to-noise, signal intensity fluctuations and most importantly the flow displacement artefact on the accuracy of the pulsation quantification analysis (**chapter 7**). The impact of these influences on the pulsation quantification analysis should be decreased before pulsatility can be studied as a potential risk factor for rupture.

7.0 Tesla MRI is not yet used in general clinical practice. Also, the aneurysm imaging characteristics that were studied in this thesis, especially aneurysm wall thickness variation, have potential, but are not yet ready to be used in clinical practice. Previous studies have shown that 7.0 Tesla MRI is a promising technique, not only in the field of imaging intracranial aneurysms, but also for other applications, such as imaging of intracranial arterial wall enhancement in stroke, imaging of microbleeds in small vessel disease, or finding subtle structural lesions in patient with cryptogenic epilepsy.[57] However, the availability of 7.0 Tesla MRI scanners is currently limited and the scanners are not yet available for imaging in daily clinical practice. The disadvantages of the high-field strength include loud noise of the machine during scanning and the occurrence of muscle twitches, which might cause discomfort to patients. Furthermore, due to safety issues, there are several contraindications for imaging patients on 7.0 Tesla MRI, including the presence of an intracranial aneurysm clip or coil, which also affect studies with patients with previously treated aneurysms on these scanners. More and more studies are published on safety of 7.0 Tesla MRI scanning with metal objects, including cranial fixation plates and aneurysm clips.[58,59] This, and more studies showing possible clinical implications of 7.0 Tesla MRI, will probably lead to higher clinical availability of the machines.

For this thesis, we imaged more than 30 aneurysms on 7.0 Tesla MRI, and in this process we noticed that also other aneurysms characteristics than the ones we studied on 7.0 Tesla MRI (for example the morphology of the aneurysm, the position of the parent and daughter vessels, the presence of perforators on the parent vessel and the presence of intraluminal thrombus), can be imaged with high resolution. Imaging of these characteristics is essential for planning of treatment of (complex) aneurysms and currently, DSA, an imaging method with a small but nonnegligible risk of significant morbidity (including stroke) and mortality, in combination with 1.5 or 3.0 Tesla MRI and CT/CTA is often needed to study the characteristics of the aneurysm in detail before treatment.[60] If a future study shows that 7.0 Tesla MRI with CT (for imaging of calcification of the wall and the relation of the aneurysm with bony structures, which are not visible on MRI) can provide the surgeon with the same information for treatment planning as low field strength MRI and DSA, a clinical application of 7.0 Tesla MRI might be identified.

CONCLUSIONS AND FUTURE DIRECTIONS

Intracranial aneurysms is a complex disease in which both environmental and genetic factors play a role. To interfere in the cascade of events and stop the aneurysm from progressing to a ruptured state, we need to elucidate the order of the events occurring, and how these events interact with each other.

This thesis yielded one risk factor, irregular shape, which is ready to be incorporated in rupture risk prediction in clinical practice. The first next step should be a prospective cohort study including patients with unruptured aneurysms that are not undergoing treatment in which the other morphological risk factors (including aspect ratio, size ratio, bottleneck factor, height-to-width ratio, contact with the perianeurysmal environment, large volume-to-ostium ratio, and dome direction) with potential for use in clinical practice are tested for their association with aneurysm growth (as surrogate marker for aneurysm rupture) in a multivariate analysis. The risk factors that show to be independent from the already established risk factors, and the risk factor irregular shape, should then be added to a prediction model that also includes the already established risk factors included in the PHASES score. This new model can then directly improve rupture risk prediction in clinical practice.

The results of this thesis give rise to many new ideas for future studies to find new risk factors for development and rupture of aneurysms. The highest potential lies in a risk factor reflecting a process occurring in the wall which is known to be directly involved in rupture. Although there are many different processes involved in initiation and maintaining of the remodelling of the aneurysm wall, the remodelling can either lead to stabilisation of the aneurysm, or can progress and lead to critical thinning of the wall and rupture. Therefore, wall thinning is a very promising marker of rupture. In this thesis, we showed that imaging of wall thickness variation is possible on 7.0 Tesla MRI and we developed a tool to study wall thickness variation of the aneurysm. In a longitudinal study, serial imaging of wall thickness variation in unruptured intracranial aneurysms should be performed on 7.0 Tesla MRI, and the association of wall thickness variation with aneurysm growth as a surrogate marker of rupture should be studied. To reach enough statistical power, we need a large group of patients with unruptured aneurysms not undergoing preventive treatment, and therefore this study should be a worldwide collaboration of medical centres with a 7.0 Tesla MRI scanner.

REFERENCES

1. de Rooij NK, Linn FH, van der Plas JA, Algra A, Rinkel GJ. Incidence of subarachnoid haemorrhage: a systematic review with emphasis on region, age, gender and time trends. *J Neurol Neurosurg Psychiatry*. 2007;78:1365-1372.
2. Nieuwkamp DJ, Setz LE, Algra A, Linn FH, de Rooij NK, Rinkel GJ. Changes in case fatality of aneurysmal subarachnoid haemorrhage over time, according to age, sex, and region: a meta-analysis. *Lancet Neurol*. 2009;8:635-642.
3. Rivero-Arias O, Gray A, Wolstenholme J. Burden of disease and costs of aneurysmal subarachnoid haemorrhage (aSAH) in the United Kingdom. *Cost Eff Resour Alloc*. 2010;8:6-7547-8-6.
4. Greving JP, Wermer MJ, Brown RD,Jr, Morita A, Juvela S, Yonekura M, et al. Development of the PHASES score for prediction of risk of rupture of intracranial aneurysms: a pooled analysis of six prospective cohort studies. *Lancet Neurol*. 2014;13:59-66.

5. Vlak MH, Rinkel GJ, Greebe P, Greving JP, Algra A. Lifetime risks for aneurysmal subarachnoid haemorrhage: a multivariable risk stratification. *J Neurol Neurosurg Psychiatry*. 2013;84:619-623.
6. Alshekhlee A, Mehta S, Edgell RC, Vora N, Feen E, Mohammadi A, et al. Hospital mortality and complications of electively clipped or coiled unruptured intracranial aneurysm. *Stroke*. 2010;41:1471-1476.
7. Brinjikji W, Rabinstein AA, Nasr DM, Lanzino G, Kallmes DF, Cloft HJ. Better outcomes with treatment by coiling relative to clipping of unruptured intracranial aneurysms in the United States, 2001-2008. *AJNR Am J Neuroradiol*. 2011;32:1071-1075.
8. Naggara ON, Lecler A, Oppenheim C, Meder JF, Raymond J. Endovascular treatment of intracranial unruptured aneurysms: a systematic review of the literature on safety with emphasis on subgroup analyses. *Radiology*. 2012;263:828-835.
9. Thompson BG, Brown RD,Jr, Amin-Hanjani S, Broderick JP, Cockroft KM, Connolly ES,Jr, et al. Guidelines for the Management of Patients With Unruptured Intracranial Aneurysms: A Guideline for Healthcare Professionals From the American Heart Association/American Stroke Association. *Stroke*. 2015;46:2368-2400.
10. Steiner T, Juvela S, Unterberg A, Jung C, Forsting M, Rinkel G, et al. European Stroke Organization guidelines for the management of intracranial aneurysms and subarachnoid haemorrhage. *Cerebrovasc Dis*. 2013;35:93-112.
11. Katusic ZS, Austin SA. Neurovascular protective function of endothelial nitric oxide – recent advances. *Circ J*. 2016;80:1499-1503.
12. Bilguvar K, Yasuno K, Niemela M, Ruigrok YM, von Und Zu Fraunberg M, van Duijn CM, et al. Susceptibility loci for intracranial aneurysm in European and Japanese populations. *Nat Genet*. 2008;40:1472-1477.
13. Yasuno K, Bakircioglu M, Low SK, Bilguvar K, Gaal E, Ruigrok YM, et al. Common variant near the endothelin receptor type A (EDNRA) gene is associated with intracranial aneurysm risk. *Proc Natl Acad Sci U S A*. 2011;108:19707-19712.
14. Yasuno K, Bilguvar K, Bijlenga P, Low SK, Krischek B, Auburger G, et al. Genome-wide association study of intracranial aneurysm identifies three new risk loci. *Nat Genet*. 2010;42:420-425.
15. Laaksamo E, Ramachandran M, Frosen J, Tulamo R, Baumann M, Friedlander RM, et al. Intracellular signaling pathways and size, shape, and rupture history of human intracranial aneurysms. *Neurosurgery*. 2012;70:1565-1572.
16. Frosen J, Piippo A, Paetau A, Kangasniemi M, Niemela M, Hernesniemi J, et al. Growth factor receptor expression and remodeling of saccular cerebral artery aneurysm walls: implications for biological therapy preventing rupture. *Neurosurgery*. 2006;58:534-541.
17. Frosen J, Piippo A, Paetau A, Kangasniemi M, Niemela M, Hernesniemi J, et al. Remodeling of saccular cerebral artery aneurysm wall is associated with rupture: histological analysis of 24 unruptured and 42 ruptured cases. *Stroke*. 2004;35:2287-2293.
18. Laaksamo E, Tulamo R, Liiman A, Baumann M, Friedlander RM, Hernesniemi J, et al. Oxidative stress is associated with cell death, wall degradation, and increased risk of rupture of the intracranial aneurysm wall. *Neurosurgery*. 2013;72:109-117.
19. Tulamo R, Frosen J, Paetau A, Seitsonen S, Hernesniemi J, Niemela M, et al. Lack of complement inhibitors in the outer intracranial artery aneurysm wall associates with complement terminal pathway activation. *Am J Pathol*. 2010;177:3224-3232.
20. Hasan DM, Mahaney KB, Magnotta VA, Kung DK, Lawton MT, Hashimoto T, et al. Macrophage imaging within human cerebral aneurysms wall using ferumoxytol-enhanced MRI: a pilot study. *Arterioscler Thromb Vasc Biol*. 2012;32:1032-1038.
21. Ryu CW, Jahng GH, Kim EJ, Choi WS, Yang DM. High resolution wall and lumen MRI of the middle cerebral arteries at 3 tesla. *Cerebrovasc Dis*. 2009;27:433-442.
22. Swartz RH, Bhuta SS, Farb RI, Agid R, Willinsky RA, Terbrugge KG, et al. Intracranial arterial wall imaging using high-resolution 3-tesla contrast-enhanced MRI. *Neurology*. 2009;72:627-634.
23. van der Kolk AG, Hendrikse J, Brundel M, Biessels GJ, Smit EJ, Visser F, et al. Multi-sequence whole-brain intracranial vessel wall imaging at 7.0 tesla. *Eur Radiol*. 2013;23:2996-3004.
24. Matouk CC, Mandell DM, Gunel M, Bulsara KR, Malhotra A, Hebert R, et al. Vessel wall magnetic resonance imaging identifies the site of rupture in patients with multiple intracranial aneurysms: proof of principle. *Neurosurgery*. 2013;72:492-496.

25. Chiu JJ, Chien S. Effects of disturbed flow on vascular endothelium: pathophysiological basis and clinical perspectives. *Physiol Rev*. 2011;91:327-387.
26. Dolan JM, Kolega J, Meng H. High wall shear stress and spatial gradients in vascular pathology: a review. *Ann Biomed Eng*. 2013;41:1411-1427.
27. Malek AM, Alper SL, Izumo S. Hemodynamic shear stress and its role in atherosclerosis. *JAMA*. 1999;282:2035-2042.
28. van Ooij P, Schneiders JJ, Marquering HA, Majoie CB, van Bavel E, Nederveen AJ. 3D Cine Phase-Contrast MRI at 3T in Intracranial Aneurysms Compared with Patient-Specific Computational Fluid Dynamics. *AJNR Am J Neuroradiol*. 2013;34:1785-1791.
29. van Ooij P, Zwanenburg JJ, Visser F, Majoie CB, vanBavel E, Hendrikse J, et al. Quantification and visualization of flow in the Circle of Willis: time-resolved three-dimensional phase contrast MRI at 7 T compared with 3 T. *Magn Reson Med*. 2013;69:868-876.
30. Juvela S, Poussa K, Porras M. Factors affecting formation and growth of intracranial aneurysms: a long-term follow-up study. *Stroke*. 2001;32:485-491.
31. Backes D, Rinkel GJ, Greving JP, Velthuis BK, Murayama Y, Takao H, et al. ELAPSS score for prediction of risk of growth of unruptured intracranial aneurysms. *Neurology*. 2017;88:1600-1606.
32. Bilguvar K, Yasuno K, Niemela M, Ruigrok YM, von Und Zu Fraunberg M, van Duijn CM, et al. Susceptibility loci for intracranial aneurysm in European and Japanese populations. *Nat Genet*. 2008;40:1472-1477.
33. Foroud T, Koller DL, Lai D, Sauerbeck L, Anderson C, Ko N, et al. Genome-wide association study of intracranial aneurysms confirms role of Anril and SOX17 in disease risk. *Stroke*. 2012;43:2846-2852.
34. Low SK, Takahashi A, Cha PC, Zembutsu H, Kamatani N, Kubo M, et al. Genome-wide association study for intracranial aneurysm in the Japanese population identifies three candidate susceptible loci and a functional genetic variant at EDNRA. *Hum Mol Genet*. 2012;21:2102-2110.
35. Frosen J, Tulamo R, Paetau A, Laaksamo E, Korja M, Laakso A, et al. Saccular intracranial aneurysm: pathology and mechanisms. *Acta Neuropathol*. 2012;123:773-786.
36. Sawyer DM, Pace LA, Pascale CL, Kutchin AC, O'Neill BE, Starke RM, et al. Lymphocytes influence intracranial aneurysm formation and rupture: role of extracellular matrix remodeling and phenotypic modulation of vascular smooth muscle cells. *J Neuroinflammation*. 2016;13:185-016-0654-z.
37. Riede UN, Staubesand J. A unifying concept for the role of matrix vesicles and lysosomes in the formal pathogenesis of diseases of connective tissues and blood vessels. *Beitr Pathol*. 1977;160:3-37.
38. Frosen J, Piippo A, Paetau A, Kangasniemi M, Niemela M, Hernesniemi J, et al. Remodeling of saccular cerebral artery aneurysm wall is associated with rupture: histological analysis of 24 unruptured and 42 ruptured cases. *Stroke*. 2004;35:2287-2293.
39. Kataoka K, Taneda M, Asai T, Kinoshita A, Ito M, Kuroda R. Structural fragility and inflammatory response of ruptured cerebral aneurysms. A comparative study between ruptured and unruptured cerebral aneurysms. *Stroke*. 1999;30:1396-1401.
40. Hasan DM, Mahaney KB, Brown RD,Jr, Meissner I, Piepgras DG, Huston J, et al. Aspirin as a promising agent for decreasing incidence of cerebral aneurysm rupture. *Stroke*. 2011;42:3156-3162.
41. Hasan DM, Chalouhi N, Jabbour P, Dumont AS, Kung DK, Magnotta VA, et al. Evidence that acetylsalicylic acid attenuates inflammation in the walls of human cerebral aneurysms: preliminary results. *J Am Heart Assoc*. 2013;2:e000019.
42. Etminan N, Vergouwen MD. Acetylsalicylic Acid Plus Intensive Blood Pressure Treatment in Patients With Unruptured Intracranial Aneurysms (PROTECT-U). February 23, 2017; Available at: https://clinicaltrials.gov/ct2/show/NCT03063541, 2017.
43. Zhang B, Fugleholm K, Day LB, Ye S, Weller RO, Day IN. Molecular pathogenesis of subarachnoid haemorrhage. *Int J Biochem Cell Biol*. 2003;35:1341-1360.
44. Grond-Ginsbach C, Schnippering H, Hausser I, Weber R, Werner I, Steiner HH, et al. Ultrastructural connective tissue aberrations in patients with intracranial aneurysms. *Stroke*. 2002;33:2192-2196.
45. Park JK, Lee CS, Sim KB, Huh JS, Park JC. Imaging of the walls of saccular cerebral aneurysms with double inversion recovery black-blood sequence. *J Magn Reson Imaging*. 2009;30:1179-1183.

46. Steinman DA, Antiga L, Wasserman BA. Overestimation of cerebral aneurysm wall thickness by black blood MRI? *J Magn Reson Imaging*. 2010;31:766.
47. Monninghoff C, Maderwald S, Theysohn JM, Kraff O, Ladd SC, Ladd ME, et al. Evaluation of intracranial aneurysms with 7 T versus 1.5 T time-of-flight MR angiography - initial experience. *Rofo*. 2009;181:16-23.
48. Wrede KH, Dammann P, Monninghoff C, Johst S, Maderwald S, Sandalcioglu IE, et al. Non-enhanced MR imaging of cerebral aneurysms: 7 Tesla versus 1.5 Tesla. *PLoS One*. 2014;9:e84562.
49. Steiger HJ, Aaslid R, Keller S, Reulen HJ. Strength, elasticity and viscoelastic properties of cerebral aneurysms. *Heart Vessels*. 1989;5:41-46.
50. Scott S, Ferguson GG, Roach MR. Comparison of the elastic properties of human intracranial arteries and aneurysms. *Can J Physiol Pharmacol*. 1972;50:328-332.
51. Challa V, Han HC. Spatial variations in wall thickness, material stiffness and initial shape affect wall stress and shape of intracranial aneurysms. *Neurol Res*. 2007;29:569-577.
52. Edjlali M, Gentric JC, Regent-Rodriguez C, Trystram D, Hassen WB, Lion S, et al. Does aneurysmal wall enhancement on vessel wall MRI help to distinguish stable from unstable intracranial aneurysms? *Stroke*. 2014;45:3704-3706.
53. Liu P, Qi H, Liu A, Lv X, Jiang Y, Zhao X, et al. Relationship between aneurysm wall enhancement and conventional risk factors in patients with unruptured intracranial aneurysms: A black-blood MRI study. *Interv Neuroradiol*. 2016;22:501-505.
54. Hu P, Yang Q, Wang DD, Guan SC, Zhang HQ. Wall enhancement on high-resolution magnetic resonance imaging may predict an unsteady state of an intracranial saccular aneurysm. *Neuroradiology*. 2016;58:979-985.
55. Meng H, Tutino VM, Xiang J, Siddiqui A. High WSS or low WSS? Complex interactions of hemodynamics with intracranial aneurysm initiation, growth, and rupture: toward a unifying hypothesis. *AJNR Am J Neuroradiol*. 2014;35:1254-1262.
56. Kadasi LM, Dent WC, Malek AM. Colocalization of thin-walled dome regions with low hemodynamic wall shear stress in unruptured cerebral aneurysms. *J Neurosurg*. 2013;119:172-179.
57. van der Kolk AG, Hendrikse J, Zwanenburg JJ, Visser F, Luijten PR. Clinical applications of 7 T MRI in the brain. *Eur J Radiol*. 2011;82:708-718.
58. Noureddine Y, Kraff O, Ladd ME, Wrede KH, Chen B, Quick HH, et al. In vitro and in silico assessment of RF-induced heating around intracranial aneurysm clips at 7 Tesla. *Magn Reson Med*. 2017: 10.1002/mrm.26650 [Epub ahead of print].
59. Kraff O, Wrede KH, Schoemberg T, Dammann P, Noureddine Y, Orzada S, et al. MR safety assessment of potential RF heating from cranial fixation plates at 7 T. *Med Phys*. 2013;40:042302.
60. Hanel RA, Spetzler RF. Surgical treatment of complex intracranial aneurysms. *Neurosurgery*. 2008;62:1289-1297.

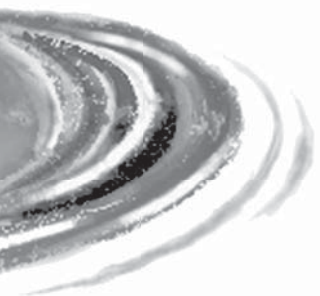

SUMMARY

Intracranial aneurysms occur in approximately 3% of the population. The pathogenesis of aneurysms is largely unknown, and is thought to be a complex process in which both genetic and environmental factors are involved. Aneurysms can rupture and give rise to subarachnoid haemorrhage, a devastating subtype of stroke with high morbidity and mortality. Treatment can prevent rupture, but carries a risk of major complications including death. The annual risk of rupture of an aneurysm lies around 1%, indicating that the majority of aneurysms never ruptures. Therefore, preventive treatment should be restricted to those aneurysms with high risk of rupture. Risk factors for rupture include geographical region, age, hypertension, aneurysm size and site, and earlier subarachnoid haemorrhage, but explain only up to 20% of the 5-year rupture risk. Thus, better risk factors to predict aneurysm rupture are urgently needed. This thesis focusses on identifying new risk factors for development and rupture of intracranial aneurysms using a literature search study, genetic and genomic studies, as well as 7.0 Tesla magnetic resonance imaging (MRI) studies.

RISK FACTORS FOR RUPTURE OF INTRACRANIAL ANEURYSMS

In the first part of this thesis (**chapter 2**), a systematic review and meta-analysis was performed to identify genetic, molecular, morphological and hemodynamic factors that would be of additional value to the factors currently used in clinical practice to predict the risk of rupture of unruptured aneurysms. Quality of the included studies was assessed by using a methodological quality score, and risk factors were categorised into strong, moderate, low and inconsistent level of evidence. 144 risk factors were identified, but only one risk factor was found to be suitable for use in clinical practice: irregular shape (evidence from 4 prospective cohort studies of high-quality; pooled odds ratio of 4.8, 95% confidence interval 2.7–8.7). Furthermore, aspect ratio (aneurysm height divided by neck size), size ratio (aneurysm height divided by the parent vessel diameter), bottleneck factor (aneurysm width divided by neck size), height-to-width ratio (aneurysm height divided by aneurysm width), contact with the perianeurysmal environment, volume-to-ostium ratio (ratio of the aneurysm volume to the area of the neck) and dome direction (downward/inferior direction) were identified as morphological risk factors with potential for use in clinical practice. However, the evidence for these factors was based on only 1 prospective study or solely on retrospective studies and therefore the value of these factors should first be confirmed in multivariate analysis and incorporated in prediction models. No genetic, molecular, and hemodynamic factors with strong or moderate evidence were identified. However, 18 genetic, morphological, and hemodynamic risk factors for rupture were additionally identified as potentially relevant for further clinical research, including the risk factor pulsatility (the change in volume of the aneurysm during the cardiac cycle).

IDENTIFICATION OF GENES AND PATHWAYS INVOLVED IN DEVELOPMENT AND RUPTURE OF INTRACRANIAL ANEURYSMS

In **chapter 3** of this thesis, the association between the six genetic risk loci identified thusfar in the genome-wide association studies on intracranial aneurysms, and aneurysm size at the time of rupture was analysed. In the study group of 624 patients with aneurysmal subarachnoid haemorrhage, no association was found between these genetic loci and size of the aneurysm. Since the six risk loci only explain a small amount of the genetic risk of aneurysms, these results do not exclude that there is an association of genetic factors with size or rupture of aneurysms.

In **chapter 4**, RNA sequencing was used to compare gene expression between ruptured and unruptured aneurysm biopsies and control intracranial artery biopsies, to increase knowledge on the genes involved in the pathogenesis of development and rupture of aneurysms. 229 differentially expressed genes in 44 aneurysm biopsies versus 16 control biopsies, and 1489 differentially expressed genes in 22 ruptured versus 21 unruptured aneurysm biopsies were found. Extracellular matrix pathways were enriched in aneurysms versus controls, whereas pathways involved in immune response and the lysosome pathway were enriched in ruptured versus unruptured aneurysms. Certain immunoglobulin genes were expressed in aneurysms, but showed no expression in controls. These results indicate that drugs targeting the immune system might be interesting treatment strategies in the prevention of aneurysm development and rupture.

7.0 TESLA MAGNETIC RESONANCE IMAGING OF INTRACRANIAL ANEURYSMS

In the last part of this thesis, we experimented with imaging of the aneurysm wall, flow, wall shear stress, and pulsatility of the aneurysm on 7.0 Tesla MRI. The ultra-high field of this scanner increases signal-to-noise ratio compared to scanners with lower field-strength, enabling imaging at a higher spatial resolution, without increasing scan time. This offers the opportunity to image those characteristics of the aneurysm for which current clinically available imaging techniques lack resolution. In **chapter 5**, the aneurysm wall was studied in 24 patients with 33 unruptured aneurysms by using a 7.0 Tesla MRI vessel wall imaging sequence with a high resolution (0.8 x 0.8 x 0.8 mm). Variation in MR signal intensity was observed in all visible aneurysm walls. The wall aligning the brain could not be imaged, because the signal of the wall is equal to that of brain tissue. With a phantom experiment, and by combining ex vivo MRI with histopathological examination of two aneurysm biopsies, we validated that signal intensity variation reflects actual thickness variation. Subsequently, in **chapter 6**, a method for semi-quantitative assessment of wall thickness variation was

developed by using vessel wall images of 9 patients with 11 aneurysms. The wall thickness variation was normalised to the signal of nearby brain to be able to compare wall thickness variation between different patients. Spatial variation in wall thickness was found in all 11 aneurysms. It was concluded that this method provides a tool to study aneurysm wall thickness variation as a risk factor for growth or rupture of aneurysms. This tool also offers the opportunity to study the relation between different characteristics of the aneurysm and wall thickness in vivo. Therefore, in the second part of chapter 6, the 7.0 Tesla MRI vessel wall sequence was combined with 3-dimensional phase-contrast MRI, to analyse the association between wall thickness and wall shear stress. In all 11 unruptured aneurysms, an inverse association between wall thickness and wall shear stress was found. This finding supports the hypothesis that high wall shear stress leads to remodelling of the aneurysm wall by activation of proteases, matrix degradation and apoptosis, probably leading to wall thinning, while low wall shear stress is associated with increased inflammatory cell infiltration and smooth muscle cell proliferation, which may lead to wall thickening.

In **chapter 7**, it was evaluated whether 7.0 Tesla MRI can quantify aneurysm volume pulsation, one of the risk factors for rupture with potential for further study identified in chapter 2. In this two staged study, 10 and 9 unruptured aneurysms were imaged with a high resolution gradient-echo sequence, and aneurysm pulsation was quantified with a semi-automatic segmentation method. In stage I, the mean aneurysm pulsation was 8% (standard deviation 7%, range 2 to 27%). The accuracy and precision of the measured volume pulsations was addressed by digital phantom simulations, and a repeated image analysis. Although repeatability was good, the accuracy analysis showed the accuracy of the quantification of volume pulsation to be influenced by contrast-to-noise ratio, intensity fluctuations, aneurysm size and, most importantly, by the flow displacement artefact. The artefactual volume pulsations measured with the digital phantom simulations were in the same magnitude as the volume pulsations observed in the patient data, even after optimisation of the imaging sequences and adding contrast enhancement in stage II of the study. Therefore, it was concluded that volume pulsation quantification with the current imaging protocol on 7.0 Tesla MRI is not accurate due to multiple imaging artefacts.

In conclusion, this thesis provides irregular shape as an additional risk factor for use in rupture risk prediction in clinical practice, and gives an overview of risk factors with potential for use in clinical practice, for which further research is needed. It confirms the role of extracellular matrix pathways in the development of aneurysms, and immune response pathways in rupture of aneurysms; and suggests a role of immunoglobulins in development and lysosomes in rupture of aneurysms. Finally, 7.0 Tesla MRI has potential for studying new risk factors for aneurysm rupture, including aneurysm wall thickness.

NEDERLANDSE SAMENVATTING (DUTCH SUMMARY)

Intracraniële aneurysmata zijn verworven uitstulpingen in de grote slagaders in het hoofd. De pathogenese van aneurysmata is nog grotendeels onbekend, maar waarschijnlijk is er sprake van een wisselwerking tussen genetische en omgevingsfactoren. Aneurysmata komen bij ongeveer 3% van de populatie voor. Door toename van het gebruik van beeldvorming van de hersenslagaders (MR- en CT-angiografie), worden er steeds meer aneurysmata per toeval ontdekt.

Een aneurysma geeft meestal geen symptomen, tenzij het barst (ruptuur). Dan ontstaat er een zogenaamde subarachnoïdale bloeding, een zeldzame vorm van beroerte (incidentie van 9 per 100.000 persoonsjaren). In tegenstelling tot de andere vormen van beroerte (intracerebrale bloeding en herseninfarct) komt de subarachnoïdale bloeding vaak op relatief jonge leeftijd voor. De kans op overlijden of blijvende invaliditeit is groot (respectievelijk 35 en 50%) en ook de patiënten die overleven hebben vaak blijvende cognitieve klachten.

Het is mogelijk om een ongebarsten aneurysma preventief af te sluiten met een behandeling via de lies (endovasculair coilen) of door een schedeloperatie (neurochirurgisch clippen), maar beide behandelingen zijn niet zonder risico. Het gemiddelde risico op ruptuur is maar ongeveer 1% per jaar en daarom zal de meerderheid van de ongebarsten aneurysmata nooit barsten. Een preventieve behandeling is dan ook alleen geïndiceerd voor de patiënten bij wie de kans op ruptuur van het aneurysma hoger is dan de kans op complicaties van de behandeling. Het is echter moeilijk om te voorspellen welk aneurysma zal gaan barsten. Er is een aantal risicofactoren gevonden die gebruikt worden om dit risico in te schatten, waaronder de geografische regio, de leeftijd, hoge bloeddruk, een eerder doorgemaakte subarachnoïdale bloeding, aneurysmalocatie en aneurysmagrootte. Deze risicofactoren verklaren echter samen maar maximaal 20% van het risico op ruptuur. Er is dus behoefte aan betere risicofactoren om de kans op ruptuur te voorspellen.

De studies in dit proefschrift richten zich op het vinden van nieuwe risicofactoren voor het ontstaan en barsten van aneurysmata. Hierbij wordt gebruik gemaakt van een literatuuronderzoek, een genetische associatie- en een genexpressiestudie, en 7.0 Tesla MRI studies.

RISICOFACTOREN VOOR RUPTUUR VAN ANEURYSMATA

Het eerste deel van dit proefschrift (**hoofdstuk 2**) beschrijft een systematisch literatuuronderzoek en meta-analyse om genetische, moleculaire, morfologische en hemodynamische risicofactoren voor ruptuur te identificeren die een aanvulling zouden kunnen zijn op de

risicofactoren die in de huidige praktijk gebruikt worden. De kwaliteit van de gevonden studies werd bepaald aan de hand van een methodologische kwaliteitsscore. De risicofactoren werden onderverdeeld in factoren met sterk, gemiddeld, laag of inconsistent bewijs voor de relatie met ruptuur. Er werden 144 risicofactoren gevonden, waarvan er één direct toepasbaar is in de klinische praktijk: een onregelmatige vorm van het aneurysma (bewijs op basis van 4 prospectieve cohortstudies met hoge kwaliteit; gepoolde odds ratio van 4,8, 95% betrouwbaarheidsinterval 2,7–8,7). Andere risicofactoren die potentie hebben om in de klinische praktijk gebruikt te worden, waren aspect ratio (hoogte van het aneurysma gedeeld door de breedte van de aneurysmahals), size ratio (hoogte van het aneurysma gedeeld door de diameter van de aanvoerende slagader), bottleneck factor (breedte van het aneurysma gedeeld door de breedte van de aneurysmahals), height-to-width ratio (hoogte van het aneurysma gedeeld door de breedte van het aneurysma), contact van het aneurysma met de omgevende weefsels, volume-to-ostium ratio (het volume van het aneurysma gedeeld door de oppervlakte van de aneurysmahals), en de richting waarin de top van het aneurysma wijst (benedenwaartse richting). Het bewijs voor deze factoren was gebaseerd op slechts 1 prospectieve studie of alleen op retrospectieve studies. Daarom moeten deze factoren eerst onderzocht worden in een multivariate analyse en toegevoegd worden aan de bestaande predictiemodellen voor ruptuur van aneurysmata, voordat ze gebruikt kunnen worden in de klinische praktijk. Er werden in het literatuuronderzoek geen genetische, moleculaire of hemodynamische risicofactoren gevonden waarvoor sterke of gemiddelde bewijskracht is. Er werden wel 18 van deze risicofactoren geïdentificeerd die relevant zijn voor verder onderzoek, waaronder de risicofactor pulsatiliteit (het veranderen van het volume van het aneurysma met de hartslag).

Het identificeren van genen en netwerken van genen die betrokken zijn bij het ontstaan en het barsten van aneurysmata

In **hoofdstuk 3** van dit proefschrift worden de resultaten beschreven van een studie naar de associatie tussen aneurysmagrootte op het moment van ruptuur en 6 genetische risicoloci. Deze risicoloci werden eerder geïdentificeerd in genoomwijde associatiestudies naar intracraniële aneurysmata. In genoomwijde associatiestudies wordt de associatie tussen de aanwezigheid van ziekte en veelvoorkomende varianten in het erfelijk materiaal (DNA) onderzocht. In de studiegroep van 624 patiënten met een subarachnoïdale bloeding die onderzocht werd in hoofdstuk 3, kon geen associatie tussen de 6 genetische risicoloci en aneurysmagrootte worden aangetoond. Aangezien deze genetische risicoloci maar een klein deel van het genetische risico voor aneurysmata verklaren, is met deze studie niet uitgesloten dat er een relatie is tussen genetische factoren en grootte of ruptuur van aneurysmata.

In **hoofdstuk 4** werden verschillen in expressie van RNA (het afbraakproduct van DNA) onderzocht in biopten van gebarsten en ongebarsten aneurysmata en in controlebiopten van hersenslagaders. Er werd RNA sequencing methodologie gebruikt om de aanwezigheid en hoeveelheid RNA op een bepaald moment in een bepaald weefsel te bepalen. RNA sequencing maakt gebruik van next-generation sequencing, een methode waarmee de nucleïnezuurvolgorde in het DNA wordt bepaald. Het doel van deze studie was om de kennis van de genen die betrokken zijn bij de pathogenese van het ontstaan en barsten van aneurysmata te vergroten, zodat uiteindelijk betere risicofactoren of zelfs gerichte behandelingsmethoden kunnen worden gevonden. In dit onderzoek werden 229 genen gevonden die verschillend tot expressie kwamen in 44 aneurysmata versus 16 controlebiopten, terwijl er 1489 genen verschillend tot expressie kwamen in 22 gebarsten versus 21 ongebarsten aneurysmabiopten. Het gennetwerk extracellulaire matrix was verrijkt in aneurysmata versus controles, en de netwerken immuunreactie en lysosomen in gebarsten versus ongebarsten aneurysmata. Ten slotte werd gezien dat bepaalde immuunglobulinegenen wel tot expressie kwamen in aneurysmata, maar helemaal niet in controlebloedvaten. De resultaten suggereren dat het onderdrukken van het immuunsysteem een mogelijke behandelstrategie in het voorkomen van het barsten van aneurysmata zou kunnen zijn.

AFBEELDEN VAN ANEURYSMATA OP 7.0 TESLA MAGNETIC RESONANCE IMAGING (MRI)

In het laatste gedeelte van dit proefschrift werd geëxperimenteerd met het afbeelden van aneurysmata op 7.0 Tesla MRI. Door de sterkere magneet in deze scanner is er een hogere signaal-ruis-verhouding dan op lagere veldsterkten, waardoor er met een hogere spatiële resolutie kan worden gescand, zonder dat de scanduur toeneemt. Dit biedt mogelijkheden om karakteristieken van het aneurysma af te beelden die met de huidige MRI-scanners niet goed kunnen worden afgebeeld door te lage resolutie, waaronder de aneurysmawand, beweging van het aneurysma met de hartslag (pulsatiliteit), de bloedstroom in het aneurysma en de stress van het bloed op de wand van het aneurysma (wall shear stress). In **hoofdstuk 5** werd de aneurysmawand in 24 patiënten met 33 ongebarsten aneurysmata bestudeerd op de 7.0 Tesla MRI met een vaatwandsequentie met hoge resolutie (0,8 x 0,8 x 0,8 mm). In alle onderzochte aneurysmata werd een variatie in intensiteit van het signaal van de MRI gevonden ter plaatse van de aneurysmawand. Het deel van de aneurysmawand dat tegen de hersenen aan lag, kon niet worden afgebeeld, omdat het signaal van de hersenen gelijk is aan het signaal van de wand. Om te bewijzen dat het verschil in MRI-signaalintensiteit dat gezien werd in de patiëntenscans overeenkomt met echte variatie in dikte van de aneurysmawand, werd er een ex vivo experiment gedaan. Hierbij werden

een fantoom met een bekende variatie in dikte en twee aneurysmawandbiopten gescand met dezelfde vaatwandsequentie. Van de aneurysmawandbiopten werd de echte dikte gemeten onder de microscoop. De variatie in signaalintensiteit van de MRI kwam overeen met de variatie in dikte van de aneurysmawandbiopten en van het fantoom. Daaropvolgend werd in **hoofdstuk 6** een methode ontwikkeld om de variatie in dikte van de wand te kwantificeren (bij 9 patiënten met 11 aneurysmata). Het signaal van de aneurysmawand werd genormaliseerd naar het signaal van de hersenen die vlak rond het aneurysma lagen, om het mogelijk te maken om variatie in dikte van de wand tussen verschillende patiënten te vergelijken. In alle 11 aneurysmata werd een variatie in dikte gevonden. De ontwikkelde methode kan gebruikt worden om de associatie tussen wanddiktevariatie en groei of ruptuur van een aneurysma te onderzoeken. Daarnaast kan de methode ook gebruikt worden om de relatie tussen wanddiktevariatie en andere karakteristieken van het aneurysma te bestuderen. Daarom werd in het tweede deel van hoofdstuk 6 de relatie tussen wanddikte en wall shear stress onderzocht door de vaatwandsequentie op 7.0 Tesla MRI te combineren met een 3-dimensionale fase-contrast MRI. Er werd een omgekeerde relatie tussen wanddikte en wall shear stress gevonden in alle 11 aneurysmata. Dit ondersteunt de hypothese dat de wand dunner zou kunnen worden als er een hoge stress op de wand is die leidt tot activatie van proteasen, matrixdegradatie en apoptose. Andersom kan een lage stress op de wand leiden tot het dikker worden van de wand door het aantrekken van ontstekingscellen en proliferatie van gladde spiercellen in de wand.

In hoofdstuk 2 werd pulsatiliteit (het veranderen van het volume van het aneurysma met de hartslag) geïdentificeerd als risicofactor met potentie voor verder onderzoek. In **hoofdstuk 7** werd onderzocht of de pulsatiliteit van het aneurysma kan worden afgebeeld met 7.0 Tesla MRI. De studie bevatte twee stadia, waarin respectievelijk 10 en 9 ongebarsten aneurysmata werden afgebeeld met een hoge resolutie gradiënt-echo sequentie. De pulsatie van het aneurysma werd gekwantificeerd met een semiautomatische segmentatiemethode. In stadium I bleek dat de pulsatie in aneurysmata gemiddeld 8% was (standaarddeviatie 7%, met een range van 2 tot 27%). De accuraatheid en precisie van de gemeten volumepulsaties werd getest door simulatie van een digitaal fantoom en een herhaling van de originele metingen. De reproduceerbaarheid van de metingen was goed, maar de accuraatheidsanalyse toonde dat de kwantificatie van volumepulsatie beïnvloed wordt door de contrast-ruis-verhouding, fluctuaties in signaalintensiteit, aneurysmagrootte en voornamelijk door het artefact veroorzaakt door flow (bloedstroom) verplaatsing. De artificiële pulsatie gemeten in de fantomen was in dezelfde orde van grootte als de pulsatie gemeten in de patiëntendata, zelfs na optimalisatie van de MRI-sequentie en het toevoegen van intraveneus contrast in stadium II van de studie. Op basis van deze resultaten werd geconcludeerd dat volumepulsatie op 7.0 Tesla MRI met het huidige protocol niet accuraat kan worden gekwantificeerd door meerdere artefacten.

Concluderend heeft dit proefschrift geleid tot een extra risicofactor (onregelmatige vorm van het aneurysma), die gebruikt kan worden voor het voorspellen van ruptuur in de klinische praktijk. Daarnaast geeft het een overzicht van risicofactoren die potentie hebben om gebruikt te worden in de klinische praktijk, maar die nog verder onderzoek behoeven. Dit proefschrift bevestigt verder de rol van de extracellulaire matrix bij het ontstaan van aneurysmata en de rol van de immuunreactie bij de ruptuur van aneurysmata, en suggereert een rol voor immunoglobulinen bij het ontstaan van aneurysmata en een rol voor lysosomen bij ruptuur. Tenslotte laat het zien dat 7.0 Tesla MRI potentie heeft voor het bestuderen van nieuwe markers voor ruptuur, zoals aneurysmawanddikte.

DANKWOORD (ACKNOWLEDGEMENTS)

Promoveren doe je niet alleen. Daarom wil ik iedereen die heeft bijgedragen aan dit proefschrift hartelijk danken. Een aantal mensen wil ik in het bijzonder noemen.

Om te beginnen de patiënten en hun vertegenwoordigers, die bereid waren deel te nemen aan de beschreven studies, zonder hen was dit proefschrift niet tot stand gekomen.

Prof.dr. L. Regli, dear Luca, it was a pleasure working under your supervision. Thank you for your critical questions on the results presented by Emine and me, and for improving my spoken English by stating that research meetings should always be in English. I really enjoyed the hours I spent in your OR observing the actual (vascular) anatomy of the brain and the intraoperative aspect of aneurysms.

Prof.dr. G.J.E. Rinkel, beste Gabriël. Na mijn wetenschappelijke stage naar Moyamoya ziekte gaf je mij de kans om een promotieonderzoek naar intracraniële aneurysmata te doen. De samenwerking tussen de neurologie, neurochirurgie en de biologie, met zowel genetische als imaging studies, maakte het een zeer veelzijdig project. Het was een mooie uitdaging om de verschillende vakgroepen en de resultaten van de verschillende studies samen te brengen. Bedankt voor je begeleiding hierin en natuurlijk voor je altijd weer grondige correcties van mijn stukken.

Dr. Y.M. Ruigrok, beste Ynte, dank voor je betrokken begeleiding tijdens mijn promotietijd. Ik heb veel van je geleerd, met name om meer pragmatisch te zijn. Ik vind het bewonderingswaardig hoe jij je passie voor het onderzoek naar de genetica van aneurysmata combineert met je gezin en klinisch werk. Je deur stond altijd voor me open en je vroeg altijd even of het, naast het onderzoek, ook nog goed met mij ging. Bedankt dat je al die tijd het volste vertrouwen in mij hebt gehad.

Dr. B.H. Verweij, beste Bon. Als copromotor vanuit de neurochirurgie maakte je mij wegwijs op de operatiekamers. Tijdens onze overleggen had je altijd veel nieuwe ideeën en brainstormden we over hoe we dachten dat een aneurysma zou barsten. Ik heb goede herinneringen aan het congres op Hawaii, waar je Wilco en mij meenam op een roadtrip langs de surfers aan de North Shore in een blauwe Ford Mustang cabrio. Bedankt voor de leuke tijd!

Prof.dr. B.K. Velthuis, Prof.dr. A. van der Zwan, Prof.dr. L.H. van den Berg, Dr. M.J.H. Wermer en Prof.dr. Y.B.W.E.M. Roos wil ik hartelijk bedanken voor hun bereidheid om plaats te nemen in de leescommissie.

Dr. J.J.M. Zwanenburg, beste Jaco, terwijl het aneurysmaproject op de 7.0 Tesla MRI eigenlijk meer een hobby van je was, heb je toch veel van je tijd in mijn begeleiding gestopt. Ik ben

onder de indruk van je kennis en betrokkenheid, en de manier waarop je zowel studenten met een technische achtergrond als artsen zoals ik weet te begeleiden. Bedankt voor je hulp bij het schrijven van de 7.0 Tesla MRI stukken en voor het blijven geloven in de publiceerbaarheid van het pulsatiliteits-artikel.

Beste Fredy, bedankt voor de vele uurtjes die je achter de 7.0 Tesla scanner hebt gezeten om mijn protocol weer verder te verbeteren. Hugo, bedankt voor je hulp bij het aneurysmawand artikel. Prof.dr. P.R. Luijten, bedankt voor de mogelijkheid om onze patiënten op de 7.0 Tesla MRI te scannen. Onderzoekers van de 7.0 Tesla groep, bedankt voor jullie flexibiliteit in het ruilen van scantijd als ik weer eens niet in mijn eigen tijdsblok kon plannen. Laboranten, beste Guus en Gerrit, bedankt voor jullie tomeloze inzet bij het scannen met mijn eigenlijk net iets te lange protocol. Pim, bedankt voor je hulp bij de WSS- en flowanalyses.

Beste Jan Andries, de samenwerking met jou en Emine in het Focus&Massa project zorgde voor een veel bredere kijk op de pathogenese van aneurysmata, dank voor het bijspijkeren van mijn kennis van de celbiologie! Emine, it was a pleasure working with you on this project, and sharing our ups and downs with a cup of tea and some sweets from Turkey. I hope you are happy with your new job, and I wish you all the best in the future.

Beste Bart van de Zwan, Sen Han, Jan Willem Berkelbach, Peter van Rijen en Peter Gosselaar, hartelijk dank voor jullie bereidheid om weefsel af te nemen voor die onderzoeker met dat kannetje stikstof in de hoek van de OK. Zonder jullie hulp had ik deze studies niet kunnen doen.

Dames van het trialbureau neurologie en Judith, Cora en Albi, hartelijk dank voor al jullie hulp bij het regelen van afspraken en paperassen, maar vooral voor de gezellige praatjes tussendoor!

Afdeling genetica van het UMC Groningen, Pieter van der Vlies en Patrick Deelen, dank voor jullie uitleg en hulp bij het voor mij helemaal nieuwe RNA sequencing. Marja van Blokland van het lab Pathologie in het UMCU, bedankt voor de hulp bij de RNA extractie. Jan Veldink, dank voor je hulp en begeleiding bij het uitvoeren en interpreteren van de RNA sequencing analyses. Fabrizio Giuliani, thank you for helping me with the quality analysis and designing the figures. Dr. De Muynck en Prof.dr. Van Damme, hartelijk dank voor het uitvoeren van het validatie-experiment in hoofdstuk 4. Jelena, dank dat je mij hebt leren pipetteren!

Roos, Erwin, Bram, Ali en Bas, het was super leuk om met jullie als studenten Technische Geneeskunde samen te werken. Bedankt voor jullie bijdrage aan de 7.0 Tesla MRI stukken. Nikki, bedankt voor je hulp bij de systematic review en de lange adem die je daarvoor nodig had. Frank en Ingeborg, nu zelf onderzoeker/neuroloog in opleiding, bedankt voor jullie hulp bij de dataverzameling van hoofdstuk 3.

Beste Prof.dr. C.J.M. Klijn, beste Karin. Als student deed ik bij jou mijn eerste onderzoek, naar Moyamoya ziekte. Het was bijzonder leerzaam om alleen aan deze zeldzame ziekte te werken onder de begeleiding van Gabriël, Luca en jou. Je hebt me geweldig ondersteund en de basis gelegd voor mijn interesse in wetenschappelijk onderzoek, waarvoor dank.

Prof.dr. Y.B.W.E.M. Roos, Prof.dr. I.N. van Schaik en Prof.dr. J.H.T.M. Koelman. Beste Yvo, Ivo en Hans. Bedankt voor het vertrouwen om mij als niet-AMC'er aan te nemen voor de opleiding. Beste collega AIOS en staf neurologie AMC, bedankt voor de goede sfeer, het gezamenlijk gevoel van verantwoordelijkheid voor de patiëntenzorg en natuurlijk de gezellige borrels! Jaargenoten, Madieke, Leroy, Sven en Esther, allemaal in hetzelfde drukke schuitje, maar met onze regelmatige etentjes is het goed vol te houden.

Arts-assistenten neurologie en neurochirurgie in het UMCU, bedankt voor de leuke vijf jaar met talloze gezellige activiteiten, zoals de toffe weekendjes in het 'neuro-huis' in de Ardennen, de dagelijkse lunch, de vele congressen en het tijdens-werktijd-boottochtje bij 30° Celsius. Celine, Stijntje, Daan, Charlotte C, Femke en de andere aneurysma-onderzoekers, dezelfde promotor hebben geeft toch een soort band. Het was gezellig om met jullie in het clubje te zitten!

Beste medebewoners van kamertje 1, beste Yael, Sophie, Susanne, Willem, Manon, Lieza, Janneke, Eduard, Merel, Joyce, Marcel en Onno. Bedankt voor alle gezelligheid. Ik hoop dat jullie onze traditie van kerstontbijt met YouTube haardvuur en paasontbijt met verse eitjes van Geert Jan ook op jullie nieuwe werkplekken in stand houden.

Naast het promoveren moet er ook tijd zijn voor ontspanning. Lieve vrienden van de 'Angeren'-groep, Larissa en Djamille, Sabine en Marijn, Kim-My en Barry, en Jacinthe en Rob, zonder alle leuke activiteiten, etentjes, vakanties en weekendjes weg was deze tijd een stuk zwaarder geweest. Meiden van Popcorn, bedankt voor de muzikale ontspanning. Karina, Bart-Jan, Amani, Annette, Jonathan en David, sinds we in jaar 3 van geneeskunde 'groepje 2' werden, hebben we meerdere life events met elkaar gedeeld, waarvan mijn promotie er weer één is!

Lieve Iris, vriendin en "schone" nicht. Bedankt voor het maken van het prachtige schilderij voor mijn kaft. Het is helemaal geworden zoals ik het in gedachten had. Nu na mijn promotie mijn favoriete hobby wegvalt, kunnen we ons misschien gaan storten op onze carrière als 'kermis-duo'? ;-)

Lieve schoonfamilie. Altijd geïnteresseerd in de voortgang van mijn onderzoek. Nou, het is klaar! Op naar al het moois dat nog komen gaat.

Paranimfen, lieve Karina. Wat een mooie ervaringen hebben we samen opgedaan, onder andere in Kenia en Laos. Bedankt voor je hulp bij de laatste loodjes van deze promotie. Lieve Marieke, mijn kleine zusje, die inmiddels niet meer zo klein is. Ik vind het super dat

we allebei in Utrecht wonen en elkaar veel zien. Bedankt dat je altijd voor me klaar staat en natuurlijk dat jij vandaag naast mij staat!

Lieve oma Miek, altijd ongekend trots op mij. Ik vind het heel erg fijn dat u alle belangrijke momenten in mijn leven tot nu toe heeft meegemaakt. Dat er nog maar vele mogen volgen.

Lief broertje, Tim en natuurlijk ook Mirjam en Stefan, bedankt dat jullie er altijd zijn en natuurlijk voor alle gezellige etentjes, spelletjes en potjes Mario op de Nintendo.

Lieve papa en mama, jullie hebben me altijd gesteund in wat ik graag wilde en hebben mij het vertrouwen gegeven dat ik het ook kon. Zonder jullie vangnet was het me niet gelukt. Bedankt voor alle extra oppas-, strijk- en schoonmaakacties in de afrondende periode van dit proefschrift.

Lieve Wilco, wat ben ik een enorme bofkont met jou! Als er iemand is zonder wie dit proefschrift er niet was geweest, dan ben jij het wel. Jij geeft mij alle ruimte om mijn dromen na te jagen. Ik heb respect voor je enorme geduld en je zorgzame karakter. Bedankt voor je onvoorwaardelijke liefde en op naar een mooie toekomst met ons gezinnetje!

Lieve Isabel, ons zonnetje in huis, wat een geluk dat jij er bent!

ABOUT THE AUTHOR

CURRICULUM VITAE

Rachel Kleinloog was born on October 2nd, 1985 in Delft, the Netherlands. She grew up in Wohlenschwil, Switzerland and IJsselstein with a younger brother and sister. She graduated from the Oosterlicht College in Nieuwegein in 2004 (Gymnasium). In the same year she started studying Medicine at the Utrecht University. After one year she obtained her propedeuse (cum laude), and as part of her medical training she went abroad for two internships: Gynaecology and Obstetrics in Garissa, Kenya, and Public Health in Savannakhet, Laos. In 2009 she started a research project on Moyamoya disease under supervision of Prof.dr. C.J.M. Klijn, Prof.dr. G.J.E. Rinkel, and Prof.dr. L. Regli at the department of Neurology and Neurosurgery of the University Medical Center Utrecht. After her graduation in 2010 she started a new research project on intracranial aneurysms under supervision of dr. Y.M. Ruigrok, dr. B.H. Verweij, Prof.dr. L. Regli, and Prof.dr. G.J.E. Rinkel, resulting in this thesis. In July 2014 she started working as a resident at the department of Neurology of the University Medical Center Utrecht. Since January 2015, she is trained to become a neurologist at the Academical Medical Center in Amsterdam (Prof.dr. Y.B.W.E.M. Roos, Prof.dr. I.N. van Schaik, Prof.dr. J.H.T.M. Koelman), and she expects to finish her training in 2021. Rachel is married to Wilco, and they live in Utrecht with their daughter Isabel.

LIST OF PUBLICATIONS

This thesis

Kleinloog R, van 't Hof FN, Wolters FJ, Rasing I, van der Schaaf IC, Rinkel GJ, Ruigrok YM. The association between genetic risk factors and the size of intracranial aneurysms at time of rupture. *Neurosurgery*. 2013;73:705-708.

Kleinloog R, Korkmaz E, Zwanenburg JJ, Kuijf HJ, Visser F, Blankena R, Post JA, Ruigrok YM, Luijten PR, Regli L, Rinkel GJ, Verweij BH. Visualization of the aneurysm wall: a 7.0-tesla magnetic resonance imaging study. *Neurosurgery*. 2014;75:614-622.

Blankena R, **Kleinloog R**, Verweij BH, van Ooij P, Ten Haken B, Luijten PR, Rinkel GJ, Zwanenburg JJ. Thinner regions of intracranial aneurysm wall correlate with regions of higher wall shear stress, a 7T MRI Study. *AJNR Am J Neuroradiol*. 2016;37:1310-1317.

Kleinloog R, Verweij BH, van der Vlies P, Deelen P, Swertz MA, De Muynck L, Van Damme P, Giuliani F, Regli L, van der Zwan A, Berkelbach van der Sprenkel JW, Han KS, Gosselaar P, van Rijen PC, Korkmaz E, Post JA, Rinkel GJ, Veldink JH, Ruigrok YM. RNA sequencing analysis of intracranial aneurysm walls reveals involvement of lysosomes and immunoglobulins in rupture. *Stroke*. 2016;47:1286-1293.

Kleinloog R, de Mul N, Verweij BH, Post JA, Rinkel GJ, Ruigrok YM. Risk factors for intracranial aneurysm rupture: a systematic review. *Neurosurgery*. 2017;doi 10.1093/neuros/nyx238. [Epub ahead of print]

Other publications

Kleinloog R, Regli L, Rinkel GJ, Klijn CJ. Regional differences in incidence and patient characteristics of moyamoya disease: a systematic review. *J Neurol Neurosurg Psychiatry*. 2012;83:531-536.

van 't Hof FN, Kurki MI, **Kleinloog R**, de Bakker PI, von und zu Fraunberg M, Jääskeläinen JE, Gaál EI, Lehto H, Kivisaari R, Laakso A, Niemelä M, Hernesniemi J, Brouwer MC, van de Beek D, Rinkel GJ, Ruigrok YM. Genetic risk load according to the site of intracranial aneurysms. *Neurology*. 2014;83:34-39.

Farlow JL, Lin H, Sauerbeck L, Lai D, Koller DL, Pugh E, Hetrick K, Ling H, **Kleinloog R**, van der Vlies P, Deelen P, Swertz MA, Verweij BH, Regli L, Rinkel GJ, Ruigrok YM, Doheny K, Liu Y, Broderick J, Foroud T. Lessons learned from whole exome sequencing in multiplex families affected by a complex genetic disorder, intracranial aneurysm. *PLoS One*. 2015;10:e0121104.

Korkmaz E, **Kleinloog R**, Verweij BH, Allijn IE, Hekking LHP, Regli L, Rinkel GJE, Ruigrok YM, Post JA. Comparative ultrastructural and stereological analyses of unruptured and ruptured saccular intracranial aneurysms. *J Neurol Exp Neurosci*. In press.